ALMA MATER STUDIORUM
UNIVERSITÀ DI BOLOGNA

DOTTORATO DI RICERCA IN

Nanoscienze per la medicina e per l'ambiente

Ciclo XXXVII

Settore Concorsuale: 03/B1 – Fondamenti delle scienze chimiche e sistemi inorganici

Settore Scientifico Disciplinare: CHIM03 – Chimica generale ed inorganica

Luminescence-based techniques for water quality monitoring

Presentata da: *Filippo Ingargiola*

Coordinatore Dottorato
Prof. Matteo Calvaresi

Supervisore
Prof. Luca Prodi

Esame finale anno 2025

Table of Contents

Abstract

Water quality monitoring is a key aspect for providing and maintaining clean water supplies for the whole world. Water pollutants are many and heterogeneous in chemical nature so numerous sensing techniques and platforms are needed to provide a comprehensive analysis of water samples. In this context, sensors with an optical signal transduction mechanism can provide numerous advantages such as cost-effectiveness, ease of use, and rapid outputs. This PhD thesis describes three different approaches for the sensing of polluting chemical species relevant to water quality, employing luminescent based techniques.

Detection of nonsteroidal anti-inflammatory drugs (NSAIDs), representing the category of "emerging pollutants", was performed employing supramolecular fluorescent sensors capable of binging NSAIDs via hydrogen bonds and hydrophobic interactions in organic medium. Two different sets of sensors were developed, characterized and tested against common NSAIDs.

Luminescent Eu(III) metal complexes were used to sense inorganic anionic species relevant to water quality monitoring. The peculiar photophysical properties of Eu(III) allowed us to obtain different outputs to different analytes; moreover, the high Lewis acidity of Eu(III) made the complexes able to bind anions in aqueous environment. An electrochemiluminescence-based immunosensor for the detection of Listeria was developed - in collaboration with Diatheva s.r.l. - as proof of concept, employing the architecture of an already existing immunoassay, to see how the assay's performances could be enhanced, with minimal changes to the design. The architecture of the assay was adapted from a commercial ELISA developed by Diatheva and modified to be used in ECL, with the aid of magnetic micro-beads technology, obtaining promising results. Overall, this thesis presented valid optical-based sensing techniques applicable to environmental water quality monitoring. Moreover, this work represents a promising advancement in the field of sensing techniques development.

1. Introduction

1.1 Water quality

Water has always been the most precious resource for humanity and the planet, being fundamental to the development and sustaining of all life forms, and a key element for the equilibrium of Earth's ecosystem. Water is not scarce on the planet, but its good quality is not assured, mainly because pollution of accessible water sources renders them unusable not only for human consumption and activities, but also for animal proliferation and wellbeing; it is also important to note that the majority of water on the planet is salty and unusable for consumption. Recent reports estimated that nearly a quarter of the world's population cannot access safe drinking water, with critical locations, such as India and Africa where the percentage is much higher.[1] Pollution has plagued water systems for long times, probably since even before the advent of the industrial revolution, mainly because of the belief that water bodies could be used as self-renewing waste disposal sites;[2] from agricultural and industrial byproducts to municipal waste, water accumulated trough time all sorts of pollutants. Nowadays most of the countries of the world have implemented strict legislation and plans to face water quality necessities.[3]

Together with remediation techniques, one of the key aspects for water quality is its precise and frequent monitoring; understanding where and how water sources get contaminated is crucial to developing plans to maintain a clean water supply for the whole world. There are numerous ways of approaching water quality analysis; the more traditional one involves the collection of samples and their transport to a laboratory, where they are analyzed by trained personnel, utilizing high-end instrumentation and cutting-edge techniques. Conventionally, different filtration and fermentation techniques, DNA amplification, electrophoresis,

chromatography, and mass spectroscopy[4,5] are the common tools of laboratory-based analysis. The benefits of this approach have long been recognized and it is widely recognized as the gold standard for the classification and quantification of pollutants, although this type of analysis is often relatively expensive, due to the cost associated with the complex instrumentation required, and not easily capable of providing real time results, especially when dealing with complex analytes such as organic pollutants or biomolecules. While commercial platforms for online monitoring of basic water parameters like pH, turbidity, and ionic strength are already available on the market, significant progress is still needed to enable real-time detection of more complex pollutants. On-site measurements and monitoring are nowadays the preferred approaches for water monitoring; technological advancement of analytical techniques allows the construction of versatile sensors that are cheap to fabricate, easy to use, and capable of on-site deployment, circumventing the necessity to transport samples to laboratories and their treatment, allowing the real-time collection of data. In this context, chemosensors are a valuable tool to be employed for water monitoring.[1] This does not mean that more refined and complex analytical techniques should be replaced by chemosensors, since it would be difficult to reach the same levels of precision; chemosensors can be advantageously introduced as a complementary technology to more laborious and accurate analytical techniques, to ease the process of routine monitoring of waterbodies.

1.2 Pollution and pollutants

There are many ways to categorize the many substances and compounds that can be considered water pollutants, the easiest being to differentiate organic, inorganic and biological pollutants; each of these categories presents unique challenges for the construction of adequate sensing systems.

The category of inorganic pollutants is probably the most known and understood; metals such as antimony, cadmium, chromium, cobalt, lead, manganese, mercury, but also non-metallic compounds like fluorides, cyanides, nitrates, sulphates, phosphates, are just a few examples of substances with known detrimental effects on the environment that are routinely monitored in water bodies. Many different techniques are employed to monitor inorganic components in water, from simple colorimetric assays to more sophisticated electrochemical or chromatographic techniques; the most limiting factor of the already employed methods is that each analyte is quantified singularly, so many different analyses are required to obtain the full characterization of a water sample.[6]

Organic pollutants are a more recently understood problem to the environment; many of such polluting substances are referred to as "chemicals of emerging concern" (CECs); the name stems from the fact that the interest for these substances is fairly recent. CECs are usually persistent chemicals that are not monitored in routine analysis and whose concentration is not yet subject to regulation. CECs are usually categorized in "emerging pollutants" (EPs), referring to chemicals with known and scientifically proven detrimental effects to the environment and could be inserted in routine analysis, and "emerging substances" (ESs) that still need more proof to be considered pollutants.[7] Among EPs we can find numerous categories of chemical such as pharmaceuticals, personal care products, plasticizers, pesticides, surfactants, coming both from industrial and private settings. The biggest challenge about EPs is their number and heterogeneity both in chemical structure and effects on the environment; since the number of compounds in the EP's family is always increasing, there is the need for analytical platforms to facilitate the monitoring of these compounds.

Water pollution is not limited to chemical compounds, it can also be caused by biological sources; waterborne pathogens, such as bacteria, viruses, protozoa, parasites, and related diseases are a major concern worldwide, not only because of the morbidity and mortality they cause, but also because these diseases are related

to the deterioration and pollution of water bodies. It is estimated that more than 3% of deaths globally are attributable to unsafe water caused by poor sanitation and hygiene, and the global cost of waterborne diseases is about 12 billion US dollars annually.[8]

Currently there is no unified method that encompass the collection and analysis of water samples for all pathogenic microorganism of interest; the traditional techniques for waterborne pathogens are mainly culture-based techniques, polymerase chain reaction (PCR)-based techniques and immunological techniques, and even if they are all efficient, each of them presents some limitations[9] Culture dependent methods, for example, are limited by low sensitivity, excessive time needed to obtain results, and false negatives that can be given by non-culturable pathogens in the samples. PCR and immunological methods suffer from the need for sample pre-treatment, which can be time consuming, and given the high sensitivity of these techniques, they are at risk of false positive results. Another significant limitation of monitoring biological water pollution is the sheer quantity of pathogens to be considered: the classic approach is to select and analyze for "index pathogens", like *E. coli*, the presence of which indicates a large quantity of pathogens in water. Although this approach is easy and inexpensive, there is the risk of missing microorganisms not correlated with the chosen index pathogens.[10] It is important to mention in this context that most of the legislations, parameters and agencies who regulate water quality are mostly local, national or international at best, so there is a distinct lack of an "universal" code to parametrize water pollution; moreover, different categories of waterbodies may present different requirements.[11] Lastly, for some of the pollutants mentioned above, especially EPs, since there is still research to be done to understand their effects on the environment, there are still no defined limit for their presence in waterbodies.

1.3 Optical chemosensors

The International Union of Pure and Applied Chemistry (IUPAC) defined chemosensors as “devices that transform chemical information, ranging from the concentration of a single analyte to total composition analysis, into an analytically useful signal”.[12] To do that a chemosensor need a sensible part of the structure, capable of interacting with the analyte creating a variation in the part of the sensor that transduces this interaction in a readable signal. Different types of interactions can be used to effectively bind the analyte to the sensor, including covalent chemical bonds as well as noncovalent interactions such as hydrogen bonding, hydrophobic forces, and electrostatic interactions; depending on the target analyte and its chemical nature and structure one or more of these interactions can be employed. It is important to underline that the interactions between the chemosensor and the analyte should be reversible thus allowing the sensor to follow concentration changes; if the analytes are bound in an irreversible way the chemosensor should be referred to as a “chemodosimeter”. In the same way as the binding unit of the sensor, also the signal transduction mode can be chosen and tailored to the need of the specific sensor. For example, electrochemical sensors, monitoring properties such as voltage, impedance or amperage, are often used to continuously determine different water properties.[13]

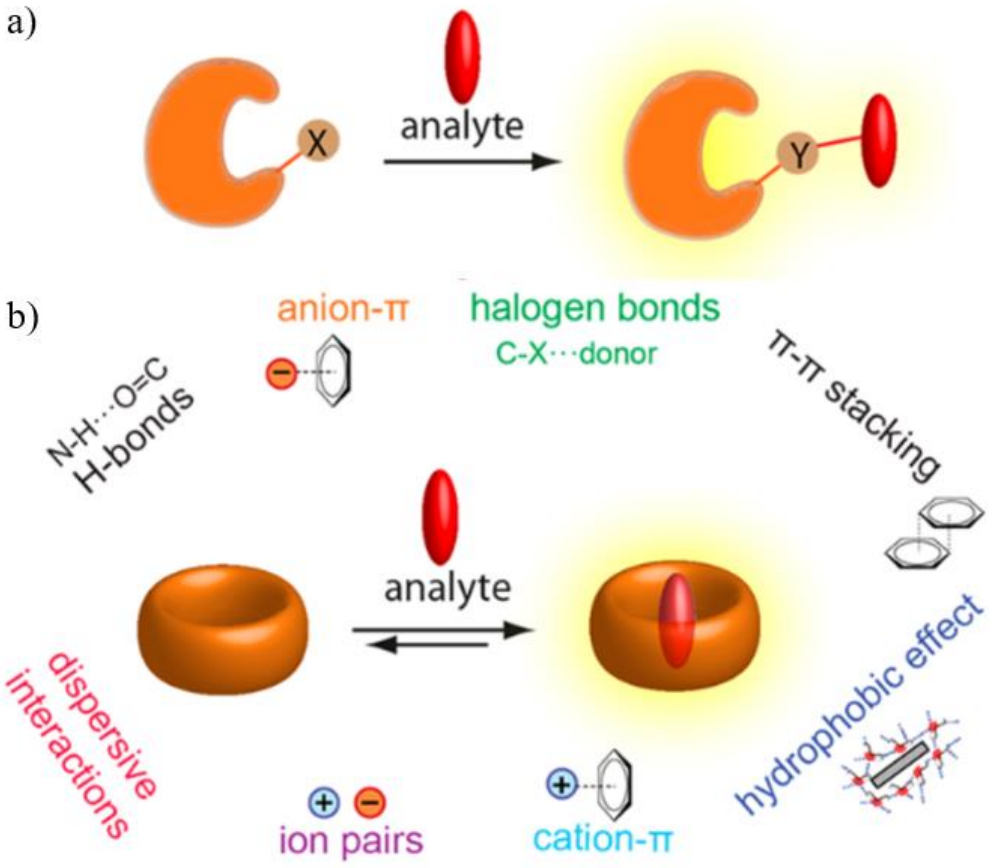

Figure 1. *Schematic representation of: a) a chemodosimeter forming a covalent bond with the analyte. b) a chemosensor and non-covalent interaction that can be employed to interact with the analyte. Adapted from [14].*

A common and versatile class of chemosensors is that of optical sensors; this category of sensors operates transducing chemical information into an optical signal, such as absorbance (color development), reflectance, scattering, and luminescence, and each of this type of signal generation has its own advantages.[15] A colorimetric chemosensor – *i.e.*, a sensor capable of change in color upon analyte detection – offers the possibility of performing very rapid analysis that often can be interpreted with the naked eye, without the need of expensive instrumentation or skilful personnel. Fluorescent sensors offer the possibility of reaching very high sensitivity, high spatial and temporal resolution, while phosphorescent sensors with long lived emissions offer the possibility to do time resolved analysis with very low signal to noise ratio. Nowadays, the technology to collect and analyze luminescent signals is very cheap, so these kinds of techniques are becoming more

and more affordable, and many routine monitoring are already being conducted with optical chemosensors.[1]

1.4 Lock&key approach vs. differential sensing

Traditionally chemosensors have been designed following the "lock & key" principle: taking inspiration from nature's highly specific and sensitive binding interactions, such as enzyme-substrate or antibody-antigen recognition. Historically the "lock & key" principle was postulated by Emil Fisher in 1894[16] and it can be summarized as "the better the geometric fit between the substrate (key) and the active site (keyhole), the stronger the interaction". Nowadays it is understood that the formation of a host-guest complex does not depend on the optimal geometric fit between the two. Allosteric interactions, induced fit, hydrophilic and hydrophobic interactions, are just some of the factors that influence the formation of a stable complex between the substrate and the active binding site. In time the concept of "lock & key" chemosensor has become associated with the idea of having a highly sensitive and highly selective sensor developed for the sensing of a single analyte.

Chemists nowadays hold all the tools needed for synthesizing chemosensors that possess binding moieties endowed with high degree of sensitivity toward a single specific analyte. Even though the process of rational design and computation modelling needed to develop receptors with good selectivity for many classes of small molecules has been vastly understood, this is not the only strategy – and in some case, not the best one – that can be used for chemosensing. In more recent times the approach of "differential sensing" (or combinatorial sensing), has gained a lot of research interest. Taking again inspiration from nature's sensing tools, in this case the olfactory and gustatory systems, differential sensing is based on the use of libraries of receptors whose binding characteristics are more generalized rather than specialized. Using this approach, one can analyze the composite signal

of the whole library of sensors, with appropriate pattern recognition protocols, and obtain information for a given single analyte, but most importantly for multi-analyte samples in a single measurement.[17] Differential sensing arrays can generate large quantities of data, so for this approach having adequate statistical techniques to interpret this data is as important as building the sensor array itself. Numerous pattern recognition methods to interpret sensor array data have been developed; principal component analysis (PCA), hierarchical clustering analysis (HCA), linear discriminant analysis (LDA), artificial neural networks (ANN) are among the most recognized, but many more approaches can be applied to this type of data, each one presenting different advantages and disadvantages.[18,19]

Both approaches are valid and both present advantages and disadvantages; the lock & key approach is vastly understood and has been proven to be effective for the development of highly sensitive and selective sensors for both simple targets, such as metal cations, and more complex analytes like pathogens and toxins. Differential sensing on the other hand might require more effort to develop a sensing platform, needing both numerous chemosensors and an adequate protocol for signal interpretation, but is able to provide multi-analyte data in a single measurement.[20] Following this approach Peng et al. were able to develop a sensor array based on Au-nanoparticles, capable of quickly discerning breath samples of healthy people, form those affected by lung cancer, by analysing 42 different volatile organic compounds and their relative concentration in breath samples.[21] One of the main aspects to keep in mind when deciding to use one or the other approach is the type of analytes present in the sample and the information needed: when dealing with the determination of multiple analytes, especially if the interest of the analysis lies in a vast category of compounds similar to each other, differential approach could provide numerous advantages; if the interest lies in a single specific analyte at a very low concentration, or with a complex structure like a pathogen, the lock and key approach might be favored.

1.5 Aim of the thesis

Optical sensing is an extremely versatile approach for developing environmental monitoring platforms, since it offers many different strategies, both for the binding of analytes and the signal transduction modes; this can offer a multitude of strategies that can be tailored to suit many different needs in the field of water quality analysis.

The aim of this project is to develop optical sensing platforms, using different approaches to tackle the detection of three different classes of water pollutants. The first work described in the thesis will be focused on the approach used to develop fluorescent and colorimetric sensors for the detection of nonsteroidal anti-inflammatory drugs as an example of organic pollutants, utilizing a supramolecular approach for the binding of the analytes. The second part of the thesis will tackle the detection of common inorganic anionic species commonly monitored during standard water quality analysis; the peculiar optical and coordination properties of luminescent europium (Eu) metal complexes will be exploited to bind and sense anionic species, following a differential sensing approach to sense multiple analytes. Lastly, the third section of the thesis will tackle biological pollution; selecting Listeria Monocytogenes as case study, to develop an electrochemiluminescence (ECL) bioassay as an alternative to culture-based methods for the sensing of pathogenic organisms.

2. Luminescent sensors for NSAIDs sensing

2.1 Introduction - Nonsteroidal anti-inflammatory drugs as emerging pollutants

Emerging Pollutants, as stated before, are a vast and very heterogeneous family of chemical, in which many categories of compounds belong, such as pharmaceuticals, plasticizers, surfactants, personal care products and many more.[22] Among the pharmaceuticals compounds belonging to the EPs category, Nonsteroidal anti-inflammatory drugs (NSAIDs), together with antibiotics, are the most common to be found in the environment.[23] NSAIDs are extensively used, both in humans and in animals, for their analgesic, antipyretic and anti-inflammatory action, based on the inhibition of prostaglandins production by COX enzymes. NSAIDs compounds are many and can be classified by their chemical nature; salicylic acid derivates (aspirin, diflunisal), acetic acid derivatives (diclofenac, ketorolac), propionic acid derivatives (ketoprofen, naproxen, ibuprofen), anthranilic and enolic acids derivatives, and non-acid NSAIDs (benzidamine, nabumetone). Chemical properties of NSAIDs, such as their acidity (although they are commonly sold as sodium or lysine salts), polarity and high excretion rate by human body, and the fact that common water treatment facilities do not remove this type of chemicals, cause these compounds to be found in water bodies around the world, at relative high concentration, in the range of ng/L to ug/L; the most common to be found are ketoprofen, ibuprofen, naproxen, and diclofenac, but as many as 26 different NSAIDs have been found in different water systems around the world.[24] It is also important to note that due to their chemical

characteristics, NSAIDs are hardly degraded in the environment; one of the more promising advances in this field is the use of microorganism to break down NSAIDs in water bodies and water treatment plants. Since much work on the fate of NSAIDs in nature has still to be done, this work will be mainly focused on NSAIDs molecule as they are, not considering the various byproducts of natural or chemical-induced degradation.

NSAID's impact on the environment has been proven to be detrimental to many types of life forms. Due to NSAIDs propensity to accumulate in water, aquatic wildlife such as fishes, molluscs, crustaceans, and amphibians, are the first organisms to be effected, but detrimental effects caused by NSAIDs exposure are also present in land animals. It has been proven by numerous studies that chronic exposure to NSAIDs, even at low concentrations, can negatively affect animals in numerous ways: these compounds can act as endocrine system disruptors, thus affecting their natural hormonal equilibrium, causing problem involving reproduction, such as infertility, hermaphroditism, and development of offsprings. NSAIDs exposure has also been linked to genotoxicity, teratogenicity, hemotoxicity, cellular oxidative stress in many lives forms not limited to aquatic ones.[25] NSAIDs are usually detected in water samples using traditional chromatographic techniques such as HPLC-MS and GC-MS coupled with specialized extraction techniques or ultra-trace LC-MS/MS GC-MS/MS techniques.[26] These methods are considered a golden standard for the analysis of these types of compounds, but they also are expensive, time consuming and specialized personnel is needed to conduct them; nowadays there is the need to develop new platform to facilitate the sensing and monitoring of NSAIDs especially to facilitate routine monitoring of these chemicals around the world. In this context, since there are dozens of compounds in the NSAIDs family, the approach of differential sensing can be used to develop a sensing platform, without the need to synthetize a selective chemosensor for each compound.

2.2 Design and synthesis – Dansyl ligands

The set of chemosensors was designed considering ketoprofen (KET) and naproxen (NPX) as potential targets. KET and NPX, like many other NSAIDs, are characterized by carboxylate moiety and an overall hydrophobic skeleton. Ideally, the binding unit should possess strong hydrogen-bond (HB) donors to interact with the carboxylate, and an aromatic part to interact with the aromatic rings of the drugs, via π-π stacking and hydrophobic interactions.[27,28] Among HB donor scaffolds, squaramide (3,4-diamino-3-cyclobuten-1,2-dione derivatives) is one of the most efficient: it is in fact an aromatic four-member ring that possesses interesting physical and chemical properties, such as rigidity, aromaticity and an ability to form strong HB, caused by the increase of aromaticity of the squaramide upon HB formation.[29,30] Moreover, coupling two or more squaramide moieties in a macrocycle reinforces the binding of anionic species, especially carboxylates.[31] One of the first reported use of squaramides as receptors for carboxylates was by Costa, Ballenster and coworkers in 1998, where they demonstrated that squaramide's N-Hs can act as H-Bond donors even in highly competitive media.[32] Over the last 20 years squaramides have been successfully employed in anion binding and sensing field, acting as stronger H-Bond donor when compared to analogous ureas, even in aqueous environments, where anion binding faces the hardest challenges.[33] Squaramide-based receptors have been successfully employed to electrochemically sense NSAIDs in aqueous environment with high degree of sensitivity.[34]

With these considerations in mind, we realized four dansylated squaramide based receptors for NPX and KET (Fig.2); each receptor has two squaramides for NSAIDs complexation and one (**L2-L4**) or two **(L1**) dansyl fluorescent units for signal transduction. The receptors present structural differences between them: **L1** and **L2** have a macrocyclic topology, while **L3** and **L4** have an open receptor unit, terminating in benzyl groups in **L3** to enhance hydrophobic interactions and terminating in indole units il **L4** to further increase the HB donor number. The non

fluorescent receptor **L5**, showing the same macrocyclic topology of **L1**, has been studied for the sake of comparison.

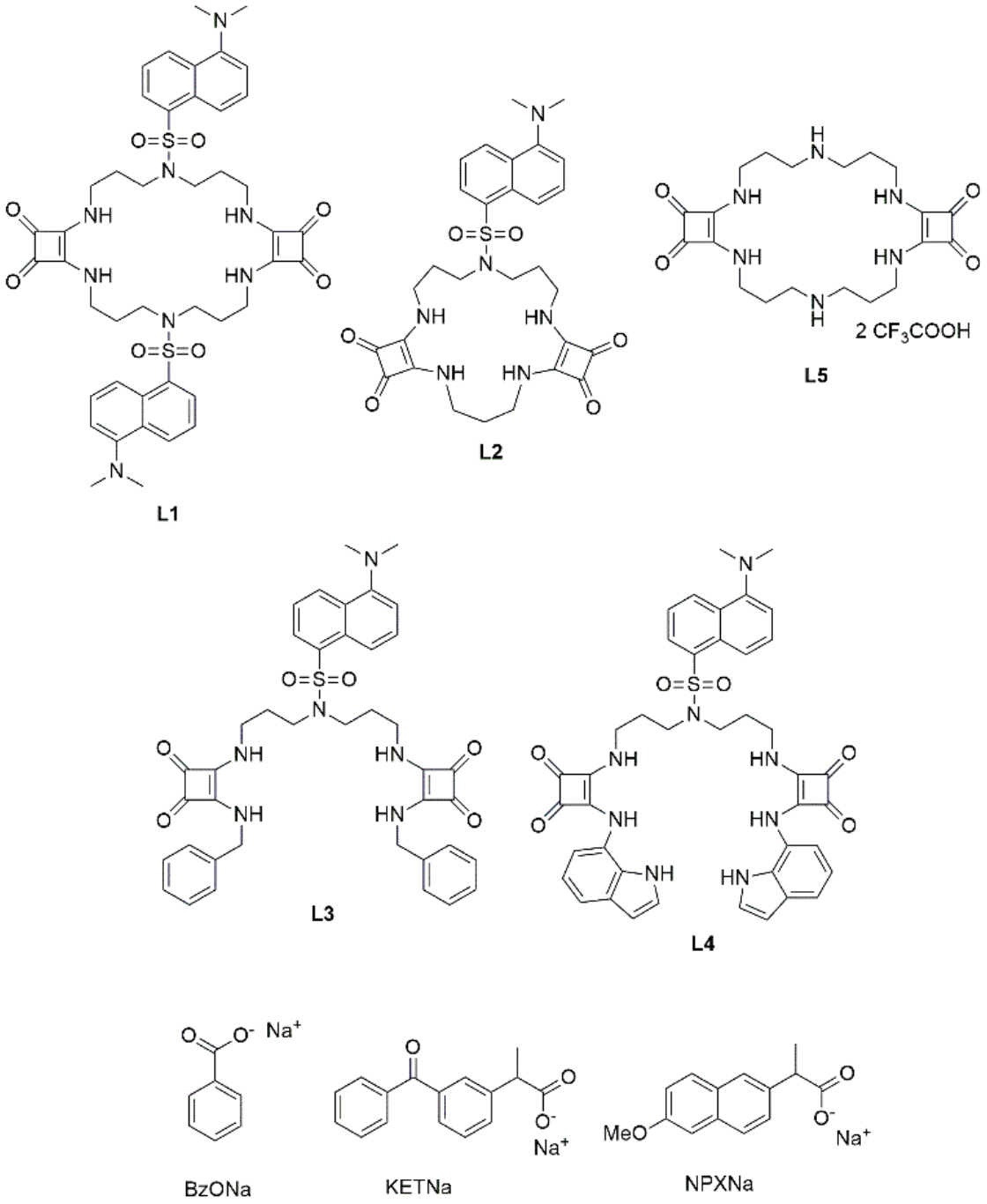

Figure 2. *Chemical structures of the ligands* ***L1-L5****, ketoprofen (KET), naproxen (NPX), and sodium benzoate (BZO).*

The ligands **L1-L5** were synthesized following the procedure described in Fig.3 by Prof. Claudia Caltagirone's group at the University of Cagliari and Prof. Vieri

Fusi's group at the University of Urbino. The synthesis of the ligands has been already discussed and out of the scope of this thesis and will not be discussed further.[35]

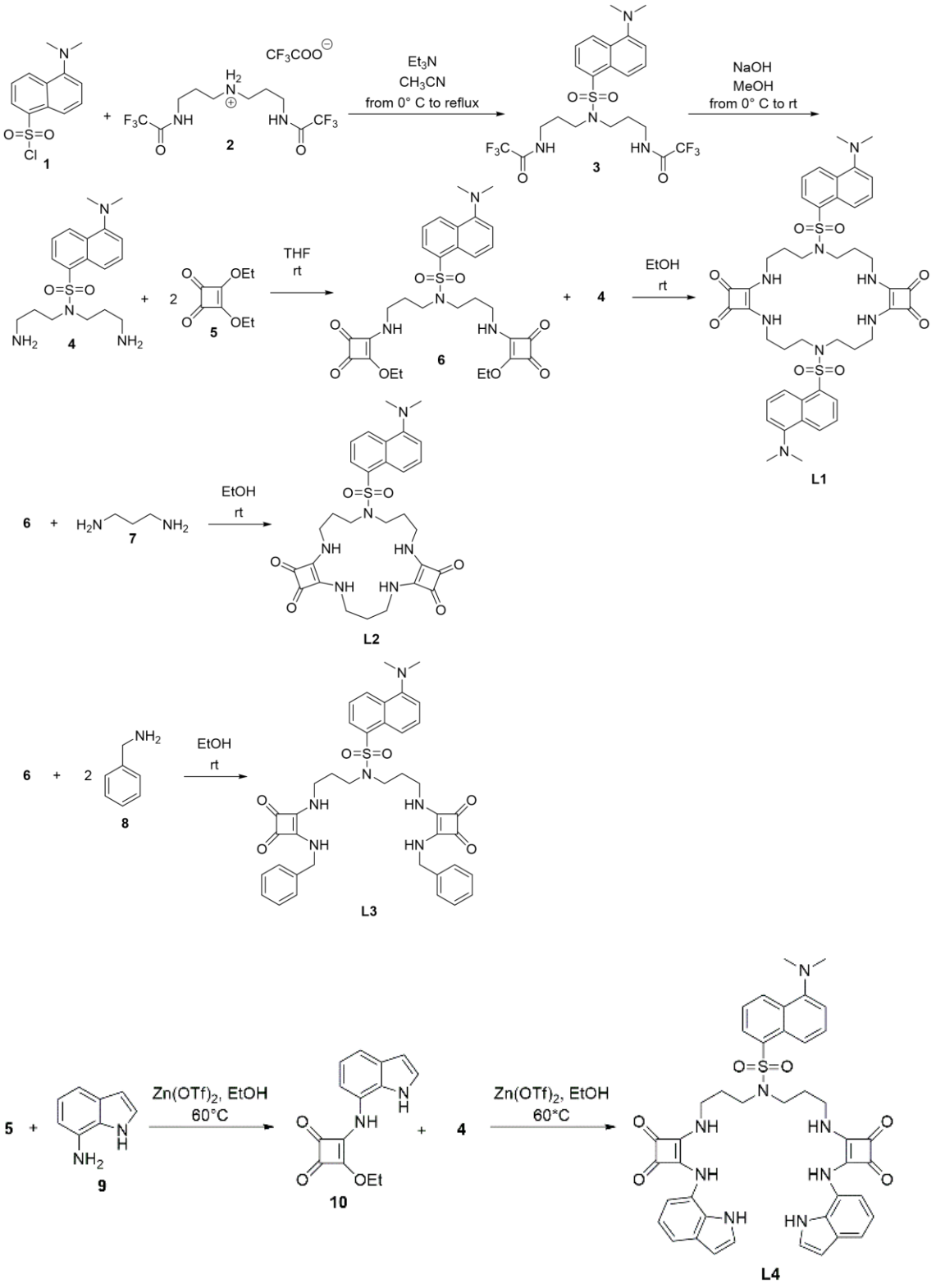

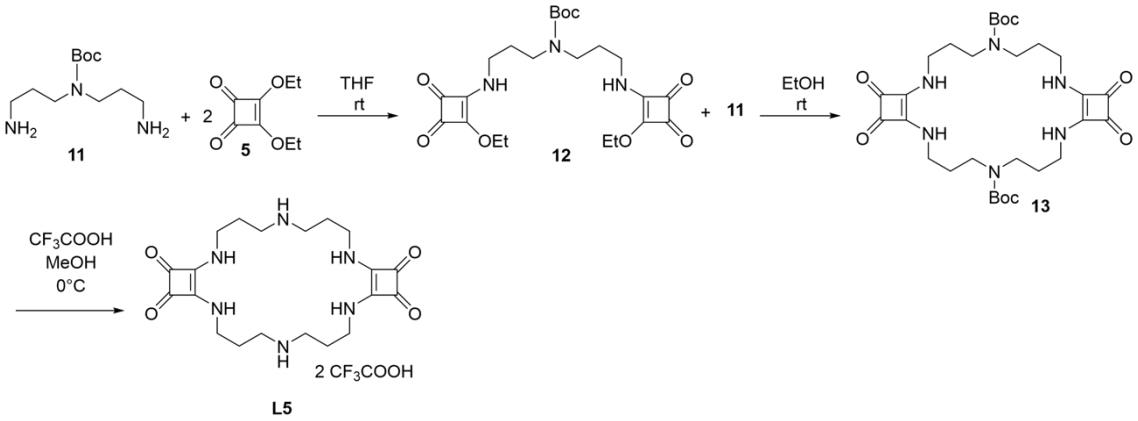

Figure 3. *Reaction scheme for the synthesis of* ***L1-L5****.*

2.3 Photophysical characterization

A detailed photophysical characterization was carried out on **L1-L5**; due to their scarce solubility in water, spectral studies could not be conducted in that solvent or in water mixtures. Preliminary studies were conducted in DMSO, which was capable of solubilizing **L1-L5**; in this solvent the ability of the ligands to interact with NSAIDs was impaired, as can be seen for **L4** with KET (Fig.4), whose absorption and emission spectra were not affected by the addition of KET. Similar results were also obtained for the other receptor.

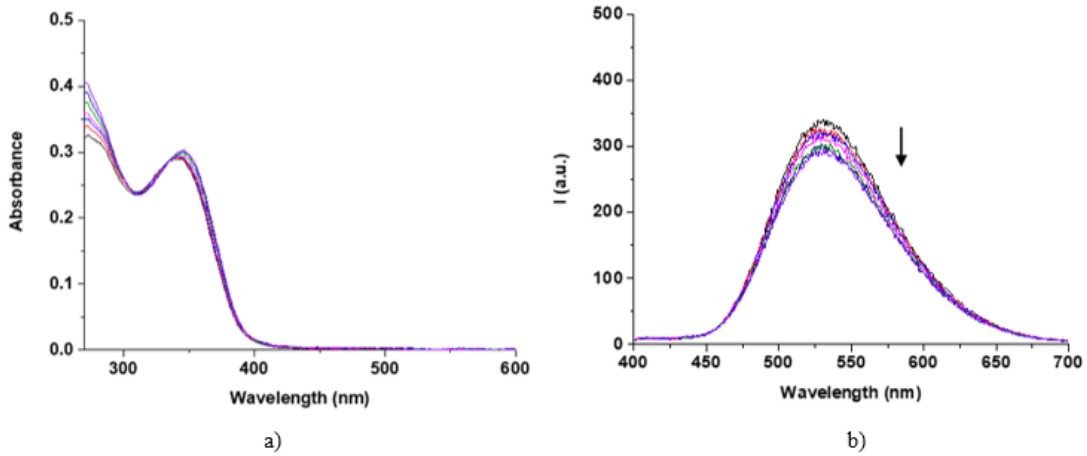

Figure 4. *Absorption (left), and emission (right) spectra of* ***L4*** *titrated with KET in DMSO.*

To enhance the optical characteristics, and NSAIDs interaction, a mixture of ACN/DMSO (90:10 v/v) – a less competitive medium – was chosen to carry out the full characterization. The absorption spectra of **L5** containing two squaramide units shows an intense band (ε = 51000 $M^{-1}cm^{-1}$) at 285nm. The spectra of **L1**, **L2** and **L3** (Fig.5) presents a shoulder in the 310-340 nm region, where the Dansyl chromophore absorbs (dansylamide shows an absorption maximum at 330 nm ε = 3800 $M^{-1}cm^{-1}$); as expected, the spectra of **L1-L3** resembles the mathematical sum of **L5** spectra and one (**L2** and **L3**) or two (**L1**) dansyl units. In the spectra of **L4**, the spectrum shows a relevant contribution by the indole units, showing a maximum at 335 nm. Concerning the emission measurements, in ACN/DMSO (9:1 v/v) at room temperature, **L5**, as expected, does not exhibit any fluorescence, while **L1-L4** show an intense emission band at 525 nm typical of the dansylamide (λ_{max} = 510nm).

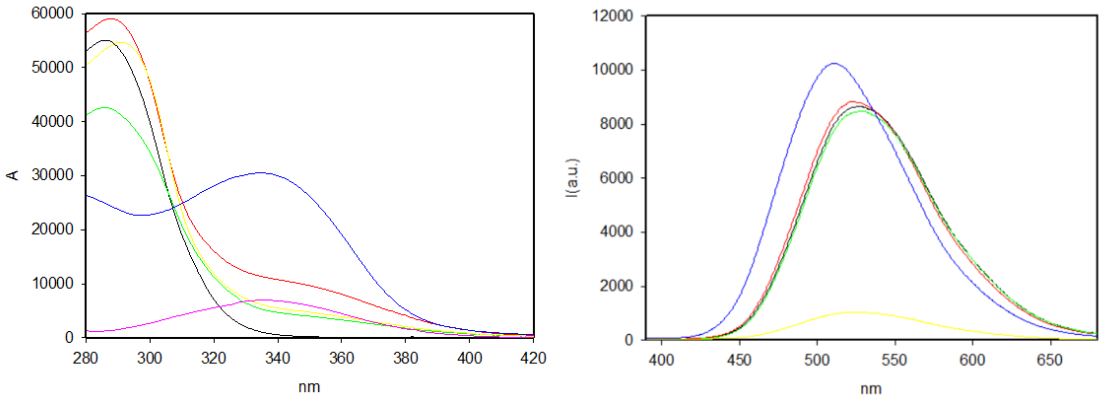

Figure 5. *Absorption spectra (left) in ACN/DMSO (9:1) of **L1** (red), **L2** (green),**L3** (yellow), **L4** (blue), **L5** (black), dansylamide (pink); emission spectra (right) λ_{ex} =350 nm of **L1** (black), **L2** (red), **L3** (green), **L4** (yellow), dansylamide (blue)*

The fluorescence quantum yields (QY) were measured using fluorescein in NaOH (Φ_{fl} = 0.92) as a reference, using Eq. 19, and the fluorescence decay lifetimes were measured via TCSPC (Time-Correlated Single-Photon Counting); the results are gathered in TAB.1. Additional information on the photophysical characterization techniques and procedures can be found in the appendix (paragraph 7.1).

Table 1. *Fluorescence decay lifetimes and QYs of* ***L1-L4*** *and dansylamide at room temperature in ACN/DMSO (90:10 v/v).*

	L1	**L2**	**L3**	**L4**	Dansylamide
τ_{fl} (ns)	13.2	12.5	17.7	11.3	12.9
Φ_{fl}	0.29	0.37	0.23	0.04	0.88

The excitation spectra of **L1-L4** are similar in shape to the absorption spectra of dansylamide, while the contribution of the squaramide is almost completely absent, indicating that there is no energy transfer from the squaramides to the dansyl. The absence of energy transfer from the binding unit to the chromophore, can also explain the lower QY of **L4**, since in this case, the dansyl contribution for the absorption at 330 nm (the excitation wavelength used to measure the QY) can be estimated at around 10%, while the remaining 90% of excitation light is absorbed by the indoles.

2.4 NSAIDs' interaction studies

The receptors' behavior was tested in the presence of KET and NPX; sodium benzoate (BZO) was also tested for comparison. The addition of KET, NPX and BZO as sodium salts to an ACN/DMSO (9:1 v/v) solution of the probes did not cause any change in the absorption spectra (neglecting the absorption contribution of the guests whose absorption spectra is reported in Fig.6 except for **L4**. In this case, the addition of guest species causes a significant red shift of the 350 nm absorption band coupled by an increase in intensity; an evident isosbestic point can be observed at 330 nm (Fig.6). These changes in absorbance can be attributed to the involvement of the indole units in HB formation.

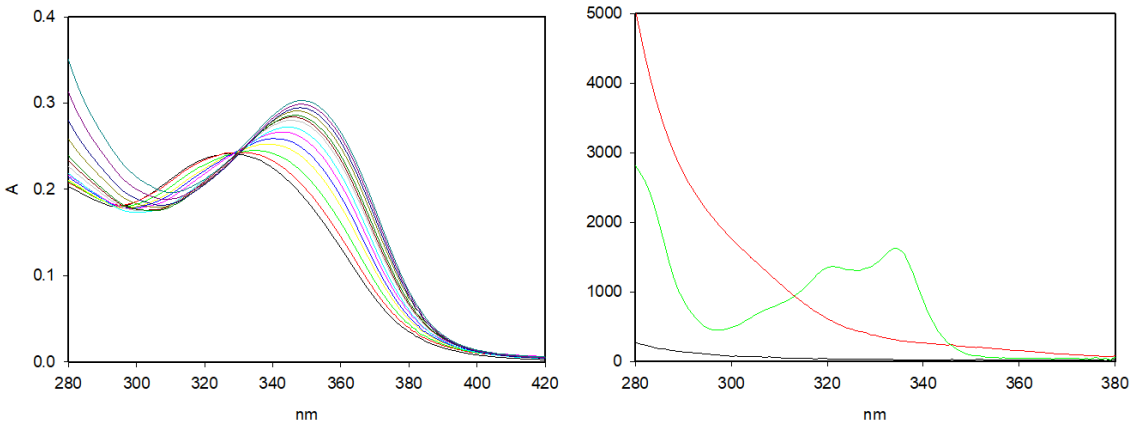

Figure 6. *Absorption spectra of **L4** titrated with KET (left); absorption spectra (right) of KET (red), NPX (green), BZO (black).*

The changes observed in emission are much more significant. In particular, in the case of the macrocyclic receptors **L1** and **L2** the fluorescence is strongly quenched (63% and 71% of the initial value respectively) upon the addition of KET, while the emission remains pretty much unvaried upon addition of NPX and BZO. From the observed quenching we were able to determine the association constants (K_a) for the 1:1 adduct with KET of both **L1** and **L2**. Together with the emission quenching, the addition of KET also perturbed the excided state decay; two distinct lifetimes could be observed for **L1** (4.5 and 9.0 ns) and **L2** (2.8 and 6.0 ns), both shorter than the one measured without guests. The titration of **L1** with KET is reported in Fig.7.

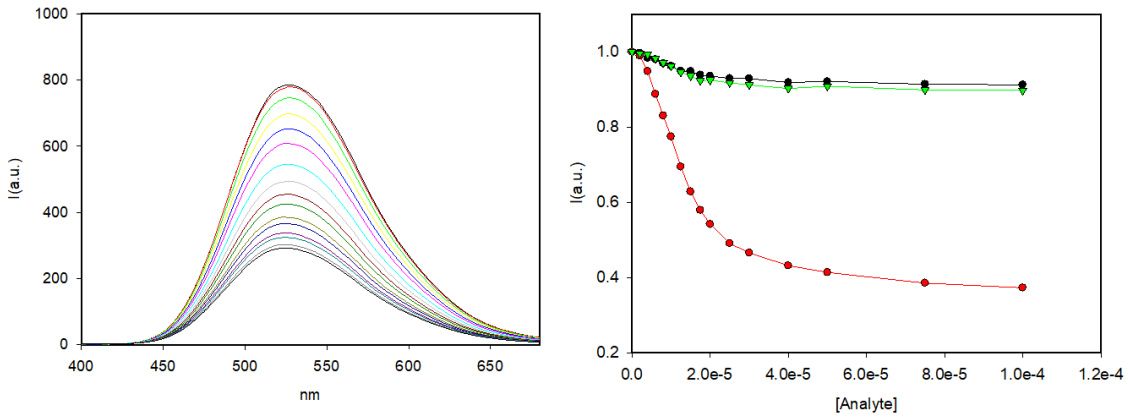

Figure 7. *Fluorescence spectra (λ_{ex} =350 nm) of **L1** titrated with KET (left); titration curves of **L1** (right) with KET (red), NPX (green), BZO (black).*

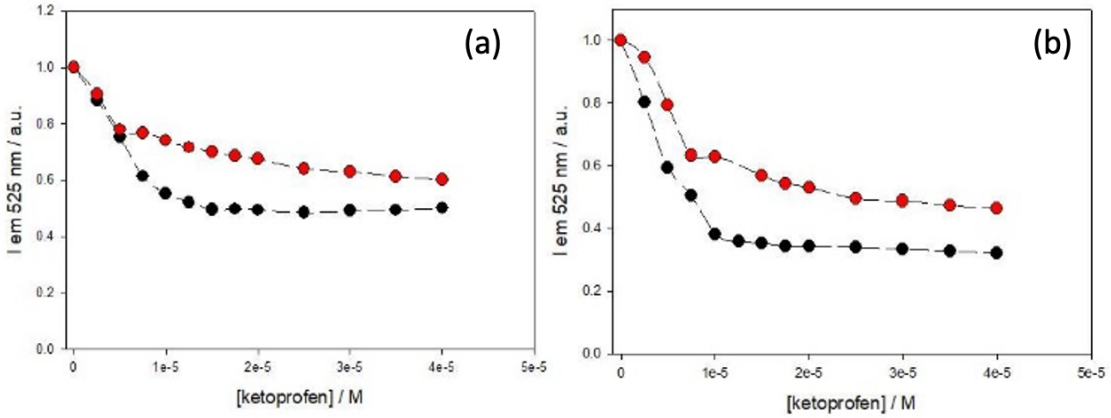

Figure 8. *Titration curves of emission intensities (λ_{exc} = 350 nm; λ_{em} = 525 nm) in CH_3CN/DMSO solution (9:1 v/v) of a)* ***L1*** *and b)* ***L2*** *upon the addition of increasing amount of KET in absence (black) and in presence (red) of BZO.*

To gain insight into possible interference by other chemicals, titrations with ketoprofen were performed also in the presence of BZO, obtaining a shift in the titration curve (Fig.8). This clearly shows that **L1** and **L2** are capable of binding BZO, but its presence does not influence the photophysical properties of the receptors, indicating that **L1** and **L2** are not selective, but sensitive to KET-.

The open receptors **L3** and **L4**, while responding in a similar way to the addition of KET (56% and 68% decrease in emission intensity respectively), underwent a decrease in fluorescence intensity also upon addition of NPX and BZO. In all cases the decrease in fluorescence is accompanied by a biexponential lifetime decay; in case of **L3** (Fig.9) with KET the observed lifetimes were 12.6 and 4.1 ns, 11.8 and 4.0 ns with BZO and 10.9 and 3.9 ns after the addition of NPX, while for **L4** the lifetimes were 2.2 and 11.1 for KET, 2.1 and 10.9 for NPX and 2.3 and 11.2 for BZO.

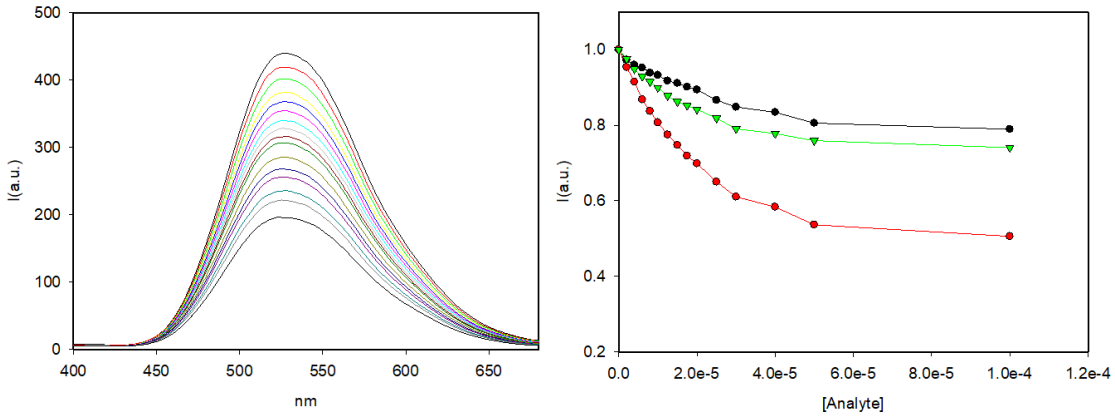

Figure 9. *Fluorescence spectra (λ_{ex} =350 nm) of **L3** titrated with KET (left); titration curves of **L3** (right) with KET (red), NPX (green), BZO (black).*

The association constants of **L1-L4** and the various analytes are collected in TABLE 2; all the constants were obtained fitting the fluorescent data using Eq.1 using SigmaPlot 10.0 non-linear regression tool.[36]

$$I = \varepsilon_F \varphi_F [F]_t + (\varepsilon_A \varphi_A - \varepsilon_F \varphi_F) \times \frac{[F]_t + [Q]_t + \frac{1}{K_a} - \sqrt{([F]_t + [Q]_t + 1/K_a)^2 - 4[F]_t \times [Q]_t}}{2} \qquad (Eq.1)$$

In general, the affinity of **L3** and **L4** to KET is similar to the one obtained for **L1** and **L2** (KET gave the highest quenching for all the receptors), which are also comparable to that with NPX, while BZO gave slightly lower results. Association constants of **L1-L2** for NPX and BZO were not calculated due to the absence of quenching of the ligands fluorescence.

Table 2. *Association constants (Ka) for L1-L4.*

Association constants (K_{ass})			
Receptor/analyte	KET	NPX	BZO
L1	$1.26*10^{5}$ M^{-1}	-	-
L2	$1.71*10^{5}$ M^{-1}	-	-

L3	$0.8*10^{5}\ M^{-1}$	$0.6*10^{5}\ M^{-1}$	$0.3*10^{5}\ M^{-1}$
L4	$3.64*10^{5}\ M^{-1}$	$0.83*10^{5}\ M^{-1}$	$3.85*10^{5}\ M^{-1}$

The photophysical study on these assemblies has been supported by TD-DFT computational studies in order to investigate the mode of interactions between the receptors and the anionic form of the investigated NSAIDs. As expected, the DFT study showed that the main force driving the formation of a ligand-analyte complex is of electrostatic nature; calculated electrostatic potential show that the most negative potential is around the carboxylate of the NSAIDs and the most positive potential around the squaramide's NH. Moreover, calculation showed that a single COO^- could form a double hydrogen bond with the two NH of a single squaramide or bridge two different squaramides via a bifurcated hydrogen bond. The highest stabilization was obtained with **L4** due to the presence of the indole hydrogens giving additional hydrogen bonds.[35]

Lastly, a preliminary strip test was conducted with **L1** to test the ability of the ligand to selectively discriminate KET over the other guests. A common filter paper strip was coated in a fine suspension of **L1** in ethanol and, after letting it dry, it showed the expected blue-green fluorescence when irradiated with an UV lamp for TLC reading (365 nm). The emission was drastically quenched after the deposition of a 0.1 mM solution of KET in water, while remaining nearly unaffected by NPX and BZO (Fig.10); also, the addition of NSAIDs water solution did not seem to disturb the sensors deposited on the paper. More experiments will be needed to develop a final prototype for a sensor array presenting all the receptors studied.

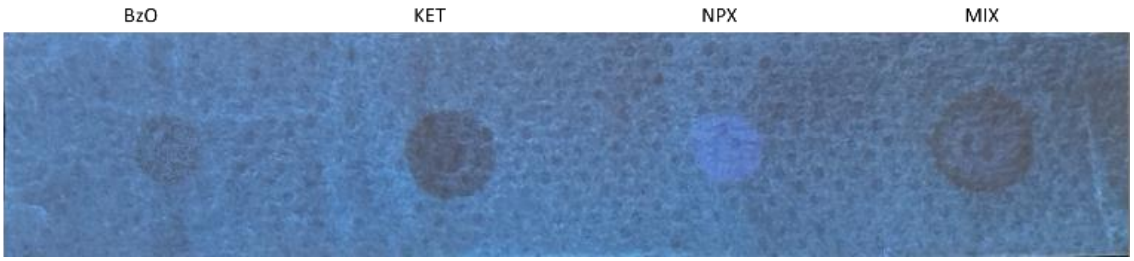

Figure 10. *Photo of the strip test performed with* ***L1****.*

2.5 Design e synthesis Coumarin ligands

Two additional squaramide-based receptors for NSAIDs sensing were synthesized by the group of Prof. Vieri Fusi at the University of Urbino, **L6** and **L7**, following the procedure reported in Fig.11. The sensors were designed to study the cooperative behavior of the squaramides as HB donors; **L7** is in constituted by a pseudo-macrocyclic binding unit possessing 2 squaramides moieties', while **L6** has only one squaramide; **L7** was designed mirroring **L6**, to see if the cooperation of 4 HB could result in a stronger interaction with NSAIDs. The dansyl fluorescent unit was replaced by a 7-trifluorometyl-7-amminocoumarine, a well-known and studied fluorophore.

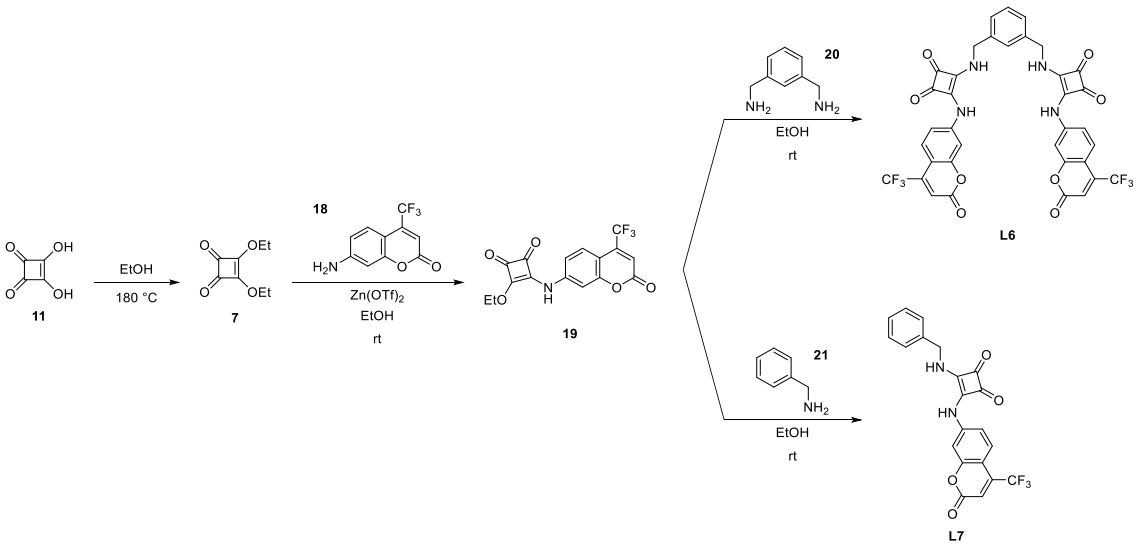

Figure 11. *Reaction scheme for the synthesis of* ***L6-L7****.*

2.6 Photophysical characterization

A complete photophysical characterization was conducted on **L6** and **L7**; the ligands were insoluble in water, so preliminary experiments were conducted in DMSO and in a mixture of ACN/DMSO (99/1 v/v). The absorption spectra in DMSO (Fig.12) shows at 400 nm the absorption maximum of the coumarin for both **L6** and **L7** and a smaller band at 515 nm relative to the deprotonated squaramide. For **L7** the absorption coefficient at 400 nm is nearly double that of **L6** ($\varepsilon_{\mathbf{L6}}$ = 45000 $M^{-1}cm^{-1}$, $\varepsilon_{\mathbf{L7}}$ = 17000 $M^{-1}cm^{-1}$). The maximum of absorbance for **L6** and **L7** in ACN/DMSO(1%) was blue-shifted to 390 nm ($\varepsilon_{\mathbf{L6}}$ = 48000 $M^{-1}cm^{-1}$, $\varepsilon_{\mathbf{L7}}$ = 25000 $M^{-1}cm^{-1}$) and the band of the deprotonated squaramide was absent.

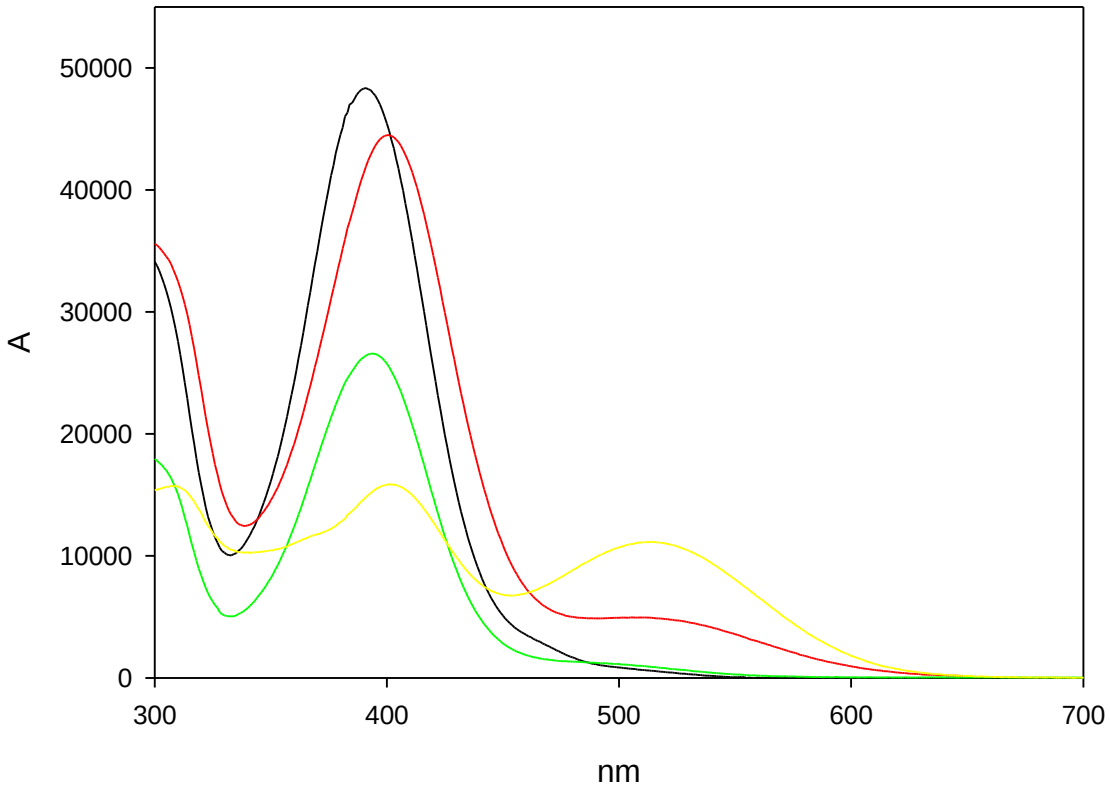

Figure 12. *Absorption spectra of **L6** in DMSO (red) and ACN (black) and of **L6** in DMSO (yellow) and ACN (green).*

The emission of both **L6** and **L7**, $\lambda_{max(DMSO)}$ = 475 nm $\lambda_{max(ACN)}$ = 485nm, (Fig.13) is relatively weak if compared to similar coumarins.

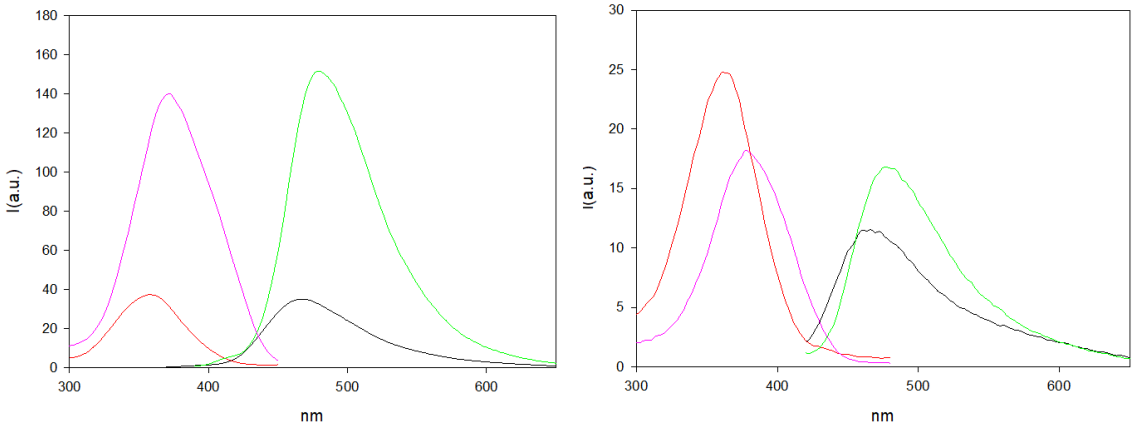

Figure 13. *Emission (λ_{ex} = 400nm) and excitation spectra (λ_{em} = 480nm) of* ***L6*** *(left) and* ***L7****(right) (Green and pink for ACN, red and black for DMSO).*

We hypothesized that this behavior could be caused by either a deactivation of the excited state of the coumarin by oxidative PET to the squaramide, or by a non-emissive twisted intramolecular charge-transfer state (TITC); deeper photophysical studies are needed to clarify this aspect. The lifetimes resulted to be 4.9 ns for both **L6** and **L7**. The fluorescence QYs were measured against quinine sulphate in H_2SO_4 (Φ_{fl} = 0.54) using Eq. 19; as expected from the low emission of **L6** and **L7** the QYs are very poor if compared to data relative to C151 (7-(amino)-4-(trifluoromethyl) coumarin, $\Phi_{fl\ (dmso)}$ = 0.48 $\Phi_{fl\ (acn)}$ = 0.57)[37], being lower than 1% in both ACN and DMSO.

2.7 Acid-base studies

The ability of squaramides to strongly bind anionic species has been explained[38] as an effect of their high acidity that deeply depends on the physiochemical properties of the solvent, such as polarity, dielectric constant and donor number. To investigate the acid base behavior of **L6** and **L7**, base titrations were performed utilizing an ionic base (tetramethylammonium hydroxide, TMAOH) and two electrically neutral bases (1,5-diazabiciclo(5.4.0)undec-7-ene, (DBU) and N,N-diisopropylethylendiamine, (DIPEA) both in ACN and DMSO.

The absorption spectrum of **L7** is similar in both solvents showing the main coumarin absorption band located at 390 nm in acetonitrile and at 400 nm in DMSO. Upon dropwise addition of a TMAOH solution both bands decrease in intensity and a new band appears at 500 nm (acetonitrile) or 515 nm (DMSO). This bands around 500 nm are attributed to the anionic form of the ligand in which the squaramide NH group linked to coumarin is deprotonated. In DMSO the deprotonation band is clearly visible also in absence of base meaning that in this solvent the ligand is sufficiently acid to be present in both protonated and deprotonated species at the equilibrium in not negligible concentrations. Additional evidence for the stronger acidity of **L7** in DMSO, compared to other solvents, is that in acetonitrile complete deprotonation is only achieved after the addition of an excess of 5-6 equivalents of TMAOH (Fig.15), indicated by the 500 nm band reaching a plateau. In DMSO, however, quantitative deprotonation requires only a single equivalent of base (Fig.14).

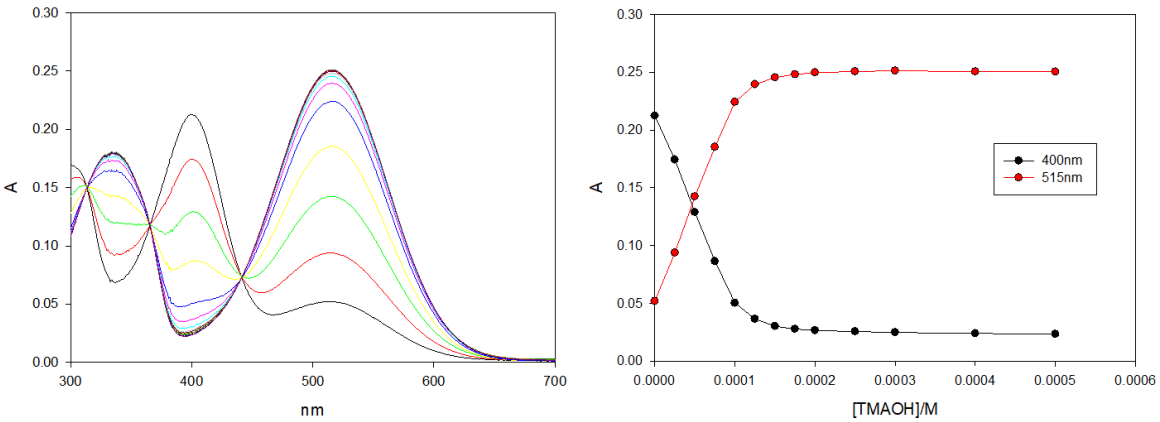

Figure 14. *Absorption spectra (left) of* ***L7*** *10 uM titrated with TMAOH in DMSO; titration curves (right).*

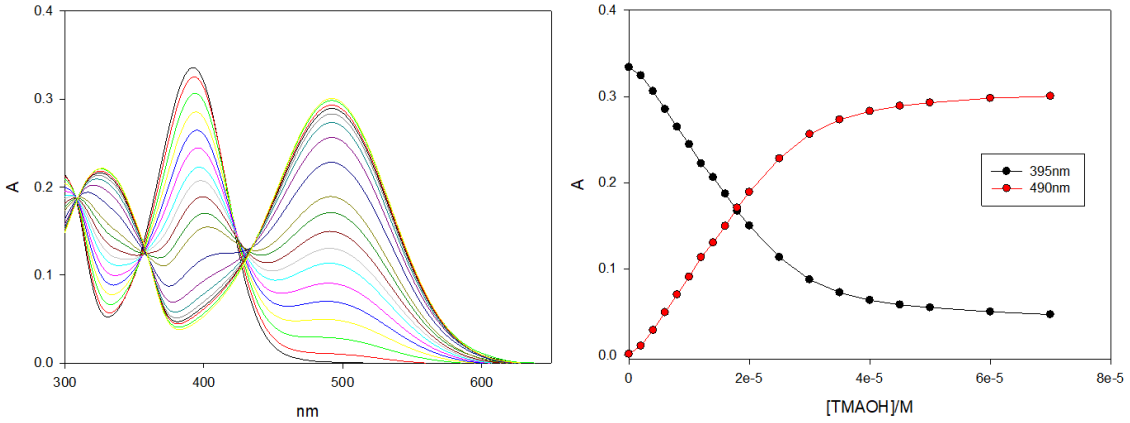

Figure 15. *Absorption spectra (left) of* ***L7*** *10 uM titrated with TMAOH in ACN; titration curves (right).*

Similar experiments were conducted with the two organic electrically neutral bases DBU and DIPEA. DBU was found able to deprotonate **L7** in both solvents with the difference that in acetonitrile the full deprotonation was reached upon addition of one equivalent of base while in DMSO only one half of equivalent is required, denoting the formation of a stable **L7**–H···**L7** homo-conjugate – hydrogen bonded adduct of neutral acid with its anion. The less basic and more steric hindered DIPEA is instead not able the deprotonate **L6** and **L7**.

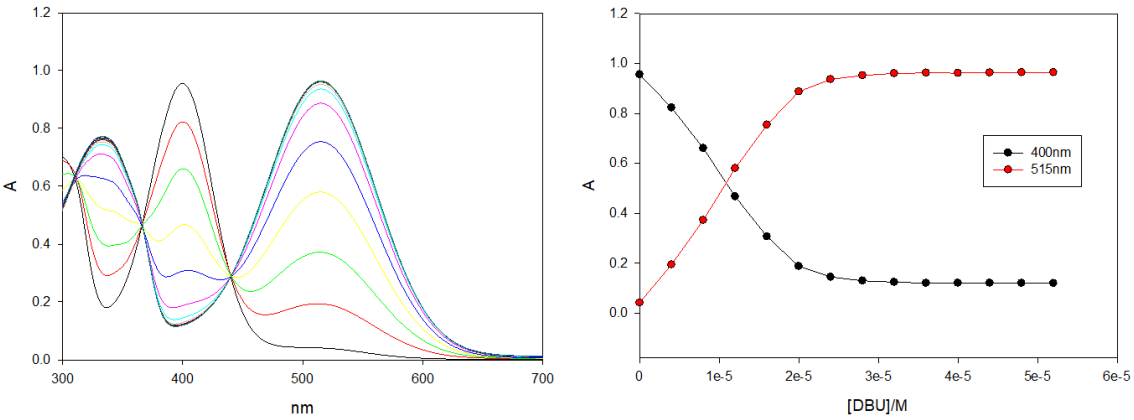

Figure 16. *Absorption spectra (left) of* ***L6*** *20uM titrated with DBU in DMSO; titration curves (right.)*

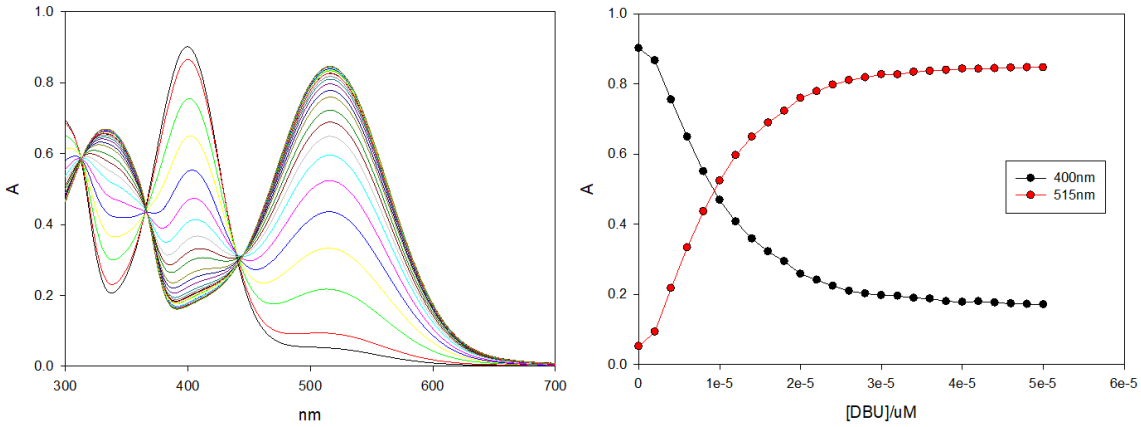

Figure 17. *Absorption spectra (left) of* ***L7*** *40uM titrated with DBU in DMSO; titration curves (right).*

It is important to note that, even in the presence of an excess of base, the emission of the deprotonated ligands remained almost unaltered, suggesting that the ligands quickly get protonated at the excited state.

The cause of the great acidity of squaramides in DMSO is the combination of elevated donor number and dielectric constant that on the one hand stabilizes the H^+ cation (leading to the formation of DMSO-H^+)[39], and on the other hand favours the ionization of covalent bonds. The high donor number constitutes the principal factor that differences DMSO from the other solvents tested, in particular with ACN that is similar to DMSO as far as the dielectric constant and dipole moment are concerned.

2.8 NSAIDs' interaction studies

KET, NPX, IBU and BZO were added to DMSO and ACN/DMSO(1%) solutions of **L6** and **L7** to test their ability to bind NSAIDs and eventually signal their presence. Unfortunately, in all cases the intensity and lifetime of the ligands fluorescence resulted in being totally unaffected by the interaction with NSAIDs. The absorption spectra resulted to be – instead – more indicative. In DMSO, the spectroscopical response of **L6** and **L7** is similar to the one observed in the

previous paragraph in the case of base titrations; as it can be seen in Fig.18, after the addition of NSAIDs salts and sodium benzoate to **L7**, the absorption peak located at 400 nm decreases while the one at 515 nm increases, suggesting the deprotonation of the ligands rather than the formation of a complex. The only exception to this behavior is **L6** titrated with KET- (Fig.19); in this case together with an overall decrease, the 400 nm peak shifts to longer wavelength while the increase of the 515 nm peak is more modest, suggesting that the type of interaction between **L7** and KET is not just an acid-base reaction.

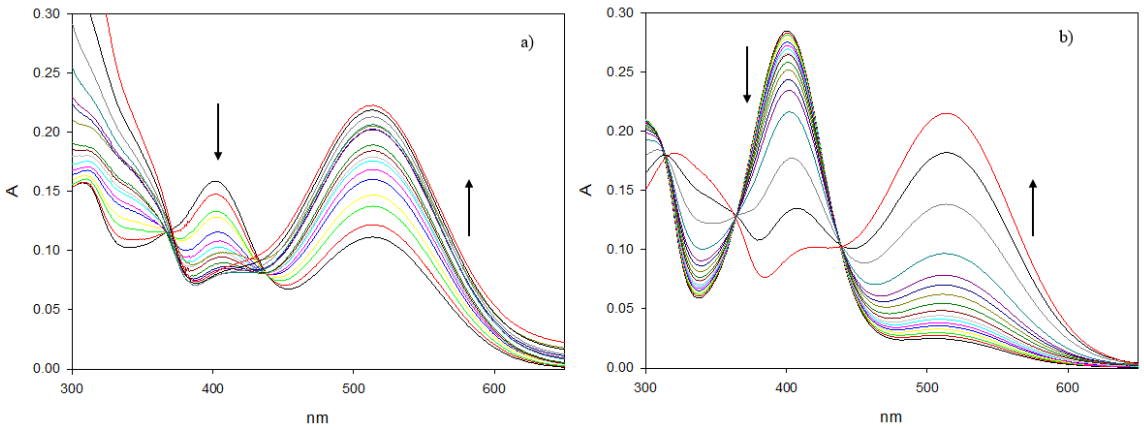

Figure 18. *Absorption spectra of **L7** titrated with KET (left) and with IBU (right) in DMSO.*

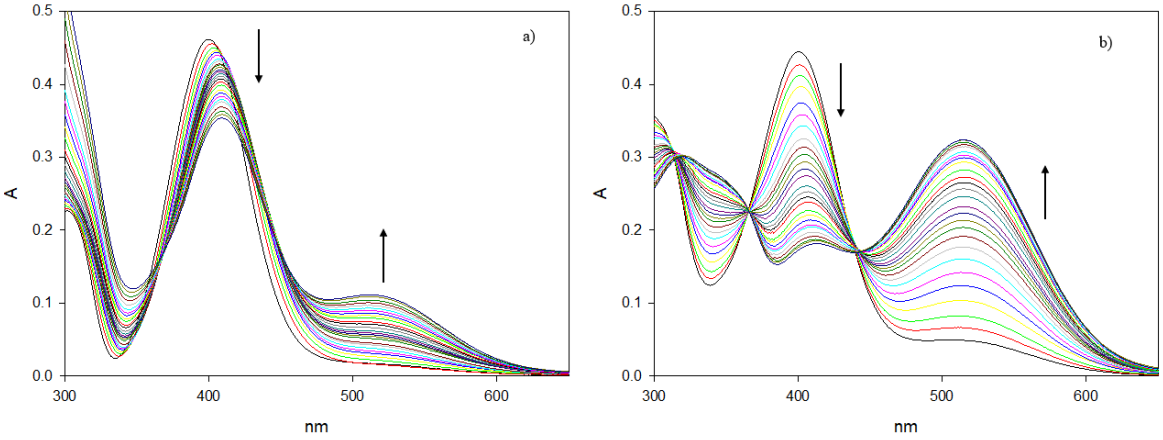

Figure 19. *Absorption spectra of **L6** titrated with KET (left) and with IBU (right) in DMSO.*

This different behavior is more evident for the titrations performed in ACN/DMSO(1%); in this case, for both **L6** and **L7**, the interaction with NSAIDs and BZO produced a shift of the 390 nm absorbance peak towards longer wavelength (Fig.20). If taking into account the behavior of the dansylated ligands,

which showed binding to NSAIDs in ACN and not in DMSO, it's safe to hypothesize that also in the case of **L6** and **L7**, binding happens only in ACN, explaining the different spectroscopic outcome of the titrations performed in different solvents. Although the formation of host-guest complexes of **L6** and **L7** is more evident in ACN, the spectral output of the titration cannot exclude deprotonation of the ligand, since also for this titration, together with the shift of the 390nm peak, there is also a slight increase of the absorbance at 500 nm, consistent with deprotonation; since all the NSAIDs and BZO are all weak bases, it is reasonable to hypothesize that the spectral behavior of **L6** and **L7** is a sum of complex formation and deprotonation.

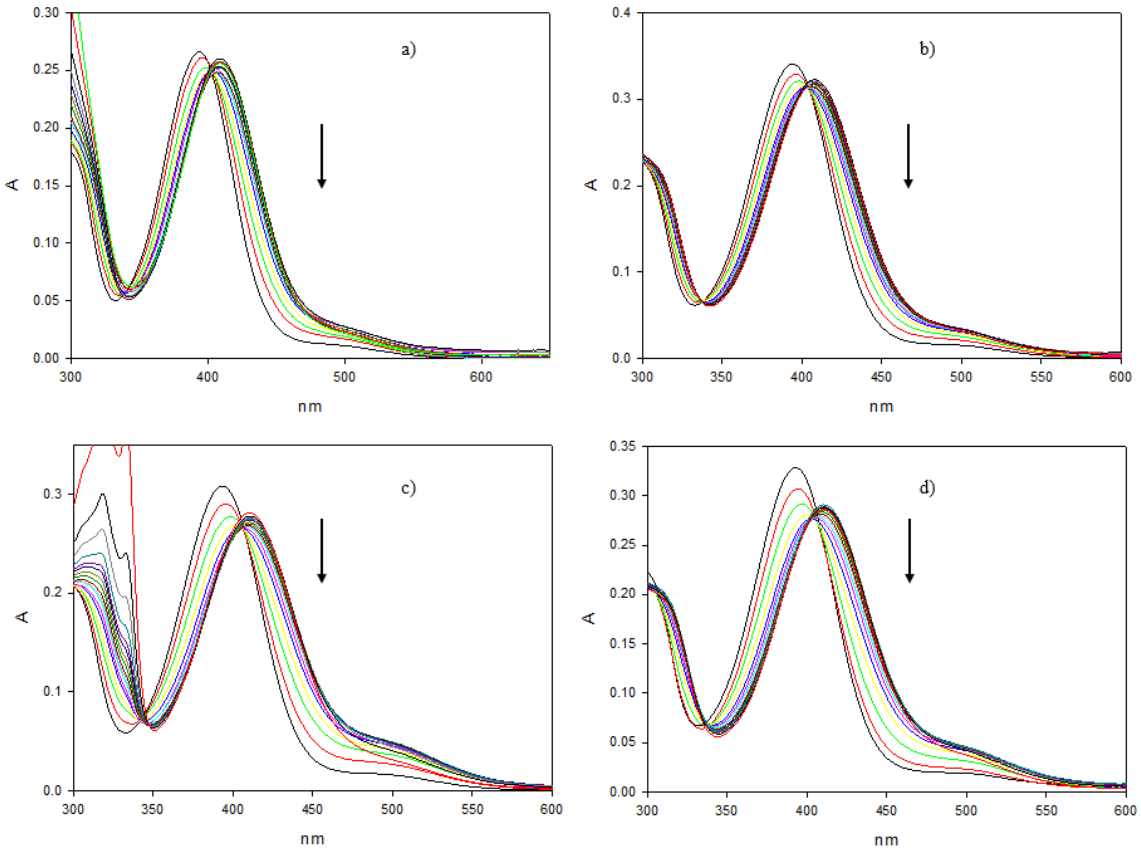

Figure 20. *Absorption spectra of* ***L7*** *titrated with KET (left), BZO (b), NPX, and with IBU (right) in ACN.*

Association constants (Table 3) were determined using BindFit.[40] Unfortunately the algorithm was not able to fit the titrations of **L7** for a 2:1 host:guest model.

Table 3. *Association constants (K_a) for* ***L6****.*

Association constants (K_{ass})	
Analite	**L6**
KET	$7.49*10^4$ M^{-1}
NPX	$5.95*10^4$ M^{-1}
IBU	$7.49*10^4$ M^{-1}
BZO	$1.45*10^5$ M^{-1}

2.9 ESI-MS

The mass spectra of **L6** and **L7** alone and in the presence of NSAID adducts were recorded to verify the formation of host-guest complexes. To avoid the use of DMSO, saturated solutions of **L6** and **L7** were prepared with pure ACN. The peaks corresponding to the deprotonated ligands [**L7-H**] m = 413 (Fig.21) and [**L6-H**] m = 749 (Fig.22) mass is clearly visible; for both **L6** and **L7** adducts with Cl- and NO_3^- were observed, with **L6** having the tendency to prefer a 2:1 stoichiometry (2 hosts:1 guest). Further UV-Vis studies confirmed that even if **L6** and **L7** can complex Cl^- and NO_3^-, the interaction does not affect the spectroscopic characteristics of the ligands. Then, to the samples of **L6** and **L7** an arbitrary amount of ketoprofen, ibuprofen, naproxen and benzoate (as sodium salts) was added. Adducts of **L7** and NSAIDs were visible: [**L6+IBU-Na**] m = 995, [**L6+KET-Na**] m = 1003 (Fig.22), [**L6+NPX-Na**] m = 979, while no adduct with benzoate was detected. Also, **L7** adducts with NSAIDs were present, but with a 2:1 stoichiometry: [**2xL7+IBU-Na**] m = 1033, [**2xL7+KET-Na**] m = 1081 (Fig.21), [**2xL7+NPX-Na**] m = 1057, and again no adduct with benzoate was

detected. These results confirm the ability of the ligands to effectively form host-guest complexes with NSAIDs. The mass spectra were recorded using a Xevo G2-XS QTof system by Waters, the solutions were directly injected into the ESI-QTof system in negative polarity mode.

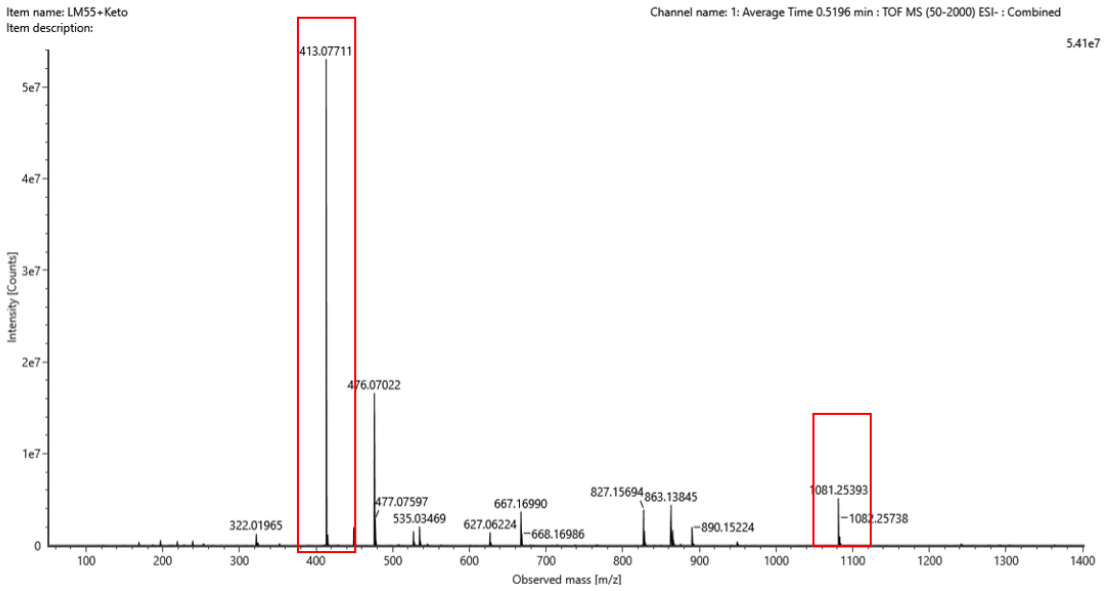

Figure 21. *Mass Spectrum of* ***L7*** *with KET. Peaks relative to* ***[L7-H]*** *m = 413,* ***[2xL7+KET-Na]*** *m = 1081 are highlighted in red.*

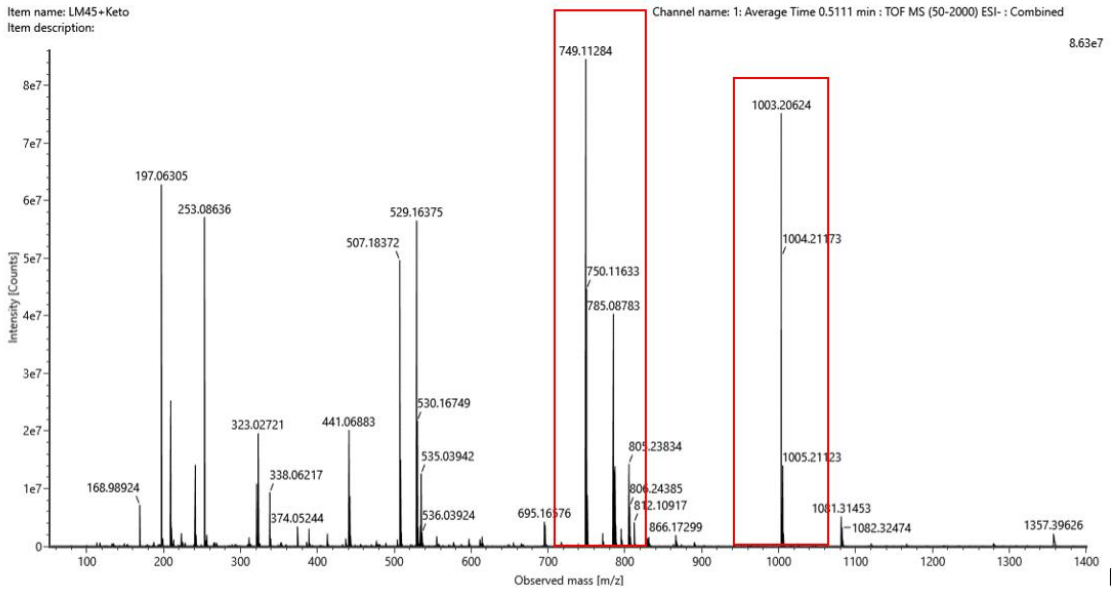

Figure 22. *Mass Spectrum of* ***L6*** *with KET. Peaks relative to* ***[L6-H]*** *m = 749,* ***[L6+KET-Na]*** *m = 1003 are highlighted in red.*

2.10 Conclusions

In this chapter two different sets of supramolecular receptors for NSAIDs detection were studied; both sets of ligands were designed, using supramolecular chemistry strategies, to form host-guest complexes with NSAIDs via hydrogen bonding and hydrophobic interactions. The first set of receptors showed good affinity in respect of the guests chosen for the interaction studies (KET, NPX, BZO) in organic solvent. Notably, only the macrocyclic systems **L1** and **L2** show a specificity in the fluorescent response to ketoprofen. In fact, the open chain receptors **L3** and **L4** undergo quenching of the fluorescence upon addition of KET, NPX and BZO, while the macrocycles **L1** and **L2** were quenched only by KET. This aspect highlights the role of a highly organized binding unit in improving selectivity and specificity of chemosensors. **L1** retained its ability to discriminate KET from the other guests also in the solid-state experiments, which is a promising result for the development of sensor arrays for NSAIDs differential sensing. We believe that this result is particularly significant for the field of optical chemosensors, especially considering that most research in this area remains at the academic level, only rarely leading to real-world applications with fully developed devices[41] but for some rare successful application such as the GlySure system[42] or the OPTI medical system, a fluorescence based platform capable of quickly measuring Na^+, K^+, $Ca^{2+}$and CO_2 in blood samples.[43]

Concerning the second set of ligands, **L6** and **L7** were able to form host-guest complexes with NSAIDs, as demonstrated by the mass spectra. Unfortunately, the acidic character of the squaramide hydrogens affected the spectral response of the probes, since deprotonated ligands possess different absorption properties with respect of the protonated species. Moreover, the conjugation of the squaramide nitrogen to the coumarin fluorophore drastically reduced the fluorescence of the coumarin itself, limiting the spectral response of the sensors to only absorbance changes. Since the sensors' output is limited to colorimetric changes, and the absorption properties of **L6** and **L7** are influenced by both acid-base equilibria and

interactions with NSAIDs (and BZO), distinguishing between these behaviors solely with UV-VIS techniques proves challenging. As a result, the applicability of **L6** and **L7** in developing a sensing platform is limited. Further studies are required to understand the complex behavior of **L6** and **L7**, and to understand how their structure could be improved to enhance their optical properties.

3. Eu(III) based luminescent probes for anionic species sensing

3.1 Introduction – inorganic anions as pollutants

The issue of inorganic contaminants in water is complex. Water, as is found in nature, is not pure H_2O and it is in fact rich in inorganic compounds, such as metal cations and a plethora of counter anions. Excluding toxic heavy metals like cadmium and lead, many of the chemical species present in water are essential for the sustenance of life forms, but must be kept in precise ranges, otherwise, if their concentration exceeds the defined limits, they can become detrimental and make the water unusable and unsafe.[44] Fluoride is a perfect example of this fine equilibrium: a moderate amount of fluoride anions in drinking water contributes to good dental health; about 1 mg/L is effective at preventing tooth decay especially in young children, but at higher concentrations it can lead to dental fluorosis, a condition that deteriorates the teeth enamel, and even lead to impaired intellectual development at even higher concentrations. The maximum allowable level of F^- in drinking water is set between 1.4 to 4 mg/L, depending on the climate of the geographical area.[6] Many chemical parameters, such as pH, carbonates/bicarbonates, chloride, fluoride, nitrogen content (as nitrite, nitrate, ammonia), phosphates and sulphates, must be monitored to make sure their presence does not exceed the recommended quantities.

During routine water monitoring, each of the different compounds mentioned above is analyzed singularly, and different techniques are used ranging from

optical and electrochemical methods to chromatographic ones.[5] The possibilities offered by differential sensing could make a substantial impact on the way this type of analysis are carried out; being able to construct a sensor array capable of having different responses to many different analytes could mean being able to acquire in a single measurement most of the parameters needed.[19,45]

In this context, luminescent lanthanide complexes can offer valid tools for the detection of inorganic anionic species in water. Many examples of chemical sensing using lanthanides for both in vitro and in vivo applications have been reported.[46]

Lanthanide-based luminescent chemosensors offer different advantages when compared to more typical luminescent compound-based sensors. Lanthanide luminescence arises from f-f Laporte-forbidden transitions. The spectrum is characterized by sharp emission peaks, which appear always at the same wavelengths. Luminescence lifetimes are long (from tens of microseconds up to several milliseconds). These properties make Ln luminescence particularly suited for sensing purposes, since background noise during measurement is easily avoided by time-gated detection. One of the biggest drawbacks of lanthanides is their extremely low molar absorption coefficient, which is usually 0.1-10 $M^{-1}cm^{-1}$ which makes direct excitation inefficient. To circumvent this problem, lanthanide complexes are decorated with light harvesting antennae, which are chromophores with adequate excited state energies to sensitize the lanthanide emission via energy transfer. Moreover, for some of the lanthanides – and in particular for Eu(III) – the spectral shape of the emission is highly dependent on the coordination field around the metal center; specifically, some transitions are more sensible to the environment, while others are marginally affected. For example, the $\Delta J = 2$ transition of Eu(III), generally located around λ_{em} = 615 nm is called an "hypersensitive transition" and is highly dependent on the metal center coordination geometry, while the $\Delta J = 1$ around λ_{em} = 590 nm is barely effected. This property of lanthanide luminescence offers the possibility to perform

ratiometric measurement comparing the intensities of the individual Eu(III) emission bands.[47]

One of the bigger challenges in sensing anionic compounds in water is the high solvation energies that has to be overcome to effectively bind the species to a chemosensor. In fact, most anion sensing chemosensors are studied in non-competitive media, and fail to maintain their binding properties in water, that is the typical milieu of environmental analysis. Another fundamental lanthanide property, their high Lewis acidity, comes into play to overcome this limitation. Thanks to their acidity, lanthanides are able to strongly bind Lewis bases, in this case anionic species, and are thus excellent candidates for the construction of sensing arrays to be used in aqueous environment.[48]

3.2 Aim of the project

The aim of the project is to conduct a spectroscopic study on the binding capabilities of selected Eu(III) complexes (Fig. 23) towards a library of anionic species commonly found in water bodies and routinely monitored during water quality analysis. The main focus of this study was to evaluate how changes in the chemical structure of the ligand affect the Eu(III) emission, and the changes brought by binding different anions.

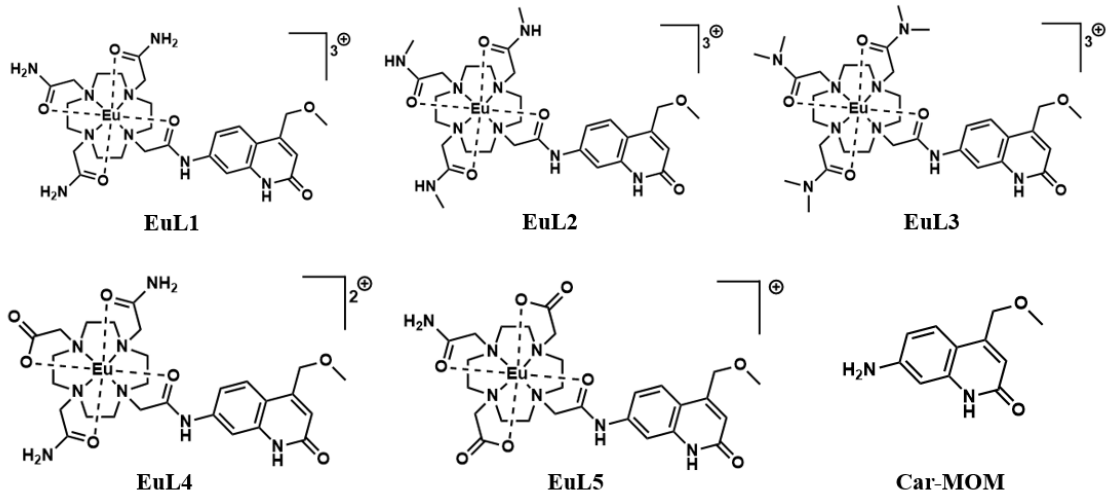

Figure 23. *Chemical structures of europium complexes* ***EuL1-EuL5*** *(europium coordinated water not depicted) and Car-MOM.*

The europium complexes are based on 1,4,7,10-tetraazacyclododecane-1,4,7-triacetic acid (DO3A), which is one of the most common chemical moieties used to stably complex lanthanides cations. The Eu(III) coordination number in the complexes is 9, eight coordination sites are occupied by the octadentate ligand, while the ninth is occupied by a water molecule (not depicted in Fig.23) which is fundamental for some of the sensing applications of these complexes. 4-methoxymethyl-7-aminocarbostyril (Car-MOM) heterocycle is linked to the macrocyclic unit by a secondary amide bond, which acts as a light harvesting antenna to sensitize the Eu(III) emission. The syntheses of **EuL1-EuL5** and Car-MOM have already been described[49] and will not be discussed.

It is important to note that the overall chemical structure is similar for all the five complexes but for one aspect: each complex presents a different number of N-H bonds in the coordination sphere of the Eu(III). This is important for the photophysical properties of the complexes, since the Eu(III) luminescence is quenched by coupling to the vibrational modes of H-X bonds (X = O, N, C). This means that having different numbers of N-H bond in the coordination sphere of the europium, each complex will have different numbers of X-H quenchers, and thus intrinsic quantum yields. The water molecule occupying the ninth coordination also strongly quenches the Eu(III) emission, and can easily be

displaced by small, hard anions (e.g. fluoride), turning the emission on, which is one of the mechanisms used to sense anionic species. Moreover, changing the medium to deuterated water leads to the exchange of the coordinated H_2O molecule with D_2O, which provides the basis for hydration state (q) analysis. q values can be calculated for Eu(III) species with Eq. 2[50]:

$$q = 1.2\left(\frac{1}{\tau \mathrm{H2O}} - \frac{1}{\tau \mathrm{D2O}} - 0.25 - m * 0.075\right) \qquad (Eq.\,2)$$

Where τ_{H2O} and τ_{D2O} are the observed lifetimes in H_2O and D_2O respectively and m is the number of nearby N-H oscillator in the Eu(III) complex. Hydration state analysis will be employed to verify the displacement of water by anionic species in the following paragraphs.

The complexes present different net charges: **EuL1-EuL3** are three times positively charged, while **EuL4** is twice positively charged and **EuL5** has just one positive charge; upon water substitution **EuL1-EuL3** will still present a net positive charge that could electrostatically attract more anions into the second coordination sphere, increasing the changes in emission properties. Overall neutral complexes were not studied as previous experiments established that these interacted minimally with anions.[51] Taking all these aspects together, each complex is expected to have a unique change in emission properties upon substitution of the coordinated water. Lastly it is important to note that both the coordination environment and the net charge of the complex affects the photoinduced electron transfer (PeT) from the excited antenna to the Eu(III) center. It has been observed that – among all Ln(III) ions – Eu(III) is the easiest to reduce, and most of the antennae employed for this type of complexes have high enough reducing potential in their excited state to easily generate Eu(II) via PeT, resulting in quenched Eu(III) luminescence. PeT can be slowed down by stabilizing the Eu(III) oxidation state or it can be favored, for example by increasing the overall charge of the complex. The balance of these processes will determine the overall response of the sensors. Having different chemosensors, each possessing unique

response to different analytes, is fundamental for constructing differential sensing arrays.

3.3 Photophysical characterization

The photophysical characterization of the complexes **EuL1-EuL5** was conducted in aqueous solution at room temperature. Since it was already known that the properties of these complexes are highly dependent on pH we decided to conduct all experiments in buffered solution; Tris-HCl buffered solution at pH 8 was chosen as a medium for all experiments. The slightly basic pH was chosen to avoid the formation of harmful substances such as HF and HCN during anion binding studies. It is also important to use buffered solutions to avoid drastic changes in pH, since many of the anionic species studied are quite basic. Changes in pH could mask the luminescent response of the complex to anion binding. To have a frame of reference for the anion binding studies, emission spectra and luminescence lifetimes of the five complexes were recorded at five different pH values: pH 4.3, pH 6, pH 7, pH 8 and pH 10. The most sensitive complex to pH changes was **EuL1** (Fig. 24-25), followed by **EuL2** and **EuL3**, while **EuL4** and **EuL5** were only affected by basic conditions.

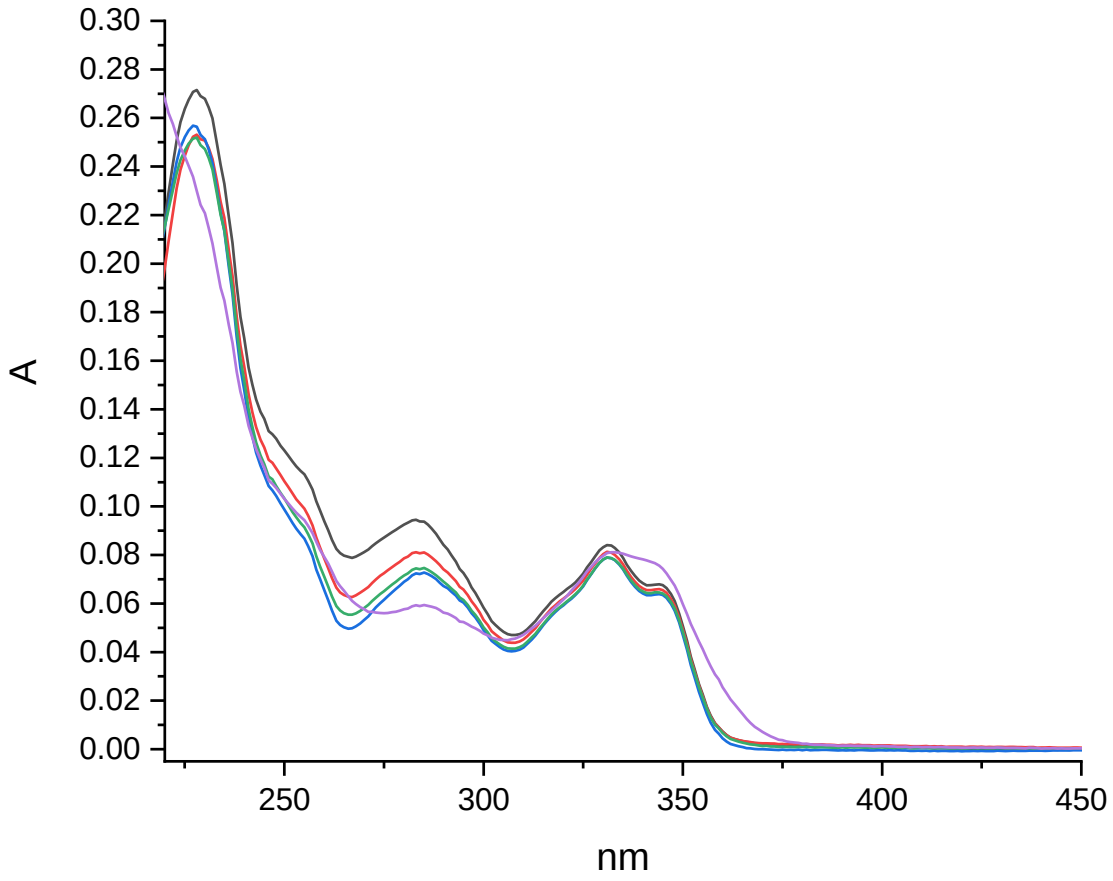

Figure 24. *Absorption spectra of* ***EuL1*** *at different pH: pH 4 (black), pH 6 (red), pH 7 (green), pH 8 (green), pH 10 (purple).*

The absorption spectrum of **EuL1** is barely affected by changes in pH, especially the region of the antenna absorption (300-340 nm), while modest changes can be observed in the region between 250-300 nm, region where the macrocyclic unit of the complex absorbs. Changes in absorption are significant only at pH 10. This effect is presumably caused by the deprotonation of the N-H groups of the complex. The increase in absorption at around 350 nm indicates the degradation of the complex: during experiments we noted that at basic pH the antenna is cleaved from the complex. This can be seen both in the absorption and emission spectra. This phenomenon will be discussed later.

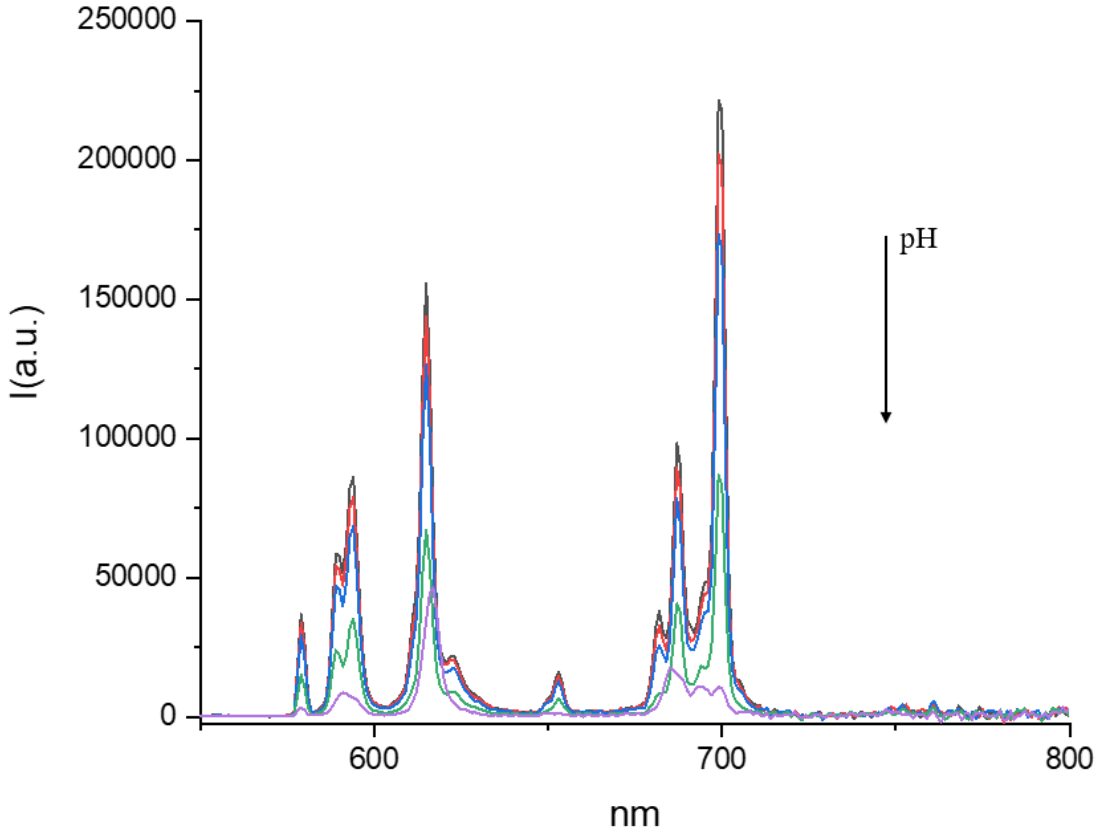

Figure 25. *Emission spectra (λ_{ex} = 330 nm) of* ***EuL1*** *(Eu phosphorescence) at different pH: pH 4 (black), pH 6 (red), pH 7 (green), pH 8 (green), pH 10 (purple).*

The emission spectra of the europium phosphorescence (Fig.25), shows the dependence of the emission intensity to pH. The more basic the environment the more quenched is the emission of the Eu(III). This is caused mainly by the deprotonation of the amide bond in the linker, which yields an antennae that is less able to sensitize Eu(III) luminescence. The other inner-sphere amides may also get deprotonated, as indicated by the luminescence lifetimes, measured both at λ_{em} = 615 and 699 nm (Table 4). Another aspect that could indicate a coordination sphere change is the ratio between the $\Delta J = 2$ and $\Delta J = 1$ emission peaks intensities: this ratio remains constant (about 2:1) up until pH 10 where it drastically changes (5:1), which indicates a change in coordination geometry around the Eu(III).

Table 4. *Phosphorescence quantum yields and lifetimes of* ***EuL1-EuL5*** *at different pH.*

	EuL1		**EuL2**		**EuL3**		**EuL4**		**EuL5**	
	Φ_{fl}(%)	τ_{obs}(ms)	Φ_{fl}(%)	τ_{obs}(ms)	Φ_{fl}(%)	τ_{obs}(ms)	Φ_{fl}(%)	τ_{obs}(ms)	Φ_{fl}(%)	τ_{obs}(ms)
pH 4.3	0.92	0.53	1.34	0.54	2.23	0.6	2.20	0.55	3.04	0.59
pH 6	0.87	0.50	1.30	0.52	2.13	0.58	2.22	0.55	3.04	0.59
pH 7	0.78	0.45	1.17	0.49	2.01	0.54	2.14	0.53	3.00	0.59
pH 8	0.40	0.25	0.76	0.32	1.48	0.4	1.84	0.44	3.00	0.58
pH 10	0.20	0.45	0.15	0.41	0.61	0.4	0.54	0.23	1.66	0.44

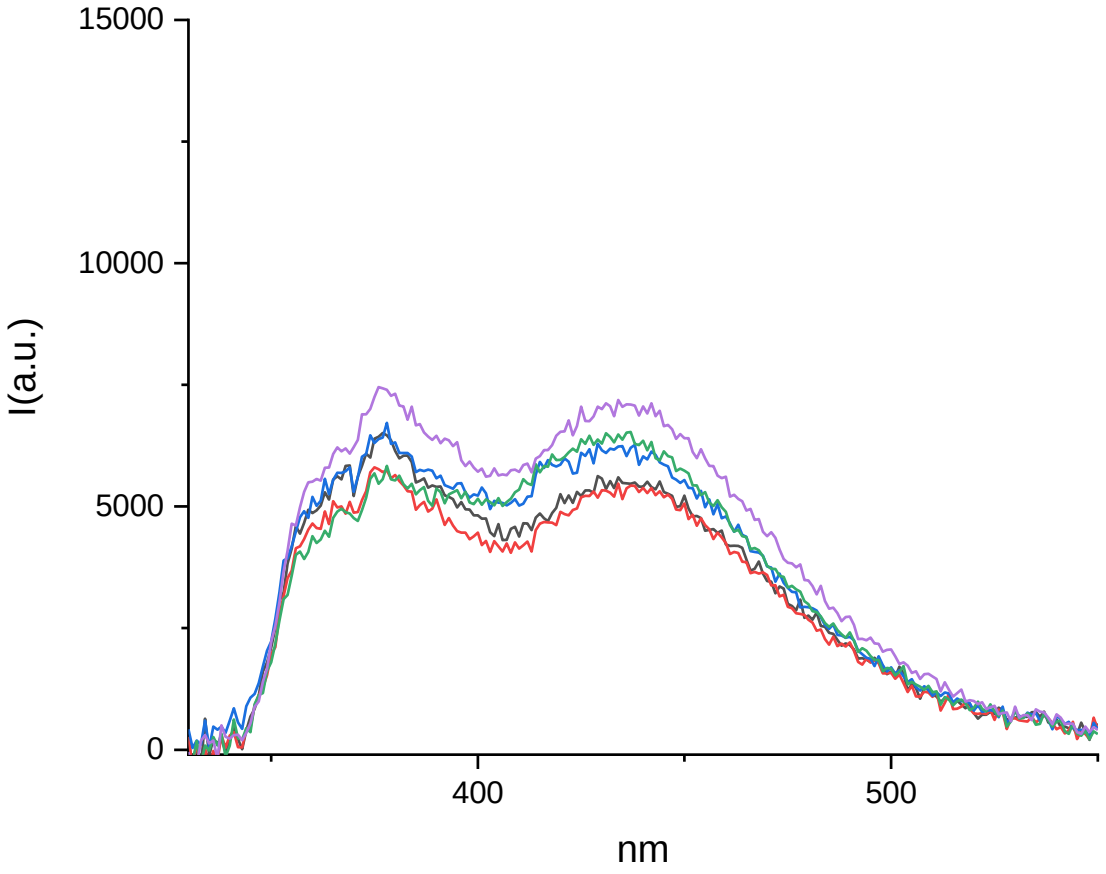

Figure 26. *Emission spectra (λ_{ex}= 315nm) of* ***EuL1*** *(Antenna residual fluorescence) at different pH: pH 4 (black), pH 6 (red), pH 7 (green), pH 8 (green), pH 10 (purple).*

The residual antenna fluorescence (Fig.26) is barely affected by the change in pH. The increase at basic pH could be due to the lowered ET efficiency caused by the ligand deprotonation, the hydrolysis of the antenna removing the carbostyril from the Eu(III) proximity. It is important to note that the spectra of the antenna fluorescence in Fig.26 should not have a peak at 445 nm, in fact the residual fluorescence of the antenna is centered at 375 nm. The emission at 445 nm is caused, as mentioned before, by the hydrolyzed antenna. Since the antenna fluorescence quantum yield is high ($\Phi_{Car\text{-}MOM}$ = 0.86), even if a small quantity of the complex gets hydrolyzed, the effect on emission spectra is significant. The degradation phenomenon was studied by preparing a fresh solution of **EuL1** and taking spectra of it immediately, after a week and after two weeks and compared

to Car-MOM (Fig.27). The hydrolysis of the antenna was also confirmed by HPLC-MS. This problem was avoided in further experiments by preparing fresh solutions for each experiment.

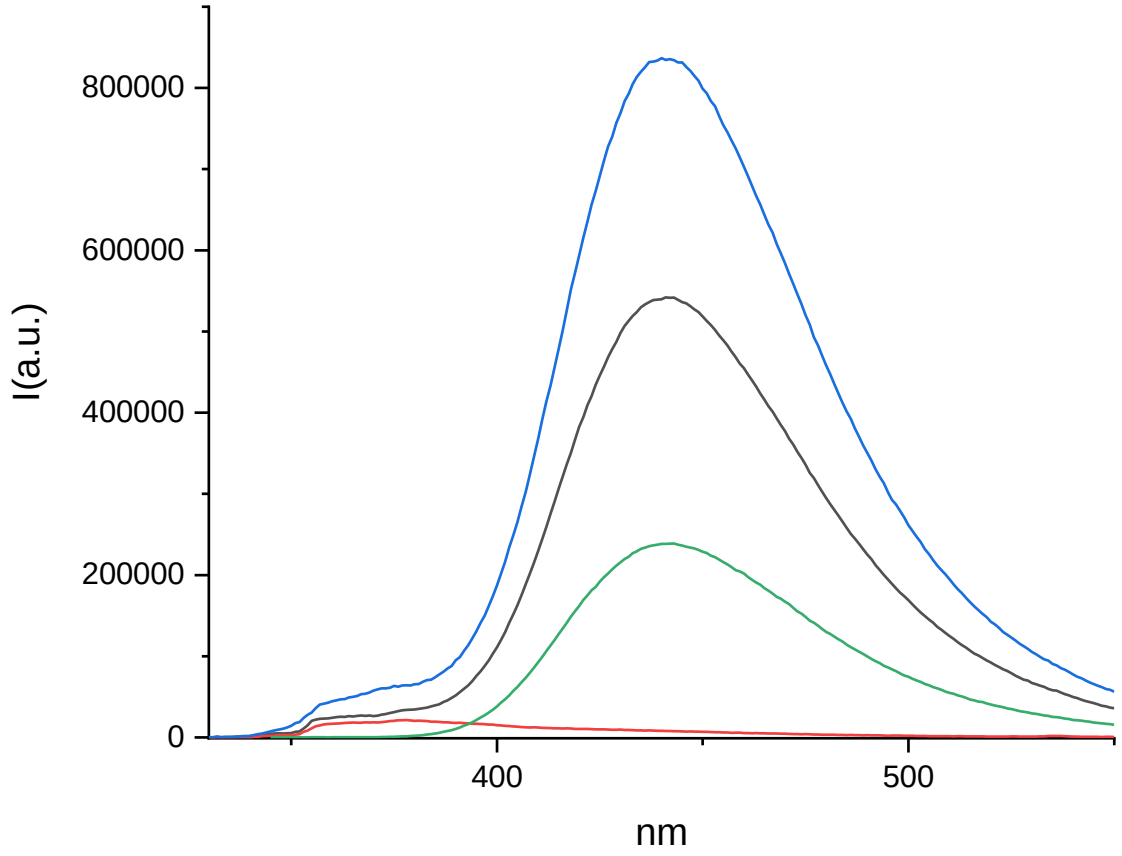

Figure 27. *Emission spectra (λ_{ex} = 330 nm) of* ***EuL1****: fresh solution (red), after 1 week (black), after two weeks (blue) compared to Car-MOM (green).*

The fact that the complexes are sensitive to pH is not to be seen as a detrimental effect; since pH is an important parameter for water quality (water for household purposes, for example, must be kept in the 6.5-8.5 pH range), the ability of these complexes to differently sense pH can be implemented in the final sensor array.

3.4 Anion binding studies

Anion binding studies were conducted in 10 mM Tris-HCl buffer solution at pH 8; it is important to note that the effect of chloride anions on the complexes was

verified before choosing the buffer. The slightly basic pH was used to ensure that the analytes are in their anionic forms and to avoid HCN and HF formation while minimally impacting the photophysical properties of the complexes. All the europium complexes were screened against a library of environmentally relevant anions: fluoride, chloride, bromide, iodide, nitrate, perchlorate, phosphate, sulphate, sulfite, sulfide, carbonate, cyanide, thiocyanate, azide, acetate, oxalate and benzoate. Sodium or potassium salts were selected for the study. Many anions (such as chloride, bromide, iodide, nitrate, perchlorate, sulfide, thiocyanate, azide, acetate, oxalate and benzoate) did not have a significant impact on the emission properties of the complexes. The largest response was given by fluoride, phosphate, carbonate, sulphate, sulfite and cyanide. To study the effect of these species, to 10 μM solutions of each europium complex a large excess (3000-fold, 30 mM) of each of the chosen analyte was added. The significant photophysical properties (absorption and emission spectra, luminescent lifetime) were measured and compared to the complex's parameters in absence of analytes. The pH of each solution was measured after the addition of the analytes to make sure that the pH value was not strongly affected, i.e. it did not change by more than 0.5 units).

3.4.1 Fluoride

Fluoride was, together with other halides, the first anionic analyte tested in the presence of the europium complexes. It was shown previously[51] that fluoride could displace the water molecules coordinated to the metal center, enhancing the Eu(III) luminescence by removing the quenching caused by O-H oscillators. Moreover, it was also shown that the presence of fluoride coordinated to Eu center stabilizes the Eu(III) state against reduction by the photoexcited antenna, which also increases emission. All the complexes were tested against fluoride, chloride, bromide and iodide, but changes in the photophysical properties were observed just for fluoride. The most significant change in emission was given by **EuL1**

(Fig.28); upon fluoride interaction the emission quantum yield of the europium (Φ_{Ln}) increased by nearly 18-fold.

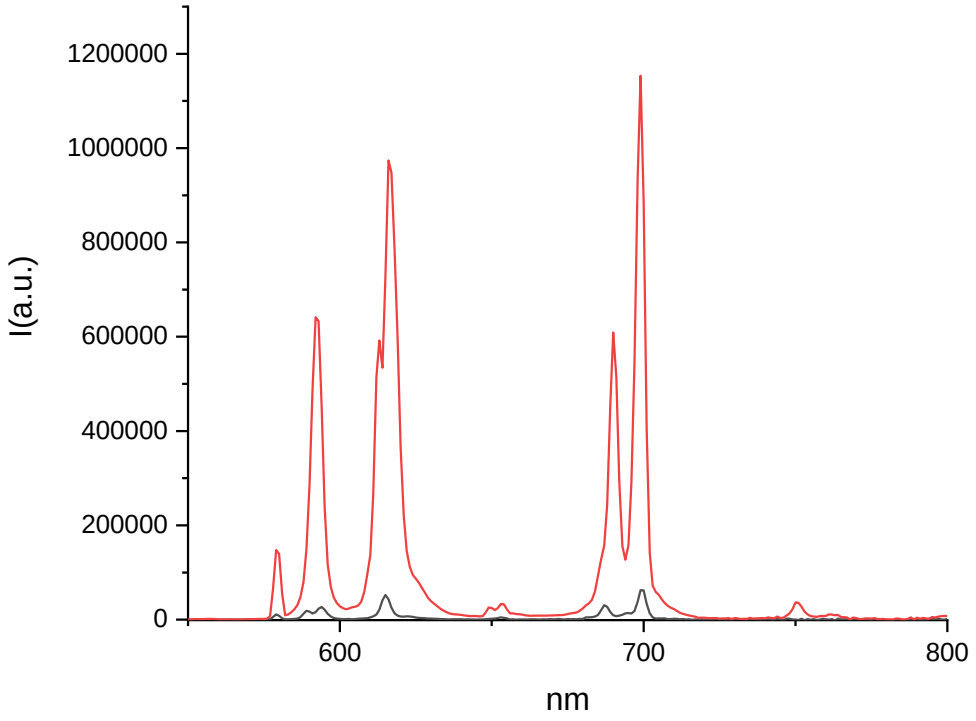

Figure 28. *Emission spectra (λ_{ex} =330 nm) of* ***EuL1*** *with (red) and without (black) fluoride.*

Together with enhanced luminescence, the luminescence lifetime was significantly lengthened, which is to be expected if the quenching water ligand is displaced. Phosphorescence lifetime decays and quantum yields of all the complexes, in presence and absence of fluoride are reported in Table 5.

Table 5. *Phosphorescence quantum yields and lifetimes of EuL1-EuL5.*

	EuL1		**EuL2**		**EuL3**		**EuL4**		**EuL5**	
	Φ_{fl}(%)	τ_{obs}(ms)	Φ_{fl}(%)	τ_{obs}(ms)	Φ_{fl}(%)	τ_{obs}(ms)	Φ_{fl}(%)	τ_{obs}(ms)	Φ_{fl}(%)	τ_{obs}(ms)
	0.30	0.25	0.60	0.32	1.48	0.40	1.60	0.44	3.00	0.58
+ F^-	5.30	0.95	5.90	1.06	7.01	1.17	4.70	0.88	3.70	0.75

The least affected complex was **EuL5**, whose quantum yield showed only a 25% increase. This difference in behavior can be explained as follows. The 3+ charged complexes, as already mentioned are the most sensible to Eu(III) reduction via PeT; thus, the relative gains in emission upon stabilizing the Eu(III) oxidation state for **EuL1-EuL3** are bigger when compared to **EuL5** where the reduction of Eu(III) is already less favorable.

When titrated with KF **EuL1** showed a very broad dynamic range (Fig.29), from µmoles to tens of mmoles, which is ideal to measure fluoride concentrations typically found in the environment (usually the maximum concentration of fluoride in drinking water is set in the 1.5-4 mg/L range). Unfortunately, we were not able to determine an association constant from the luminescence titration.

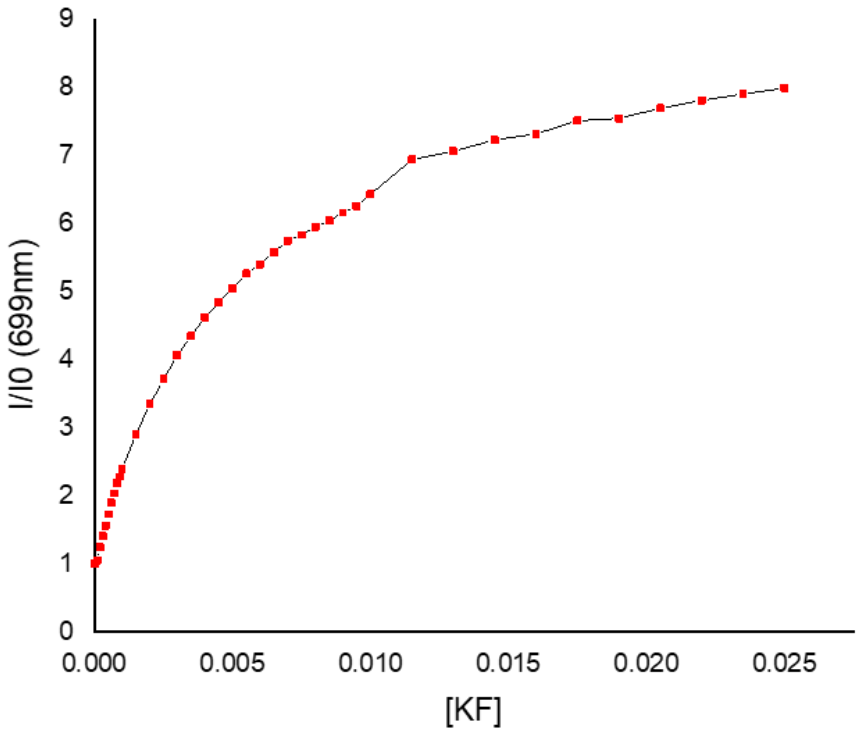

Figure 29. *I/I_0 titration curve of* ***EuL1*** *with KF.*

3.4.2 Sulfur-based anions

A variety of sulfur-based anions were tested against the five complexes (sulphate, sulfite, sulfide, thiocyanate), but only SO_4^{2-} and SO_3^{2-} affected the emission

properties of the probes. Interaction with SO_4^{2-} gave the 3+ charged complexes a very slight increase in Φ_{Ln}, while **EuL4** and **EuL5** were unaffected. As discussed before for fluoride, also for sulphate the most sensitive complex was **EuL1**, whose change in emission are reported in Fig. 30. Acceptable levels of SO_4^{2-} in water are around 250-500 mg/L Together with the increase in emission intensity, also the lifetime gets slightly longer (Table 6).

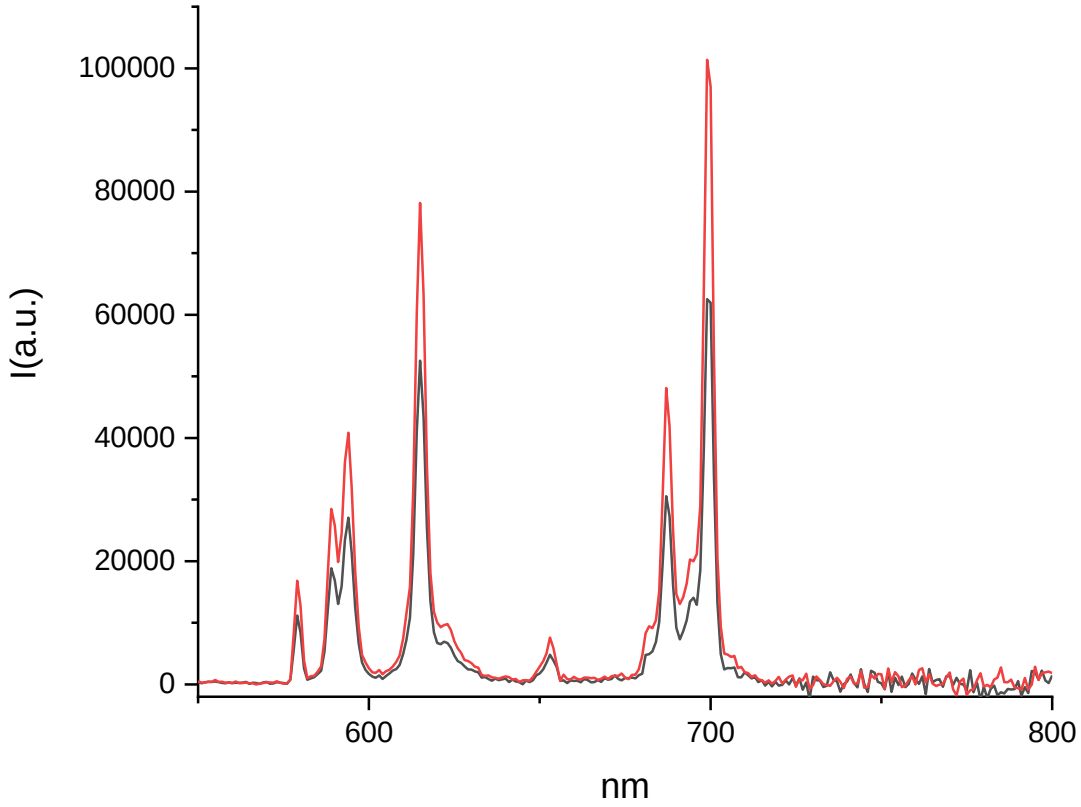

Figure 30. *Emission spectra (λ_{ex} = 330 nm) of* ***EuL1*** *with (red) and without (black) sulphate.*

Table 6. *Phosphorescence quantum yields and lifetimes of* ***EuL1-EuL5****.*

	EuL1		**EuL2**		**EuL3**		**EuL4**		**EuL5**	
	Φ_{fl}(%)	τ_{obs}(ms)	Φ_{fl}(%)	τ_{obs}(ms)	Φ_{fl}(%)	τ_{obs}(ms)	Φ_{fl}(%)	τ_{obs}(ms)	Φ_{fl}(%)	τ_{obs}(ms)
	0.30	0.25	0.60	0.32	1.48	0.40	1.60	0.44	3.00	0.58
$+SO_4^{2-}$	0.42	0.30	0.75	0.35	1.52	0.41	1.60	0.44	3.00	0.58

The overall effect of Na_2SO_4 on **EuL1-EuL3** is similar to that of fluoride and is characterized by an increased luminescence over the whole spectrum (560-800 nm) and a lengthening of the lifetime. This effect is modest compared to the one induced by the addition of fluoride. SO_4^{2-} is a bigger anion than fluoride and may not be able to displace the coordinated water molecule. The fact that the shape of the luminescence spectrum remained unaltered upon addition of SO_4^{2-} clearly indicates that this is unable to modify the first coordination sphere. *q* values calculation will be needed to rule out the coordinated water displacement.

Interaction with sulfite gave different results. The Eu(III) emission was approximately halved for all five complexes but left the luminescence lifetimes unaffected (Table 7). Acceptable levels of SO_3^{2-} in water are around 250 mg/L.

Table 7. *Phosphorescence quantum yields and lifetimes of* ***EuL1-EuL5****.*

	EuL1		**EuL2**		**EuL3**		**EuL4**		**EuL5**	
	Φ_{fl}(%)	τ_{obs}(ms)	Φ_{fl}(%)	τ_{obs}(ms)	Φ_{fl}(%)	τ_{obs}(ms)	Φ_{fl}(%)	τ_{obs}(ms)	Φ_{fl}(%)	τ_{obs}(ms)
	0.30	0.25	0.60	0.32	1.48	0.40	1.60	0.44	3.00	0.58
$+SO_3^{2-}$	0.15	0.30	0.35	0.32	0.70	0.40	0.88	0.44	2.30	0.58

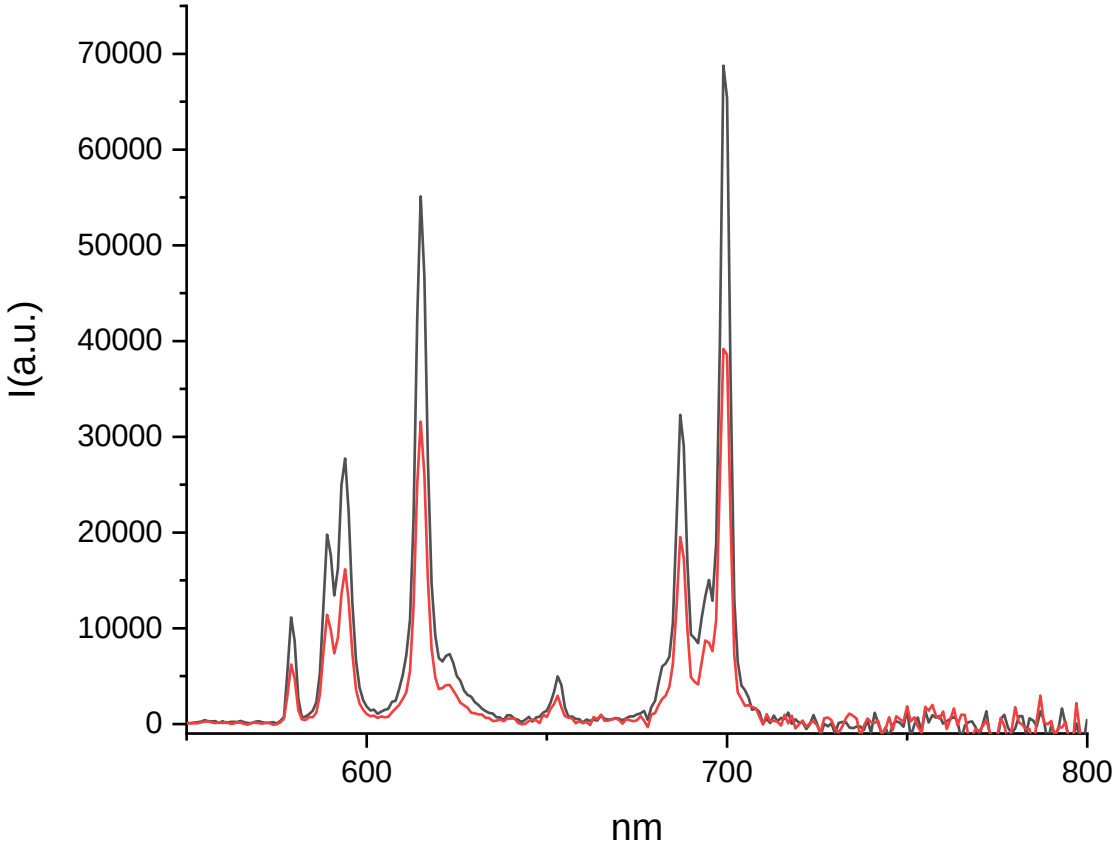

Figure 31. *Emission spectra (λ_{ex} = 330 nm) of* ***EuL1*** *with (red) and without (black) sulfite.*

As can be seen for **EuL1** (Fig.31), SO_3^{2-} quenched the emission of Eu(III) over the whole spectrum; also for the other compound the magnitude of the quenching was comparable. This consistency in quenching, together with the fact that the emission lifetimes are not affected led us to consider Eu-independent quenching mechanisms. To investigate if this could be an antenna-mediated process, we recorded the emission spectra and fluorescence lifetime of Car-MOM under the conditions described for the europium complexes in presence and absence of SO_3^{2-} (Fig.32). The emission of Car-MOM was quenched by 3000 equivalents of sulfite approximately by 30% ($\Phi_{Car\text{-}MOM}$ = 86% $\Phi_{Car\text{-}MOM(+SO3)}$ = 52%), and its fluorescence lifetime was shortened from 6.5 ns to 4.5 ns.

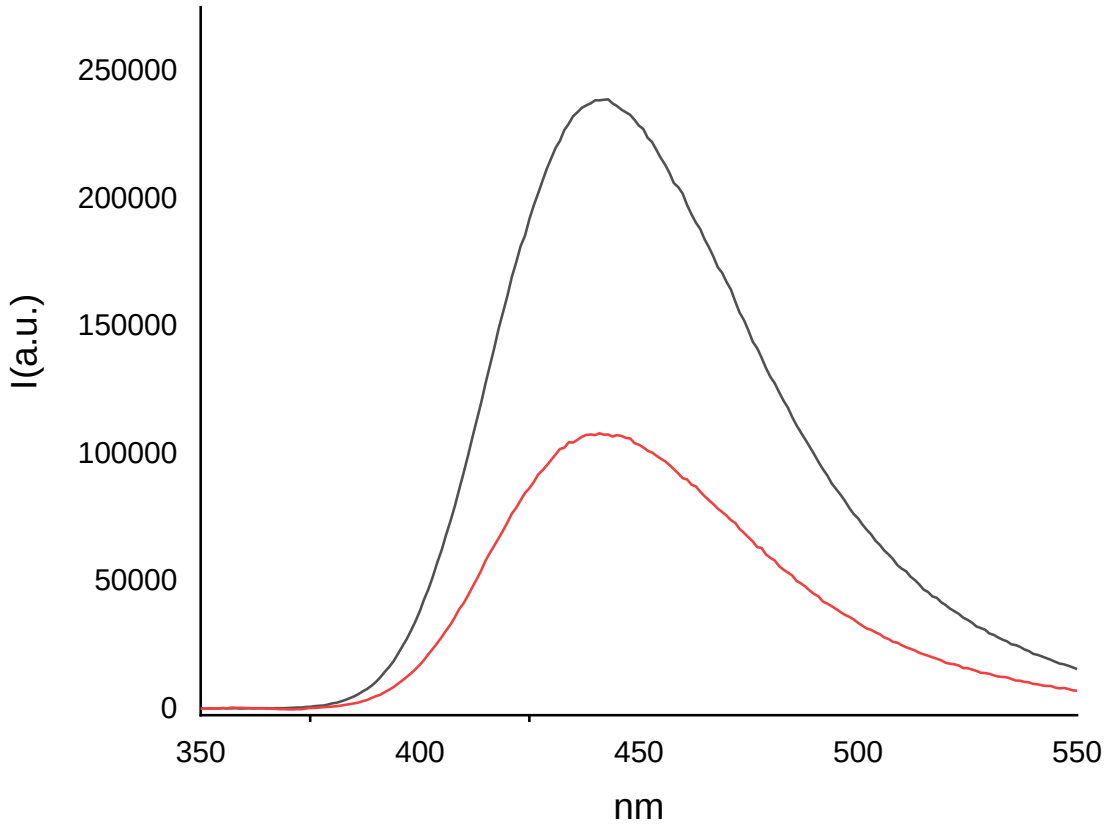

Figure 32. *Emission spectra (λ_{ex} =330 nm) of Car-MOM with (red) and without (black) sulfite.*

We believe that this quenching effect of sulfite could be caused by a photoreaction between SO_3^{2-} and the ligand/Car-mom. Further experiments are being conducted to understand the underlying mechanism.

3.4.3 Phosphates

The interaction of the europium complexes with phosphate (Na_2HPO_4 was used) produced interesting results. Maximum tolerated phosphate concentration in drinking water are set at around 1 mg/L. It is important to note that the addition of HPO_4^{2-} anions increased the solution pH to 8.6-8.7 so a small quenching of the europium phosphorescence is to be expected. This can be seen for **EuL3**, **EuL4** and **EuL5**, the quantum yields of which are marginally lowered (Table 8), while no effect is seen for **EuL2**.

Table 8. *Phosphorescence quantum yields and lifetimes of* ***EuL1-EuL5****.*

	EuL1		**EuL2**		**EuL3**		**EuL4**		**EuL5**	
	Φ_{fl}(%)	τ_{obs}(ms)	Φ_{fl}(%)	τ_{obs}(ms)	Φ_{fl}(%)	τ_{obs}(ms)	Φ_{fl}(%)	τ_{obs}(ms)	Φ_{fl}(%)	τ_{obs}(ms)
	0.30	0.25	0.60	0.32	1.48	0.40	1.60	0.44	3.00	0.58
$+HPO_4^{2-}$	0.42	0.36	0.60	0.32	1.10	0.38	1.40	0.40	2.80	0.57

EuL1 response to phosphate anions was peculiar, and it can be observed in Fig.33.

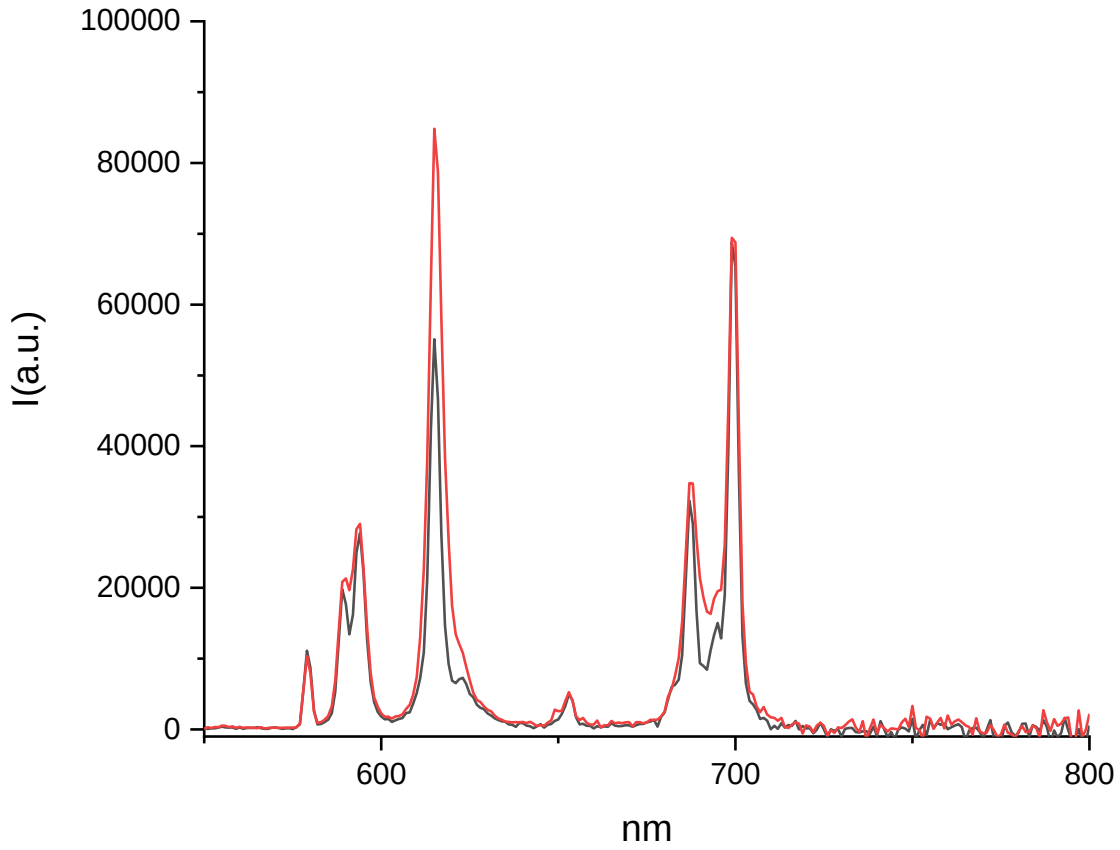

Figure 33. *Emission spectra (λ_{ex} =330 nm) of* ***EuL1*** *with phosphate (red) and without (black).*

EuL1 luminescence quantum yield increased by about 40%, which is modest when compared to the results obtained with fluoride. The interesting effect is that the increase in emission is not uniform for the whole spectrum. The intensity of the

615 nm peak, which is associated with the $\Delta J = 2$ transition, is nearly doubled, while the rest of the spectrum is mostly unaffected. The $\Delta J = 2$ is a "hypersensitive transition" meaning that this transition is particularly sensitive to the coordination environment and its geometry. It has been shown that highly asymmetric complexes have prominent $\Delta J = 2$ transition; the results obtained suggest that the binding with phosphates disrupts the symmetry of the coordination environment.[52] The fact that the emission properties of **EuL3-EuL5** are affected differently when compared to **EuL1**, and that **EuL2** is unaffected by the addition of phosphate could indicate that the luminescence is modulated by both the pH and metal-anion interactions. To clarify the mode of interaction of the phosphate anion, *q* values calculation will be needed.

3.4.4 Carbonates

Sodium bicarbonate addition yielded interesting results. Acceptable carbonate/bicarbonate levels for drinking water are set at around 500 mg/L The addition of $NaHCO_3$ increased the pH to about 8.5, so a small quenching of the europium emission is to be expected. This is true for **EuL4** and **EuL5**, whose luminescence quantum yields slightly decreased (Table 9).

Table 9. *Phosphorescence quantum yields and lifetimes of* ***EuL1-EuL5****.*

	EuL1		**EuL2**		**EuL3**		**EuL4**		**EuL5**	
	Φ_{fl}(%)	τ_{obs}(ms)	Φ_{fl}(%)	τ_{obs}(ms)	Φ_{fl}(%)	τ_{obs}(ms)	Φ_{fl}(%)	τ_{obs}(ms)	Φ_{fl}(%)	τ_{obs}(ms)
	0.30	0.25	0.60	0.32	1.48	0.40	1.60	0.44	3.00	0.58
$+HCO_3^-$	1.38	0.42	1.02	0.35	1.75	0.42	1.51	0.37	2.80	0.54

On the other hand, **EuL1-EuL3** quantum yields are increased in the presence of bicarbonate anions. Along with an increase in emission intensities, a change in the shape of the emission spectrum is seen (Fig.34) for **EuL1**.

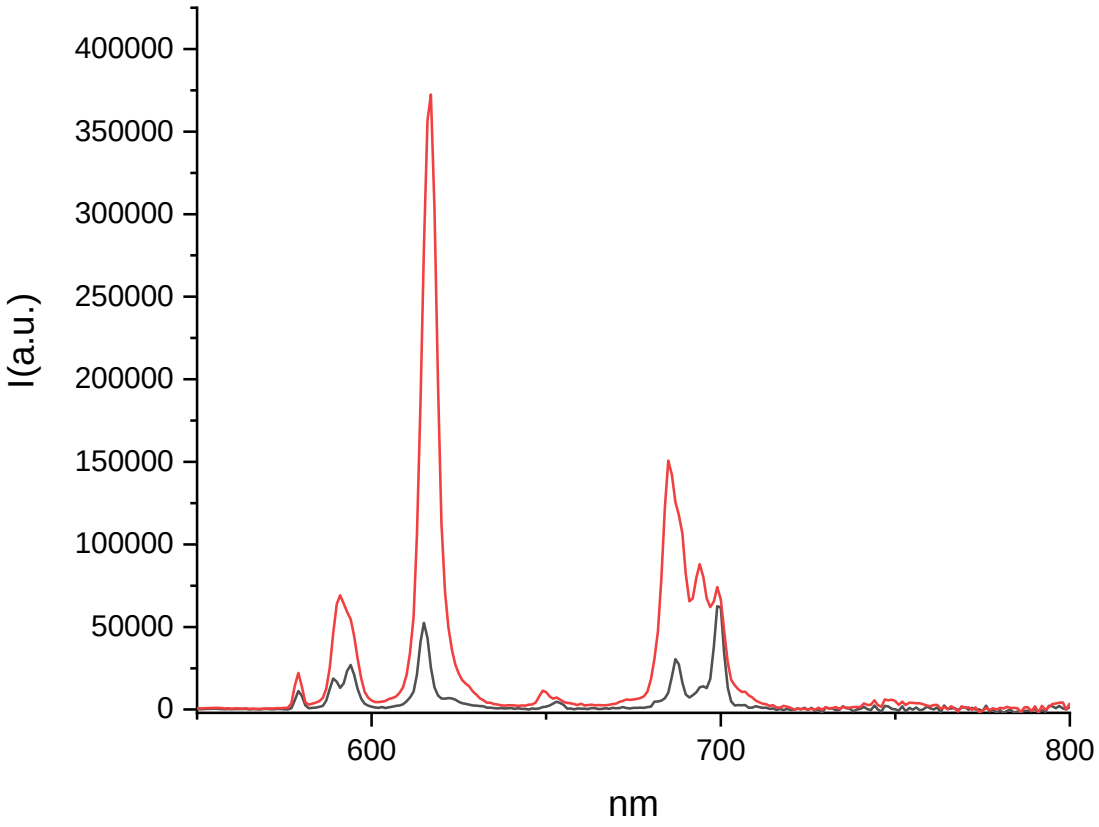

Figure 34. *Emission spectra (λ_{ex} = 330 nm) of* ***EuL1*** *with (red) and without (black) carbonate.*

Again, for the case of bicarbonate the relative intensity of the $\Delta J = 2$ peak at 615 nm increased, indicating that interaction with HCO_3^- influences the coordination geometry of the Eu(III) center. Bicarbonate binds Eu(III) in a bidentate way as it has been demonstrated in similar works[53]. Such a binding mode in these complexes would result in the displacement of both the coordinated water molecule and one of the arms of the DO3A macrocycle, which would lead to a significant change in the Eu(III) coordination geometry. To verify the displacement of water from the Eu(III) center, *q* values calculation will be performed.

3.4.5 Cyanide

Studies with cyanide were problematic for a variety of reasons. Firstly, the high basicity of CN^- made it impossible to study the same analyte concentration as the other anions without drastically changing the pH; the addition of 30 mM cyanide yielded a solution with pH 10. A preliminary study with cyanide was conducted in the same condition as for the other anions; the results are summed up in Table 10 and the spectral changes for **EuL1** can be seen in Fig. 35.

Table 10. *Phosphorescence quantum yields and lifetimes of* ***EuL1-EuL5****.*

	EuL1		**EuL2**		**EuL3**		**EuL4**		**EuL5**	
	Φ_{fl}(%)	τ_{obs}(ms)	Φ_{fl}(%)	τ_{obs}(ms)	Φ_{fl}(%)	τ_{obs}(ms)	Φ_{fl}(%)	τ_{obs}(ms)	Φ_{fl}(%)	τ_{obs}(ms)
	0.30	0.25	0.60	0.32	1.48	0.40	1.60	0.44	3.00	0.58
$+CN^-$	0.76	0.40	0.45	0.40	0.85	0.50	0.40	0.30	1.60	0.40

The changes in spectral shape of **EuL1** (also for **Eul2** and **EuL3**) upon the addition of cyanide resembled the one obtained with carbonates which may indicate a change in coordination geometry. **EuL4** and **EuL5** spectral shapes are barely affected by cyanide addition. Luminescence quantum yields are lowered for all the complexes but **EuL1**, most likely due to the significant increase in pH.

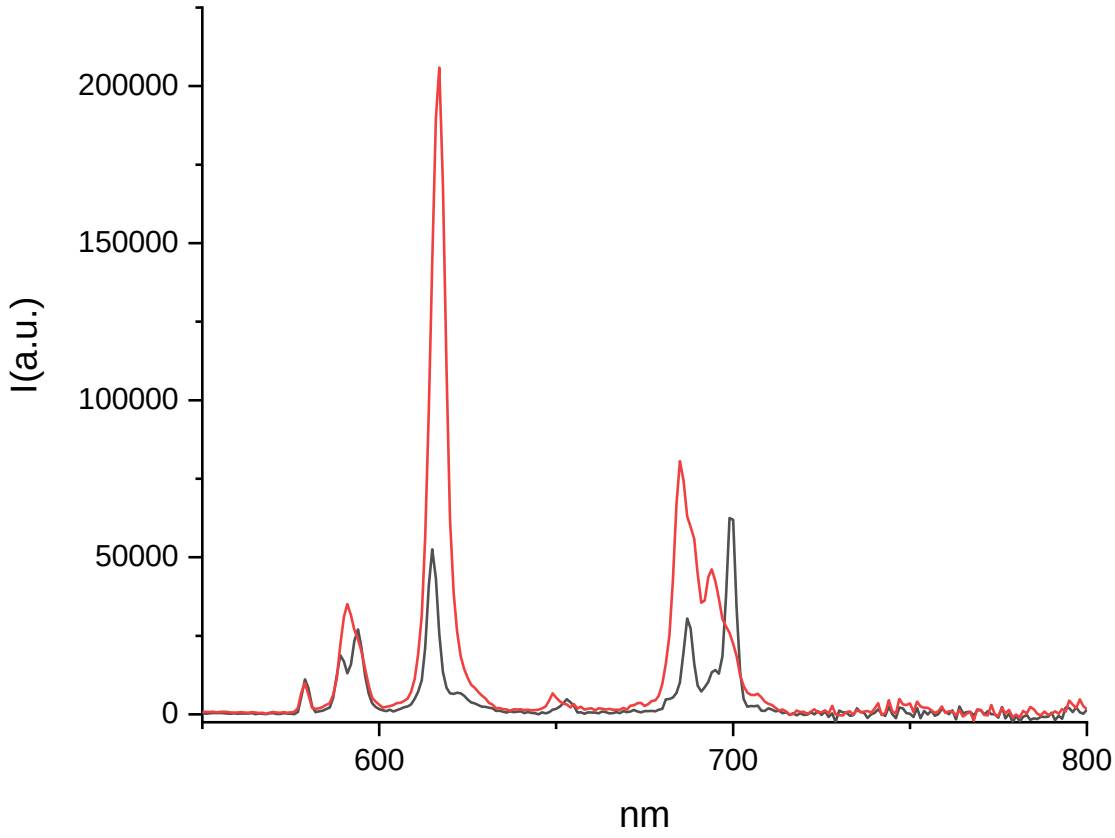

Figure 35. *Emission spectra (λ_{ex} =330 nm) of EuL1 with (red) and without (black) cyanide anion.*

To understand the interaction between cyanide and the Eu(III) complexes the previous experiments were repeated but with lower cyanide and complex concentrations to mitigate the pH change while keeping a significant excess of cyanide. The concentration of cyanide was 5 mM resulting in a final pH of 8.5, and the complex concentrations were halved to 5 µM. The change in working conditions also affected the emission response of the complexes: the emission of every complex was quenched uniformly over the whole spectrum for **EuL2-EuL4** in the same way an increase in pH would diminish the luminescence. The only exception was **EuL1**, the emission of which was drastically quenched, but this decrease was accompanied by a change in the profile of the emission spectrum (Fig.36). The overall quantum yield is lowered but the 615 nm peak was relatively less affected by the quenching. Two different luminescence lifetime values were observed for the emission at different wavelengths, 0.14 ms at λ_{em} = 699 nm and 0.26 ms at λ_{em} = 615nm.

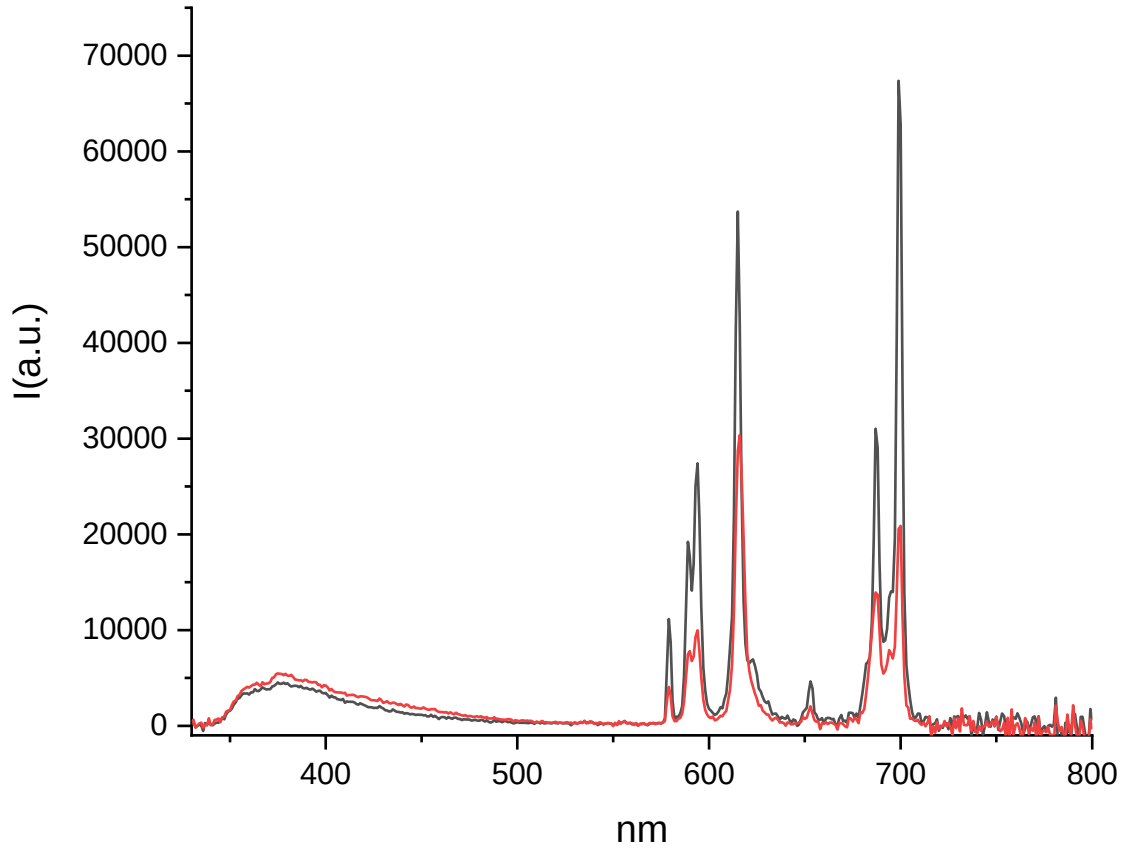

Figure 36. *Emission spectra (λ_{ex} =330 nm) of* ***EuL1*** *with cyanide (red) and without (black)-lowered concentrations.*

The luminescence lifetimes were measured in D_2O to calculate the number of inner-sphere water molecules (*q*-values). A decrease in *q*-value would be consistent with the CN^- anion coordinating to the Eu(III) center. The *q*-value calculation was conclusive for **EuL4** and **EuL5**, and water displacement was excluded. The results for the 3+ charged complexes were not as precise, probably due to pH effects. The *q* values for **EuL2** and **EuL3** remained constant after cyanide addition, suggesting that water displacement was not happening. The results for **EuL1** were inconclusive. More experiments will be needed to understand the interaction mechanism between the complexes and cyanide.

3.5 Conclusion

The full photochemical characterization of five different Eu(III) complexes was carried out. All the complexes have a water molecule coordinated to the metal center that can be displaced by anionic species, modulating the sensitized luminescence of the europium. The complexes were screened against a library of anionic compounds relevant for water monitoring purposes, with the aim of developing a novel differential sensing platform capable of sensing different chemical species in a single measurement. The chemical structure of the europium complexes was designed to give unique emission characteristics to each one and different changes in luminescence when interacting with the chosen analytes. The emissions of the complexes studied are sensitive to pH to varying degrees; this is important for water monitoring applications, since pH is a fundamental parameter for the quality of water bodies. Thanks to this feature – together with being able to sense anions in water – a sensor array constructed with these complexes could be also able to sense pH. Moreover, the pH range where these complexes are most sensitive (6.5-8.5), is the most useful pH window for this purpose.

Among the analytes tested, the compounds showed high sensitivity towards fluoride, while being completely unaffected by other halides. With respect to the other analytes, the 3+ charged complexes showed affinity to a larger set of species when compared to the +1 and +2 complexes. One or more unaffected compounds could be used in the final sensor array construction to calibrate the changes in emission of the other complexes. Interesting results were obtained for carbonate anions, that affected the spectral shape of the Eu(III) emission. This result is especially important for the final sensing platform to conduct ratiometric analysis by confronting different peaks emission intensities. It is also interesting that the complexes showed affinity towards carbonates, while being unaffected by carboxylate-bearing molecules such as acetate, benzoate and oxalate.

More work will be necessary before the application of these complexes in the development of a sensing platform. It would be interesting to understand the interaction of the complexes with anions by co-crystallization with the various analytes to resolve the structure of the EuL-anion complexes via XRD. Other investigation techniques, such as NMR and HPLC-MS will be employed to understand the interaction mechanism of CN^-. Luminescence titrations will be carried out for all the five complexes with all the anions that showed some degree of affinity to determine the analytical dynamic range of each complex toward each analyte. Competition studies will be needed to determine if the sensor will be able to provide complex responses in a multi-analyte environment. Lastly, the anion recognition properties will be tested on solid supports (such as a paper strip) to evaluate if the realization of a prototype is possible. It will also be interesting to expand the set of complexes tested including different architectures and different luminescent lanthanides such as Tb(III), Sm(III) or Yb(III) to expand the final prototype capabilities.

4. ECL-immunoassay for *Listeria* sensing

4.1 Introduction – Biological pollutants

Water pollution, as stated in the general introduction, does not stem just from chemical compounds, but also from biological components such as bacteria, viruses, and parasites. Many microorganisms present in water bodies have an essential function in nature, but some of them can be harmful for mankind and other life forms. Diseases caused by waterborne pathogens cause tens of millions of deaths each year and millions of dollars in related expenses[9], and this problem tends to be more prominent in countries where water monitoring and sanitation is not regulated. It's important to note that contamination of water sources by harmful microorganisms can lead to proliferation of said microorganisms in food production chains, in crops, and in livestock; it is thus imperative – to actively avoid contamination of products – that the monitoring of harmful pathogens includes water sources.

Presently, there are no unified methods for the collection and analysis of water for detecting all pathogenic microorganisms of interest; differences among pathogens, low concentrations in large volumes of water, and the presence of interferents in the sample are just some of the many challenges presented by the quantification of biological pollutants in water. Culture based methods are extensively used for quantification of waterborne pathogens, but they suffer from low sensitivity, the excessive time needed to obtain reliable results and the presence of non-culturable organisms. Polymerase chain reaction (PCR) based techniques offer faster results when compared to culture based methods, while providing high sensitivity; PCR

also has its limitations, such as the inability to discriminate between viable and non-viable DNA that could lead to the inability of determining the real infectious risk associated with a population, and the necessity of treatment and purification of samples to concentrate the initial sample and remove possible interferents.[8]

Moreover, the most common diseases related to waterborne pathogens (cholera, salmonellosis, shigellosis)[10] are caused by bacterial contamination by fecal matter, both human and animal, but the presence of pathogenic bacteria tends to be sporadic and erratic, the levels are usually low, and their isolation and culture can be problematic; due to these reasons routine water microbiological monitoring does not include the detection of pathogenic organisms. However, since safe water must be pathogen free, the approach for assessing the microbiological quality of water is to test for indicator bacteria. Indicator bacteria are non-pathogenic bacteria present in the gastrointestinal fauna that, if present in a water sample, indicates the presence of fecal matter contamination and the possible presence of dangerous pathogens.[54] This approach can be cost effective and facilitate analysis, since these indicator bacteria are easy and quick to quantify; however, since this approach does not lead to a real quantification of pathogens, it presents some limitations. For instance, indicator bacteria do not correlate with viruses, parasites or bacteria that do not originate from fecal contamination. Thus, the need to develop sensing platforms for the detection of harmful microorganisms is always an important topic, especially if the sensing platforms developed can avoid the use of long and delicate procedures typical of PCR or culture methods.[4]

4.2 *Listeria* case study

Listeria monocytogenes is a gram-negative bacterium of the Listeriaceae family that causes the infection listeriosis. Listeriosis is particularly of interest because even though the occurrence of listeriosis is low, approximately 1 case per million people, the mortality rate is one of the highest for foodborne/waterborne infectious

diseases (20-30%)[55], which can be higher for at risk subjects, especially for pregnant women, where bacteriemia often leads to miscarriages and stillbirths. Moreover, it has been reported in recent years that the cases of listeriosis are on the rise, even in the European Union.[56]

Listeria is often referred to as a foodborne pathogen since nearly all listeriosis cases are caused by the consumption of contaminated animal products (dairy, preserved meats) or vegetables, but the presence of pathogenic listeria in waterbodies has been reported.[57] Since listeria is a resistant bacterium, that can live even in the absence of oxygen and proliferate even at freezing temperatures and high salt concentrations, contamination of food products by using contaminated water sources can easily occur.[58]

Even though *Listeria Monocytogenes,* and other members of the Listeriaceae, are relatively common bacteria (around 10%) present in human gastrointestinal fauna , it has been reported that they have a low correlation with typical index pathogens, such as *E. Coli*, especially *L. Monocytogenes*; so, if there is need to quantify Listeria, it is mandatory to quantify Listeria itself and not measuring index pathogens.[59] Thus, the need to develop sensing platforms capable of detecting Listeria in waterbodies is as important as developing clinical assay for the determination of the disease in living patients.

4.3 *Listeriolysin-O*

Listeriolysin-O (LLO) is a pore-forming toxin produced by the pathogenic strains of Listeria. LLO plays a key role for the virulence of *L. Monocytogenes*, since its function is to pierce holes in the membranes of phagosomes, allowing the escape of the bacteria in the cytosol without damaging the plasma membrane of the infected cells, where it can grow intracellularly protected from the extracellular immune system components.[60]

Since LLO is expressed only by pathogenic strains of *Listeria*, such as *L. Monocytogenes*, this protein could be used as a target biomarker for the detection of only pathogenic strains of Listeria; many cases of immunoassays that use LLO as a recognition element for sensing anti-LLO specific antibodies for clinical tests have been reported in literature.[61] LLO has also been used to produce anti-LLO monoclonal and polyclonal antibodies, that can also be used for the development of immunoassays for the detection of LLO itself.[62,63]

4.4 Electrogenerated chemiluminescence

Electrochemically generated chemiluminescence or electrogenerated chemiluminescence (ECL), is a redox-induced light emission in which species generated on electrode surfaces undergo high energy electron transfer reaction to form excited states that emit light. Described for the first time by Bard in 1960, who observed light emissive tris-2,2'-bipyridylruthenium(II) ($[Ru(bpy)_3]^{2+}$), which is able to react under electrical stimulus to generate the excited state of the ruthenium complex which emits light at 610 nm.[64]

ECL began as just academic curiosity, but nowadays it has become one of the most powerful tools in the field of medical diagnosis techniques. The advantages offered by ECL when compared to electrochemical and spectroscopic methods are numerous: superior spatial and temporal control of the light emission, intrinsically low background noise and high sensitivity, very broad dynamic range, and very rapid measurement are just some of them. Most of the advantages of ECL when compared to photoluminescence techniques is the absence of excitation light for the generation of the emitting excited state, that not only is the reason for the low noise levels of ECL but also offers the opportunity to simplify the instrumental setup. Taking profit of the many advantages just mentioned, especially the low cost of instrumentation, in the last 20 years ECL based analytical applications have been developed and commercialized, with a particular focus on immunoassays for

the detection of molecules of biological interest such as cancer biomarkers, DNA/RNA, toxins or abuse substances.[65] A more in-depth discussion of the principles of ECL can be found in the appendix at paragraph 7.2.

4.5 Aim of the project

This work stems from a collaboration between our research group and Diatheva s.r.l., an Italian biotech company specialized in the development and manufacture of kits for the detection of multiple pathogens, both for clinical, veterinarian, and industrial purposes. The aim of this work is to develop an ECL-based immunoassay for the sensing of *Listeria Monocytogenes*; the assay is based on a commercial ELISA (enzyme linked immuno-sorbent assay) kit produced by Diatheva for the detection of anti-Listeria antibodies in humans, with the goal of improving the limits of detection of the assay. The assay architecture will be modified for the use of magnetic microbeads (MMB) technology as a support, and to accommodate the different signal transduction mechanisms. The broader concept of the work is to offer an alternative technology (ECL) to accommodate already existing assay architectures with minimal changes. The ELISA kit offered by Diatheva uses *Listeriolysin-O* (LLO), a toxin which is a key factor in Listeria virulence, to detect anti-Listeria antibodies that are produced in individuals infected by Listeriosis. The LLO is adsorbed on a 96-well polycarbonate plate, and it's able to bind anti-Listeria antibodies from clinical samples (serum, plasma); the antigen-antibody complex is then revelated using an anti-human antibody conjugated with horse radish peroxidase (HRP) that can react with the chromogenic substrate, 2,2′-Azino-bis(3-ethylbenzothiazoline-6-sulfonic acid) (ABTS).

The plan to translate the assay from ELISA technology to ECL will consist of the following: instead of adsorbing the LLO on a surface, the antigen will be conjugated with biotin, in order to utilize MMBs coated with streptavidin; using

MMB, the immunocomplex can be separated from the bulk solution with the aid of a magnet, which will also facilitate the washing steps, and aide with the deposition of the immunocomplex on the electrode surface. To obtain the ECL signal, the secondary antibody – instead of being conjugated with HRP – will be conjugated with $Ru(bpy)_3$, one of the most common luminophores used for ECL applications.

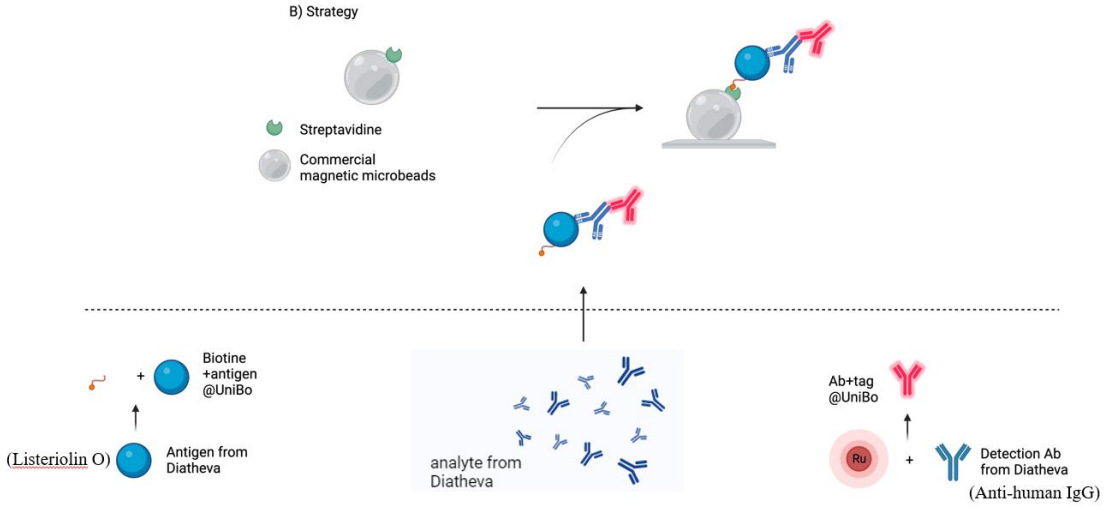

Figure 37. *Graphic representation of the assay structure and components*

4.6 ListeriaTest – Anti-LLO IgG immunoassay from Diatheva

ListeriaTest (https://www.diatheva.com/it/prodotto/listeria-test-96/) is an ELISA for the detection of anti-LLO IgGs in human serum and plasma, designed as an aid for the diagnosis of listerial infection and the screening for *Listeria* exposure designed and sold by Diatheva as a complete kit. The 96-well plate coated in LLO are incubated with collected samples. During the incubation (1h) step the anti-LLO antibodies bind to the antigen forming a specific complex. After removing sample excess by washing with the washing buffer provided with the kit, the antigen-antibody complex is revealed by incubating (1h) anti-human IgG HRP-conjugated

antibody. After an additional washing cycle, the detection is performed by incubating the samples (30min) with ABTS as a chromogen and reading the absorbance at 410 nm with a microplate reader. The samples of serum or plasma must be diluted 100-fold using the dilution buffer that comes with the kit. Each kit also comes with positive and negatives control to compare the samples' output. The absorbance of the positive control should be $A_{pos} > 1.2$, the negative should be $A_{neg} < 0.35$ while background should be $A < 0.12$; if these criteria are not met, the assay is non reliable and should be performed again. The calibrator is used to correct the real samples ABS to calculate an index value, if the index value is $I > 1.15$ the test is positive and anti-LLO antibodies are present in the sample; if the index is $I < 0.85$ the test is negative, while if the index is in between these two values the test is unconclusive and should be performed again with a fresh sample. The biggest limitation of this assay is that it cannot discriminate between current or prior infection, so the test's results can be used just as an aid for the diagnosis of listeriosis, taking into consideration patient's history, physical findings and other diagnostic procedures.

4.7 IgG labeling with $Ru(bpy)_3^{2+}$

Polyclonal FC specific goat anti-human immunoglobulin G (IgG) labeled with $Ru(bpy)_3^{2+}$ were chosen as the secondary antibody for the immunoassay. Before the labeling, the antibodies were dialyzed against PBS 1x pH 7.4 (10mM phosphate buffer, 137mM NaCl, 2.7mM KCl) to exchange the buffer of the IgGs, to eliminate possible interferent to the bioconjugation reaction with ruthenium such as tris(hydroxymethyl)aminomethane (tris base). The dialysis was conducted overnight at 4°C using regenerated cellulose (RC) dialysis membrane with an 8-10kDa cutoff. After dialysis, the IgG solution was diluted to 1 mg/ml for the coupling reaction. ($Ru(bpy)_2$-bpy-OSU), a $Ru(bpy)_3$ complex, presenting a N-hidroxysuccinimide (NHS) ester on one of the bipyridyl substituent, was solubilized in DMSO to obtain a concentrated solution (0.01M). The coupling

reaction between the IgG and Ru(bpy)$_2$-bpy-OSU was conducted at room temperature (RT) under mild stirring, covering the reaction from light. The ruthenium solution was added to the solution of IgG and left to react for 1h; at the end, an excess of Tris base was added to quench the reaction. The ruthenium labeled IgGs were then purified with dialysis against PBS 1x at 4°C overnight, covering from the light. Three different batches of labeled antibodies were prepared, with increasing amounts of Ru(bpy)$_2$-bpy-OSU, respectively 20, 50, 100 molar excesses were used, both to obtain different ratios of ruthenium per antibody, but also to better understand the correlation between ruthenium used and the degree of labeling (DOL) of the final product. After dialysis, all the samples prepared presented a yellow precipitate that did not redissolve, even under strong agitation (Fig.38).

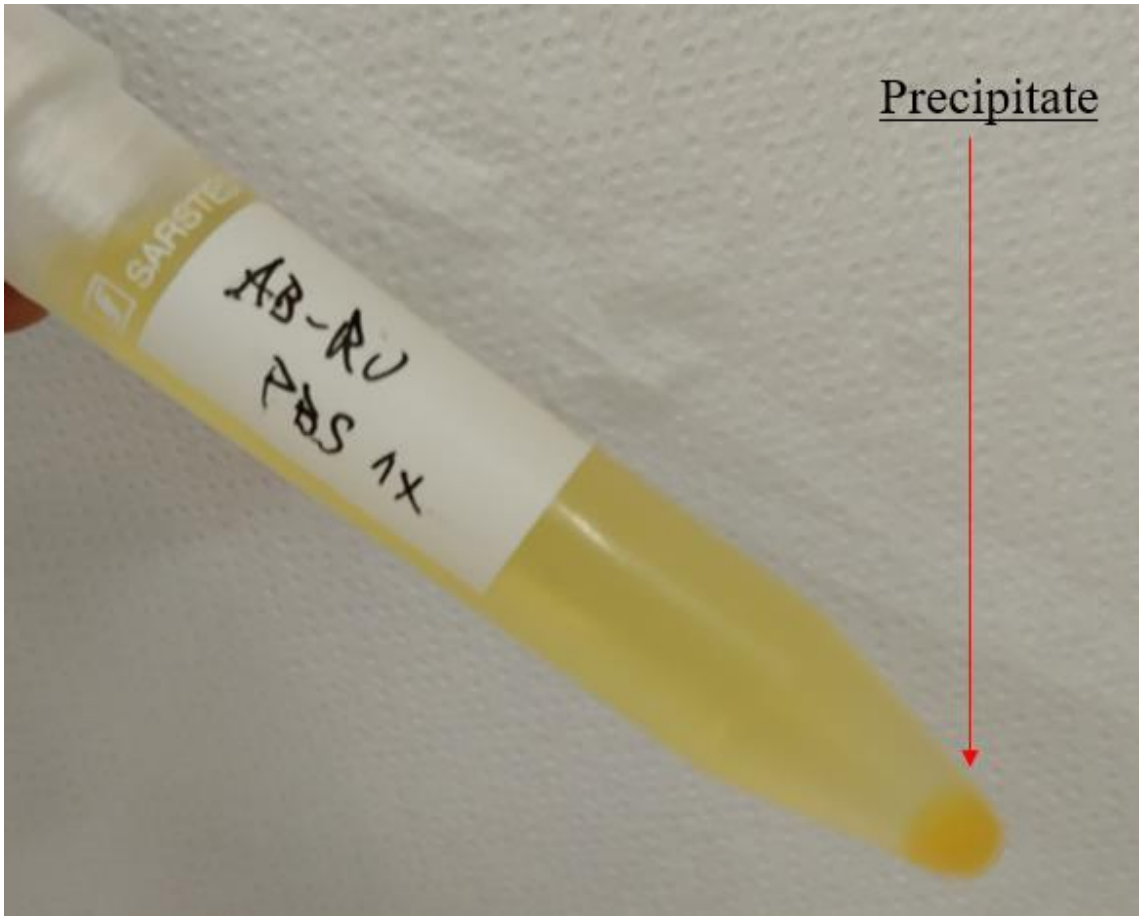

Figure 38. *Ruthenium labelled antibodies, and the precipitate formed during purification.*

The amount of precipitate did not correlate with the amount of Ru(bpy)$_2$-bpy-OSU used for the reaction; for this reason, we believe that the precipitation was not caused by an over-labeling of the IgGs. To remove the precipitate, we used polyvinylidene difluoride (PVDF) syringe filters with 0.2 µm pore size. A fourth batch of labeled IgGs was prepared, again with a 50 times molar excess of ruthenium but at a lower temperature (4°C instead of RT) and for a shorter time (30 minutes instead of 1h) to see if milder reaction conditions would prevent the precipitation of the labeled antibodies. Unfortunately, after dialysis nearly the same amount of precipitate was present. The final concentration of IgG was thus measured again after filtration using the Bradford protein assay; the DOL (degree of labeling) of the labelled IgGs was estimated spectroscopically, measuring the absorbance of the ruthenium at 452 nm and 460 nm (ε_{452nm}=14600, ε_{460nm}=14100). The calculated DOL for the different batches of IgG came out at around 20, 19, and 11 ruthenium complexes per antibody for the reactions with a 100-fold, 50-fold, and 20-fold molar excess of Ru(bpy)$_2$-bpy-OSU, respectively, while we observed a DOL = 12 when the conjugation was conducted in milder conditions. The highest DOL antibodies were chosen for the use in the assay, to maximize the ECL signal.

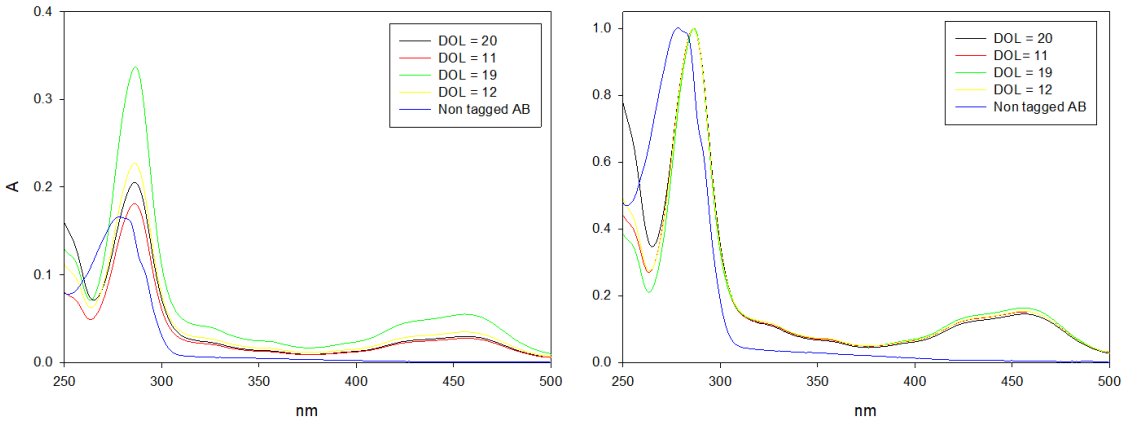

Figure 39. *Absorption spectra (normalized on the right, as is (left) of the different IgG-Ru conjugates prepared with: 100-fold excess of ruthenium (Black), 20-fold excess (Red), 50-fold excess (Green) and 50-fold in milder conditions (Yellow), compared to unlabeled (blue).*

The different batches of IgGs were analyzed with sodium dodecyl sulphate polyacrylamide gel electrophoresis (SDS-PAGE), both in reducing and non-reducing condition, following standardized protocols[66] (Fig.40).

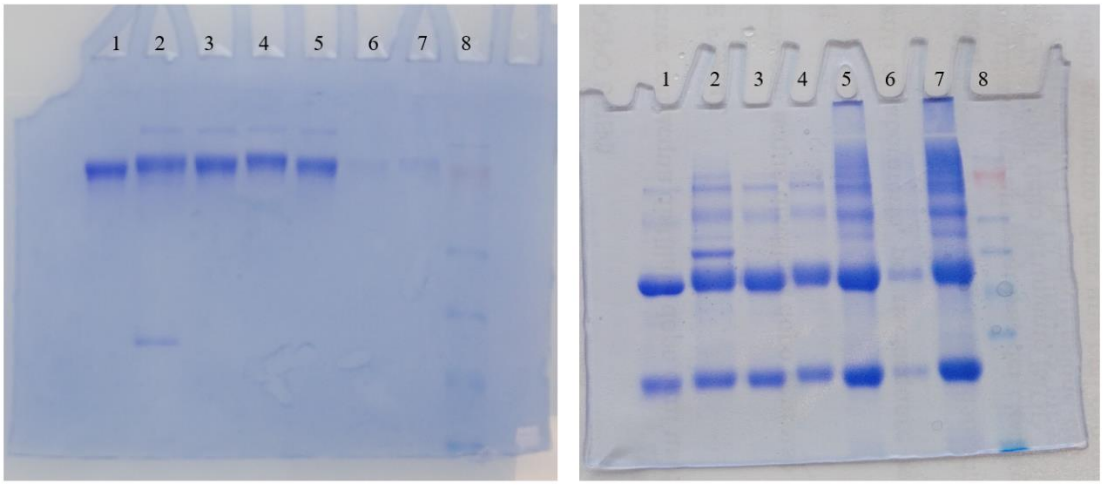

Figure 40. *SDS-PAGE gels in reducing conditions (right) and non reducing conditions (left) of the different IgG-Ru conjugates: non labeled IgG (lane 1), 100-fold excess ruthenium (2), 20-fold excess (3), 50-fold excess (4), milder conditions (5), precipitated IgGs (6-7), molecular weight standards (8).*

It is clearly visible on the non-reducing condition gel (on the left) that the conjugates with higher DOL (lane 2 and lane 4) are retained more when compared with the IgGs with lower DOL (lane 3 and 5), and they all are retained more when compared to the non-labelled IgG (lane 1). To try to make some clarity on the precipitation phenomenon occurring during the labeling rection, some precipitated antibodies were run on SDS gels together with the other antibodies (in lane 6-7 the precipitate of the same IgGs of lane 4-5 respectively). It is interesting to note that in the absence of β-mercaptoethanol (non-reducing conditions) the precipitates are hardly visible on the gel, while in reducing conditions they are more clearly visible. This may indicate that the driving force behind the precipitation of the labeled antibodies could be of electrostatic nature; since each ruthenium tag is twice positively charged, the change in the overall electrostatic charge of the protein could be so relevant that the amount of SDS to protein (standard methodologies use a ratio of 2:1 of SDS to protein) could be not enough to fully denature the IgGs, while the braking of disulfide bonds by the action of β-mercaptoethanol might be

enough to properly run the antibodies on the gels, although some precipitate is left at the top of the gel.

Lastly, since the precipitation phenomenon raised some concerns and we wanted to make sure that the labeled antibodies still possessed their recognition ability, a modified ELISA was conducted. Utilizing Diatheva's listeria assay (described in paragraph 1) as a platform, the secondary antibody (anti-human HRP conjugate) of the assay was substituted with the ruthenium labeled IgG; then an anti-goat antibody capable of binding the ruthenium labeled IgG, conjugated with HRP, was used to develop the assay. This experiment confirmed that after the labeling reaction with ruthenium the antibodies maintain their recognition ability. The results are shown in the next paragraph (Fig.43).

4.8 LLO functionalization with biotin

Recombinant Listeriolysin-O was functionalized with two different NHS esters of biotin, one of them presenting a medium length aliphatic chain, the other having a longer polyethylene glycol (PEG) chain (Fig.41). The LLO was used as received without further purification.

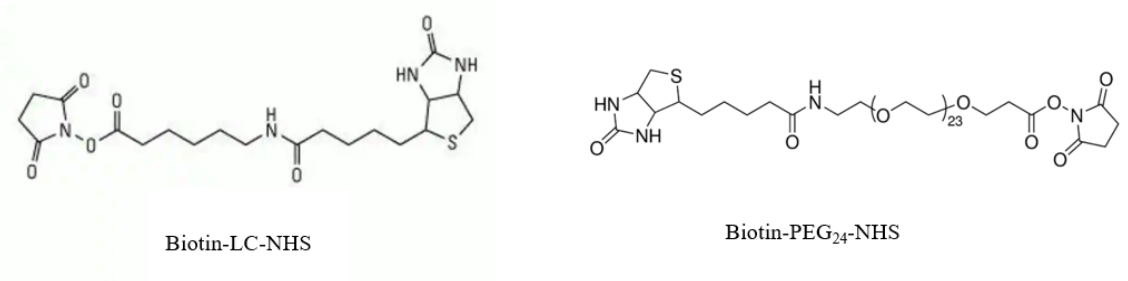

Figure 41. *Chemical structure of the two different Biotin derivates.*

A ten-fold molar excess of Biotin-NHS, solubilized in DMSO, was added to a 0.2mg/ml solution of LLO and was left to react for 30 minutes at 4°C, after which the reaction was quenched by adding an excess of tris base. The LLO-Biotin conjugate was then then purified by centrifugation aided size exclusion

chromatography using 7KDa MWCO desalting columns at 4°C, using the same storage buffer the LLO is preserved in as an eluent (50mM NaH_2PO_4, 0.5M NaCl, 2.7mM KCl, 1mM EDTA, 1mM DTT, 5%(v/v) glycerol). The final product concentration was then measured with the Bradford assay to verify that no loss of product occurred, and finally the LLO-Biotin was analysed with SDS-PAGE against pure LLO (Fig.42) although the difference in molecular weight is barely enough to see significant differences between the LLO with different functionalization.

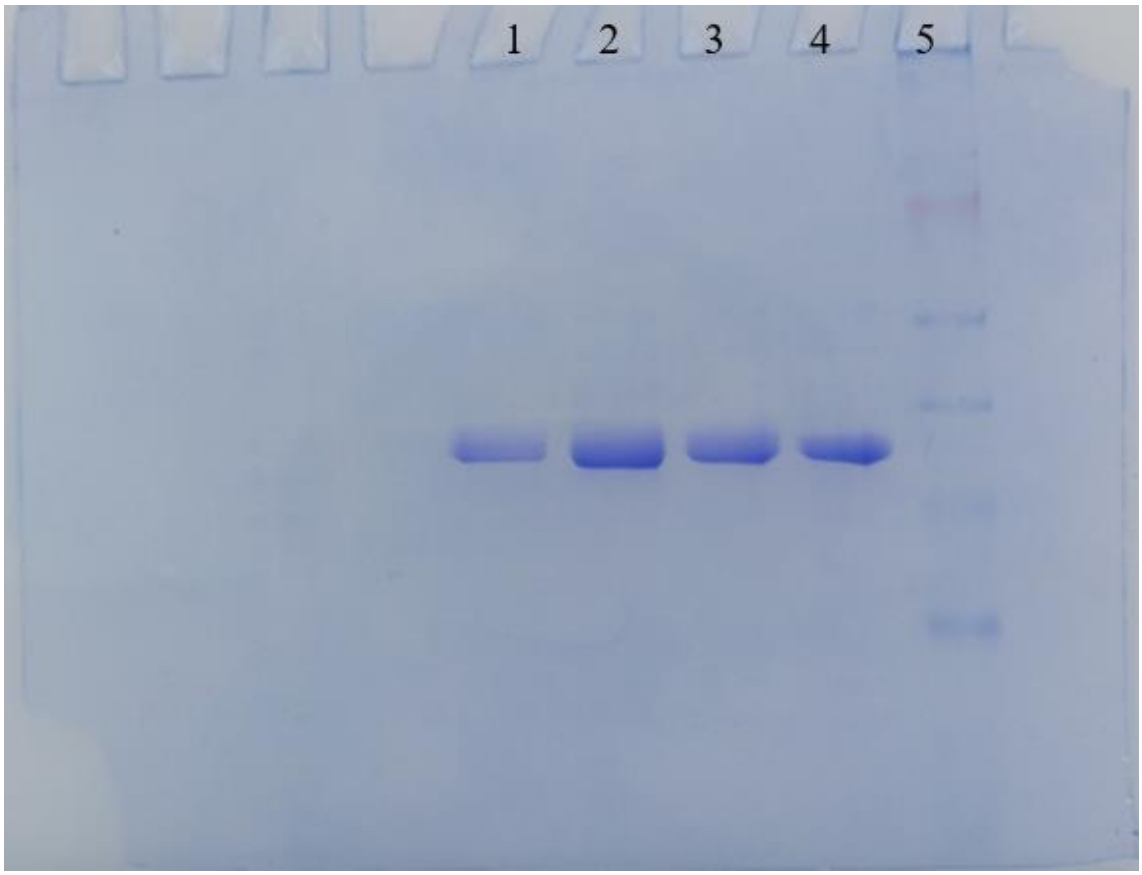

Figure 42. *SDS-PAGE gel (non-reducing conditions) for the different LLO-Biotin conjugates: LLO functionalized with Biotin-LC-NHS (lane 1), LLO functionalized with Biotin-PEG-NHS (lane 2-3), non-functionalized LLO (lane 4), MW standards (lane 5).*

To verify that the conjugation with biotin did not affect the recognition capability of the protein, a variation of the LLO assay was conducted (as introduced in the previous paragraph); instead of using a 96-well plate with LLO adsorbed on the surface, we used a 96-well plate coated in streptavidin to conduct the assay. In each

plate of the streptavidin coated plate, 100uL of 1mg/L solution of LLO-Biotin were added and incubated at 37°C for 1h; after washing the plate with the aid of an automated plate washing machine using 0.1% (v/v) Tween-20 PBS pH 7.4, positive and negative controls were added, serially diluting them from 100-fold up to a 4000-fold dilution with the control buffer solution made by Diatheva; in addition, also spiked serum and plasma positive controls were measured to assess how the matrix of the sample could make a difference in the assay; non-spiked serum and plasma samples were also tested as black samples to compare the spiked ones. The spiked serum and plasma controls were prepared adding to the buffer 1/100 (w/w) of human serum and plasma, before the addition of the positive control. The controls were incubated 1h at 37°C and then washed. Then 100 uL of a 1 mg/L solution of ruthenium labelled antibodies was added and left to incubate for 1h at 37°C and then washed. After that, HRP-conjugated anti-goat antibodies were added to each well, incubated and then washed. Lastly 100 uL of a commercial ABTS solution was added to each plate and left covered from light to let the color develop for 30 minutes. The results of the assay are reported in Fig.43; as can be seen the system manages to discriminate positive from negative control effectively, also when the biological matrix is present. Since the length of the carbon chain connecting the biotin to the LLO did not present any difference in behavior, we decided to use the longer chain for further experiments.

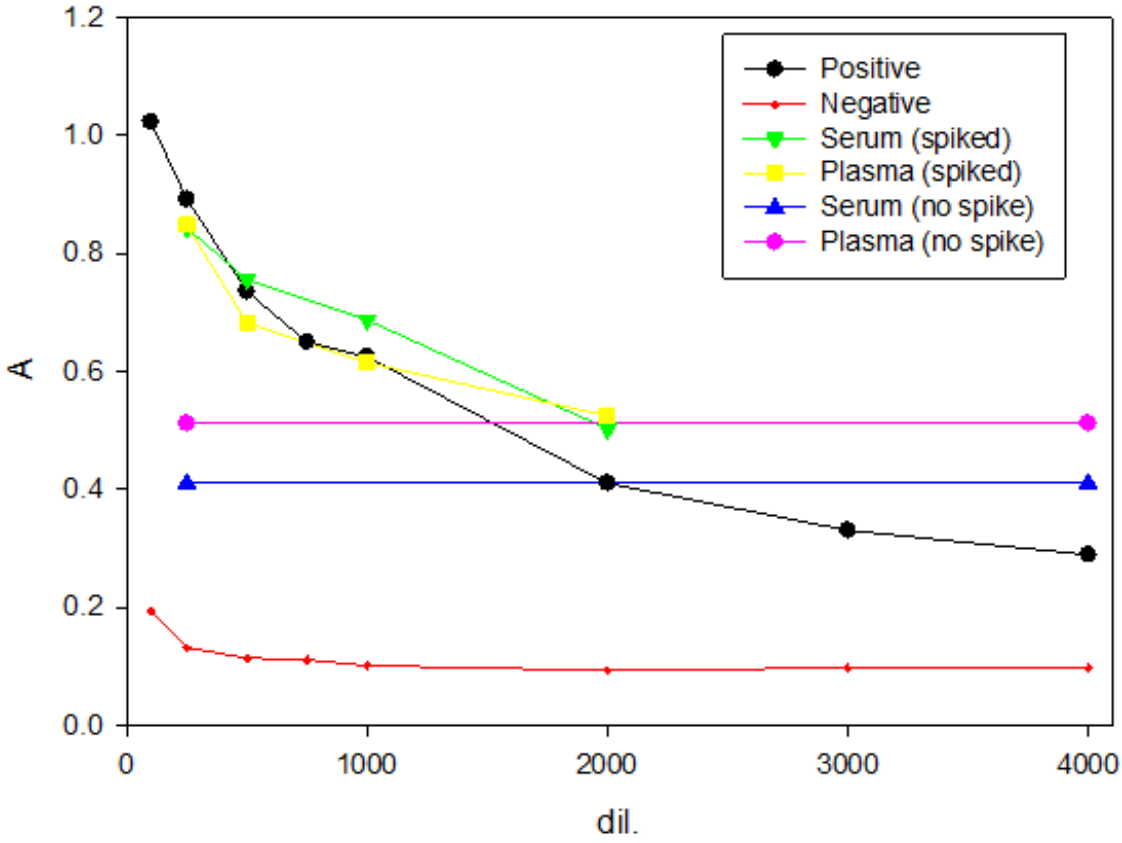

Figure 43. *Absorbance values (410nm) of the ELISA performed to evaluate the correct functioning of the LLO-Biotin and IgG-Ru.*

4.9 Chemiluminescence *Listeria* assay

As a first step, we investigated how the assay behaves by changing the reaction used to obtain the signal. The idea came from the fact that HRP-conjugated antibodies not only are able to react with chromogenic substrates, such as ABTS, to develop color, but for instance they can also catalyze the reaction between hydrogen peroxide (H_2O_2) and luminol, which is one of the most common chemiluminescence reagents couple, to generate luminescence. Since luminescence as a sensing mode can be more sensitive than absorbance, this simple change in substrates could lead to better performances for the same assay. In literature, just a single example of a chemiluminescence assay for the detection of listeria is reported[67], so we believed that this experiment could be an interesting addition to this work. The first step to accommodate the change in sensing mode

is to prepare adequate 96-well plates; typical ELISA plates are made of transparent polystyrene to be able to read an absorbance value through each well, while chemiluminescence plates are white and opaque to maximize light reflection to the detector. To prepare a plate for an assay, a 1 mg/L solution of LLO is prepared in 50 mM carbonate buffer at pH 8.5, and 100 µL of the solution are placed in each well of the plate; the plate is then covered and left to incubate over-night at 4°C. After the incubation the plate gets washed five times with PB-Tween; after that a blocking solution of 1% (w/w) BSA in PBS is added to the plate and left to incubate at 37°C for 30 minutes and washed again. The plate is then ready for incubation with positive and negative controls (we also tested some spiked serum and plasma samples), 1h at 37°C; the plate is then washed and incubated with HRP-conjugated antibodies again for 1h at 37°C. The ABST was substituted by a commercial H_2O_2-Luminol solution (Clarity ECL substrate-Biorad), which was added to each well of the plate; the solution is then left to react for 30 minutes to obtain the highest signal. The results of the experiment are shown in Fig.44.

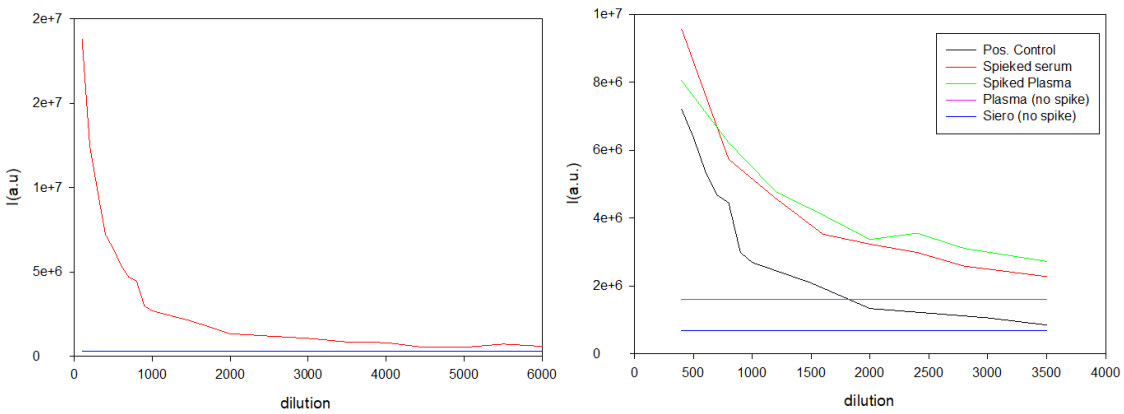

Figure 44. *Chemiluminescence listeria assay; on the right positive controls (red) and negative controls (blue). On the left, comparison between positive controls and spiked serum and plasma.*

The performance of the assay was good, being able to discriminate positive controls from negative up to 6000-fold dilution; also, for spiked serum and plasma samples the resolution was very good up to 3500-fold dilution (higher dilutions were not tested). The same type of experiment was also tried in fluorescence rather than chemiluminescence, substituting the HRP antibodies with our ruthenium labeled IgGs without the need of additional substrate. Unfortunately, in this case

we were not able to obtain satisfactory results, probably because of the low DOL of ruthenium per antibody, and the fact that $Ru(bpy)_3$ presents a relatively low brightness compared to the most common organic dyes.

4.10 ECL *Listeria* Bioassay

Once all the components of the assay were prepared and after verifying that they were working correctly we focused on developing a protocol for the preparation of samples for the ECL-bioassay. The protocol has been optimized during multiple experiments; in this paragraph the optimized protocol will be discussed, and the main optimizations made will be discussed after. The experimental setup and conditions of the ECL measurements is described in the appendix at paragraph 7.2.

First, the magnetic micro beads (Dynabeads, 2.8 µm, streptavidin coated - Invitrogen) are incubated with the LLO-biotin; in a single 2 ml vial, 320 µL of magnetic micro beads are added together with 4µg of LLO-biotin, and the volume is topped at 2ml with PBS pH 7.4, to obtain a 2 mg/L concentration of LLO-biotin. The mixture is then incubated at 37°C for 1h. It is important to give the solution a strong mix before the incubation to make sure that the MMB are well dispersed in the sample.

After incubation the MMB are washed using 0.1% (v/v) Tween-20 PBS pH 7.4 for three times. For each washing step the beads are separated from the solution, which gets discarded; then 1ml of PB-Tween is added to the beads, the sample gets vortexed to make sure the correct dispersion of the beads in the washing solution, and then the beads are separated again, and the cycle is repeated for three times.

The MMB's are then subjected to a blocking step. The blocking solution consists of a 1 % (w/w) solution of bovine serum albumin in PBS pH 7.4. 1 ml of blocking solution is added to the washed beads and incubated at 37°C for 30 minutes. After that the MMB are then washed again three times as described previously.

After the blocking step the MMB can get aliquoted for the addition of positive and negative controls. Since each ECL measurement requires 10 µL of MMB solution, and every measurement is repeated for three times, 40 µL of MMB are taken for each aliquot. The positive and negative controls are serially diluted using the control dilution buffer provided by Diatheva; to each aliquot of MMB 300 µL of control solution are added. The samples are then incubated at 37°C for 1h under mild agitation, and finally washed again as described before.

Lastly, to each sample, 300 µL of ruthenium labeled antibodies are added and the samples are incubated at 37°C for 1h. The last washing step is performed twice, for a total of 6 washes for each sample, to make sure that all the unbound labeled antibodies are removed. After washing the beads are dispersed in 40 µL of PBS and the sample is ready for measurement.

For each measurement, 10 µL of beads solution are deposited onto the electrode surface with the aid of a magnet placed behind the electrode, making sure that before the deposition the beads are well dispersed in the solution. The electrode is then placed inside the cell, together with the counter (Pt) and reference (Ag/AgCl) electrodes, the cell is then filled with TrPA buffered solution and placed in front of the PMT. For the measurements of ECL signal, each electrode is subjected to an applied potential, using the chronoamperometry technique, which consist in monitoring the current intensity generated by an applied potential as a function of time, while the PMT records the light emission from the electrode. Each electrode is subjected to a chronoamperometry cycle that lasts for 10 seconds; in the first 2 seconds the applied voltage is V = 0 and 8 seconds at 2.5 V. An example of a typical measurement is represented in Fig.45. Curves represented further in this chapter depict the maximum emission intensity as a function of analyte concentration.

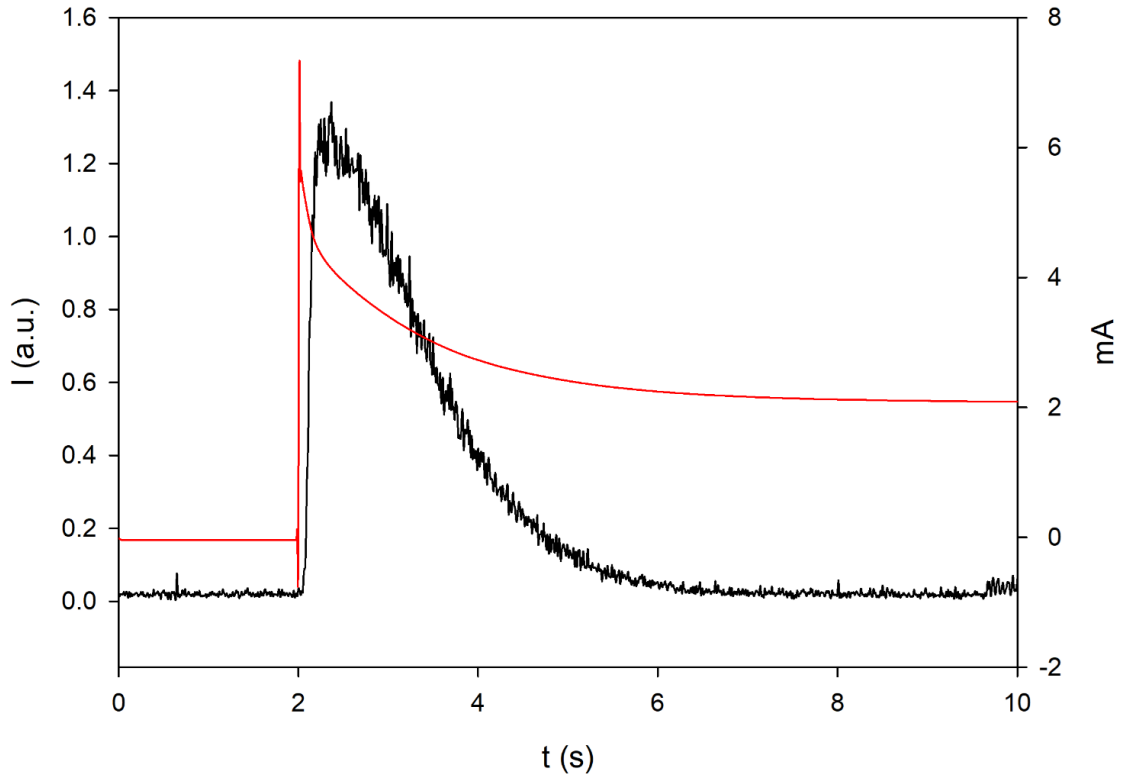

Figure 45. *Example of a typical ECL measurement. The red line represents the current, the black curve represents the light emission.*

As mentioned previously, the assay protocol was optimized in many aspects as it was developed. At the beginning of the project, one of the aims was to try to keep the sample preparation times as short as possible; to do so, one of the first approaches tried was to form the whole immunocomplex (LLO-Biotin + target IgG + secondary IgG) in a single step, to then capture the already formed immunocomplex with the streptavidin coated MMBs. A one step sample preparation would require no more than two hours total to have samples ready to measure. Unfortunately, this type of approach did not give consistent results, in particular the correlation between signal intensity and analyte concentration was inconsistent. This phenomenon can be seen in the graph in Fig.46.

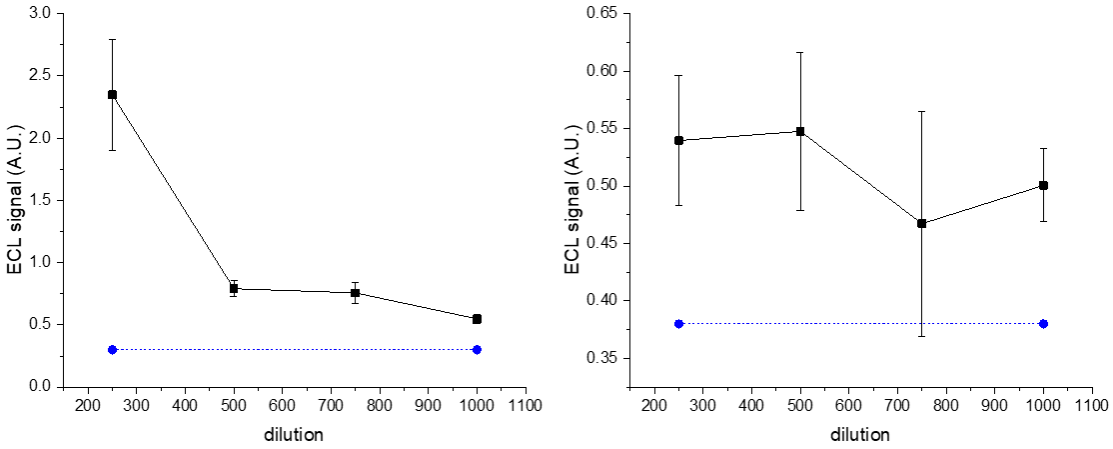

Figure 46. *Comparison between one-step sample preparation (right) and step-by-step assembly (left). Just positive controls (black) and white samples (blue) represented.*

Another fundamental step to optimize the assay was the inclusion of the blocking of the surface using bovine serum albumin. It is standard for assays such as ELISAs, to use a blocking solution after having adsorbed assay components on the plate (the LLO in our case) to avoid aspecific bindings of other components of the assay on the surface. Since we noticed that many of our assay samples that should have low ECL signals, were rather high in intensity, we hypothesized that without blocking the surface of the micro bead, after that the LLO-biotin has formed a complex with the streptavidin on the bead, in the space left unoccupied there could be aspecific adsorption of the ruthenium labeled antibody, thus leading to high signals. The most common blocking solutions for this type of purpose are made with bovine serum albumin (BSA) or nonfat-dried milk (NFDM), usually used in 1% (w/w) in buffered solution. Both types of blocking solutions were tested with our protocol, and both solutions had a positive impact on the outcome of the assay. In particular, the signals of negative control and white samples dropped significantly, with BSA having marginally better results. As can be observed in Fig.47, without a blocking step, the signals relative to negative controls (red line) are higher than positive, furthermore the white samples (in green), which should have the lowest signal among all the samples, are the highest. On the other hand, the signals of the samples prepared with blocking of the surface follow the proper trend.

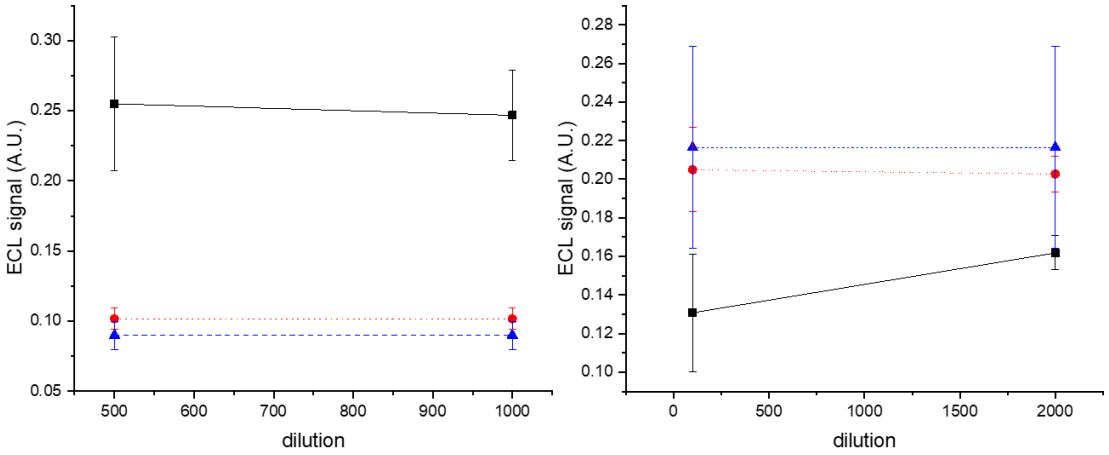

Figure 47. *Comparison between measurements performed without (right) and with BSA blocking (left). Positive controls (black), negative controls (red) and white samples (blue) are averaged from 3 measurements.*

Another important optimization of the assay was made comparing samples preparation volumes: two different approaches were investigated. The first approach – the same that has been previously described – consists in preparing replicates together, and then aliquoting the beads before the deposition on the electrode. This approach resulted in more consistent results between samples having the same dilution factor. The second approach consisted in preparing replicates of each concentration separately: instead of preparing each sample with 40 µL of MMB and doing three distinct measurement with said sample, for the second approach, 10 µL of MMB were used, and each one of the three replicates – of same dilution factor - were prepared separately and then measured, with all the volumes of the other components of the assay scaled down by a factor of 3 (100 µL). This approach was designed to better take into account the possible errors arising from sample preparation. The first major problem with this approach is related to volumes: when working with volumes smaller than 250-300 µL, the surface tension of water is too strong to allow the solution to be adequately homogenized during incubation, since the motion provided by the incubator is not sufficient to move the whole solution. We tried to tackle this problem by substituting the incubation step at 37°C, with a room temperature incubation under strong agitation, but the results obtained were worse, probably because the temperature for the incubation steps is a key factor in the formation of the

immunocomplex. The other problem related to this approach is the divergence between replicates of the same point measurement; although this problem is not absent when preparing replicates together, this erratic behavior was more evident for replicates prepared separately. This inconsistency between replicates can be seen in Fig.48.

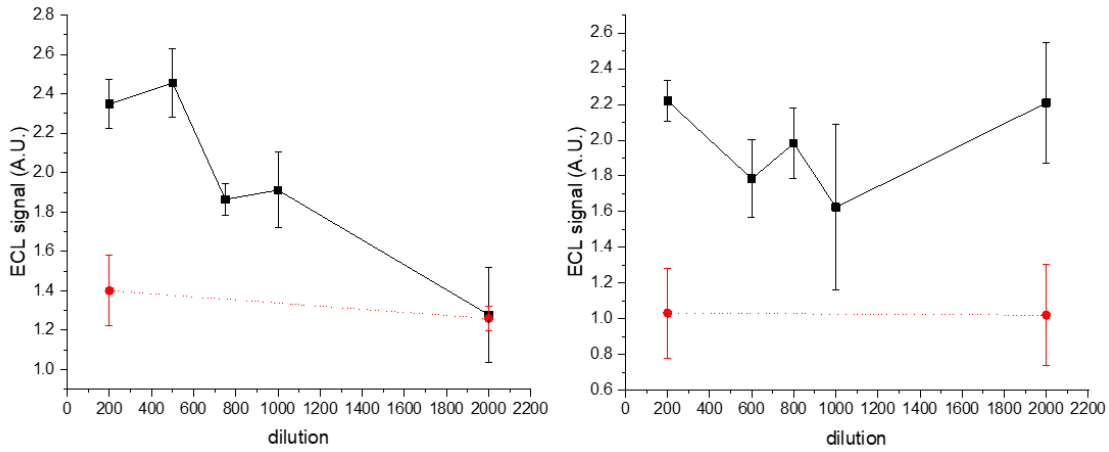

Figure 48. *Comparison of replicates prepared together (left) and separately (right); positive controls (black) and negative controls (red).*

It is important to note that both these experiments were performed without the blocking step, so the negative sample have high signals. It is still evident that the replicates prepared together (graph on the left) are more consistent, so we decide for the final protocol to prepare replicates together.

After managing to establish a protocol, the successive step for the development of the assay is to construct a calibration curve, so that we could switch to measuring real life samples. Ideally, we expected to obtain performances similar, if not superior, to the results obtained for the chemiluminescence assay. We were able to perform experiments where the assay was able to discriminate positive controls from negatives up to a dilution factor of 4000 (Fig.49).

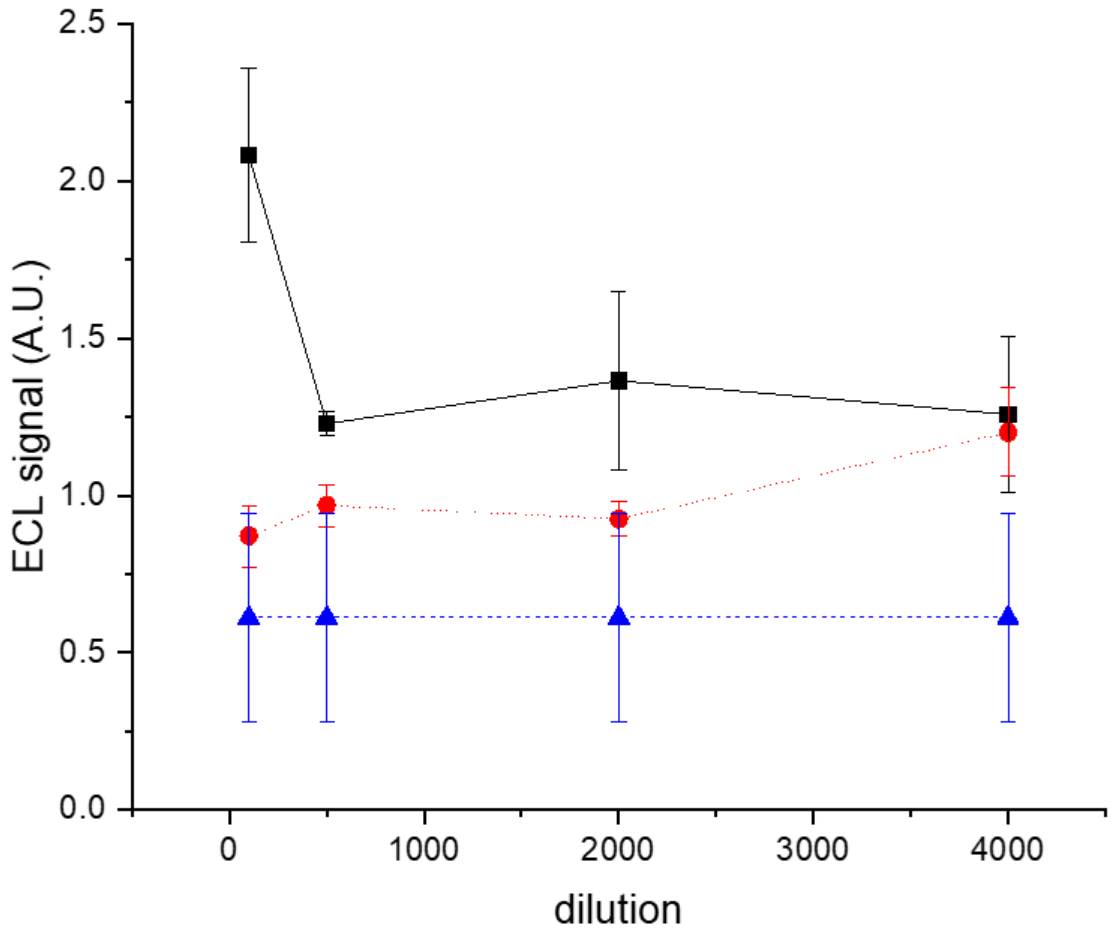

Figure 49. *Emission maxima curves: positive controls (black), negative controls (red), whites (blue) The results shown are the average of 3 replicates.*

As can be observed, the distinction between positive and negative control is clear, but other problems are still of relevance; the most important being the inconsistencies in the signals of the positive controls, that often were not coherent with the dilution factors. While some results indicate that the use of ECL for the detection of anti-listeria antibodies is promising, other optimizations should still be applied to the protocol to obtain the reliability needed for a screening test for this pathogen.

4.11 Conclusions and future perspectives

In this chapter the development of an ECL based immunoassay for the detection of anti-listeria antibodies has been discussed. The structure of the assay was

adopted from an existing ELISA developed by Diatheva s.r.l., modified and adapted to be used with ECL technology to obtain better performances. In general, this project aimed to evaluate the feasibility of translating already existing assay structures to a different sensing technique, with minimal modifications. Although many optimizations are still required for the ECL listeria assay to work properly, in general the experience gained from this project gave precious insights that will be fundamental to further optimizing this assay. Moreover, much insight has been gained regarding antibodies labeling, which then led us to investigate alternative ruthenium and iridium based luminophores that do not affect the stability of the antibodies. Future work will be focused on obtaining an efficient procedure that will lead to more repeatable output signals, and to determine the reasons behind the low correlation between concentration of analytes and ECL emission intensity. Once this objective is reached, and a good calibration curve is obtained, we will start testing real life samples. Another important step of developing an assay capable of sensing *Listeria monocytogenes* in environmental water samples, rather than clinical samples, will be to redesign the structure of the assay; by using an anti-LLO antibody, rather than LLO itself as a sensing element. Building an assay capable of sensing LLO at very low concentration would not only give the possibility of sensing *Listeria* in the environment, but also give more accurate results on the status of the infection in patients, since sensing for anti-LLO antibodies does not discriminate between current and past infections. Finally, once the assay is fully optimized, we will begin the construction of a prototype.

5. General conclusions

Water quality is a complex topic, but since water is one of, if not, the most important resources to sustain all life forms on the planet, it must be monitored with extreme care. Many standards of water quality exist in current legislations, and the vast number and heterogeneity of water pollutants can pose a significant challenge in the development of sensing platforms and methodologies capable of satisfying the required criteria.

In this context, optical-based chemosensors and techniques can offer many advantages to the water quality monitoring field. Among these advantages, one of the most important is the possibility to employ different signal transduction mechanisms. Colorimetric sensors can be easily and cheaply employed since the required instrumentation is cheap and sometimes not even needed if the color developed can be seen with the naked eye. Fluorescence based techniques can offer extremely high sensitivities. Phosphorescence offers the possibility to perform time-gated measurements to eliminate background noise. Combining different techniques, such as photochemistry and electrochemistry – as in the case of ECL – can enhance the already good performances of electrochemical or optical methods. Since many different types of chemicals – from small organic and inorganic molecules up to complex biological components such as toxins or pathogens – represent a concern for the environment, it is also important to develop efficient strategies to effectively and selectively bind the target analytes, often found in complex matrices. Coordination chemistry can be employed for small molecules such as metal cations or inorganic anions. Supramolecular chemistry can offer many advantages when sensing for more complex molecules such as pharmaceuticals. For the analysis of biological pollutants, employing nature-modeled recognition elements such as antibodies is by far the most efficient approach.

In this PhD thesis three different approaches to water pollutants sensing have been described, each one focusing on a distinct category of polluting chemicals. The first chapter of the thesis focuses on the sensing of nonsteroidal anti-inflammatory drugs (NSAIDs), the second chapter is about inorganic ionic species, while in the last chapter the detection of anti-listeria antibody was discussed.

In the first part of the thesis, two sets of supramolecular optical chemosensors developed for the sensing of NSAIDs were studied. The sensors' binding unit was based on squaramide moieties, able to interact with and bind the carboxylates of NSAIDs with strong hydrogen bonds. The first set of sensors possess a dansyl fluorescent unit for signal transduction. The interaction with NSAIDs strongly quenched the fluorescence of the probes. The binding unit of two of the four sensors (**L1-L2**) were closed macrocycles; these probes' response was affected only by ketoprofen while being unaffected by other analytes such as naproxen. Competition studies were conducted for these two probes with KET in the presence of sodium benzoate obtaining a shift in the titration curve; this clearly indicates that the sensors were sensitive, but not selective toward KET. **L1** ability to sense ketoprofen was maintained also at the solid state. The two other probes (**L3-L4**), possessing an open receptor unit, showed a different behavior. Their emission was quenched by KET, NAP and BZO, by varying degrees. This difference highlights the importance of a highly organized binding unit for improving selectivity and sensitivity of supramolecular chemosensors. The fact that each sensor had a unique response toward the analyte tested is an excellent starting point to develop differential sensing platforms for NSAIDs analysis.

The second set of sensors (**L6-L7**), also based on squaramide binding units, were synthesized with a 7-amminocoumarin as a signal transduction moiety. The two sensors were able to form complexes with NSAIDs as demonstrated by mass spectroscopy. The spectral properties of **L6** and **L7** were affected by the acidic character of the squaramide hydrogen. The deprotonated form of the ligands possesses different absorption characteristics from the protonated form. Moreover,

the emission quantum yield of the coumarin is drastically reduced by the conjugation with the squaramide, limiting the sensor spectral response to just colorimetric changes. Since the absorbance properties of **L6** and **L7** are affected similarly by both deprotonation and NSAIDs binding, the application of these two sensors is limited. More testing is required to improve the performances of **L6** and **L7** and to better understand the interaction with NSAIDs. The overall results obtained with this work are encouraging for the future development of differential sensing platforms for NSAIDs. The insight gained will also be helpful to develop similar sensing platforms for other emerging pollutants.

The second work described in this thesis focuses on the study of a set of luminescent Eu(III) metal complexes and their ability to sense different anionic species relevant for water quality monitoring. Five different Eu(III) complexes were chosen, each one possessing a unique luminescence quantum yield given by the overall net charge of the complex and by the number of N-H bonds in the coordination sphere of the europium, both affecting the luminescence of the Eu(III). The complexes present a coordinated water molecule to the Eu(III) center, which quenches the emission of the metal; displacement of this water molecule by an harder coordinating anion eliminates the O-H vibrational quenching, modulating the luminescence of the complex. The luminescence properties of the complex are also dependent on pH. This property can be exploited when employing these compounds in a sensor array, since pH is one of the most important parameters to be measured for water quality. The complexes were studied at different pH points. Importantly the pH range in which these complexes are most sensitive (6.5-8.5) is the most useful pH windows for water quality monitoring purposes.

The sensors were tested against a vast library of anionic species relevant to water quality. The complexes showed the highest affinity towards fluoride while being unaffected by other halides; the magnitude of the response towards fluoride was unique for each complex, with the 3+ charged complexes being the most effected.

Regarding the other analytes, the 3+ charged complexes showed affinity to a larger set of species when compared to the +1 and +2 charged complexes, particularly bicarbonate, sulphate, phosphate, cyanide and sulfite. This is particularly interesting because one or more unaffected compound in the final sensor array could be used to calibrate the other emission changes.

Other interesting results were obtained during the anion binding studies. Interaction with bicarbonate strongly affected not only the luminescence quantum yields of the 3+ charged complexes, but also the shape of the Eu(III) emission spectra; this result is especially useful for the final sensing platform to conduct ratiometric analysis confronting different emission peaks intensities. Moreover, it is interesting to note that the complexes showed affinity towards bicarbonate anions, while being totally unaffected by carboxylate baring small molecules such as acetate and benzoate.

More testing will be required to better understand the modes of interaction of the various anions tested with the complexes; hydration state (q) analysis will be required to verify the displacement of water by the anions. Obtaining co-crystals of the complexes with the various analytes for XDR analysis and resolving the structure would confirm not only the displacement of water, but also make clarity on the geometry changes caused by anion binding. UV-Vis titration will be needed to determine the dynamic range of the sensors towards each analyte; competition studies will be performed to evaluate the complex response of the sensors in a multi-analyte environment.

Overall, the results obtained are promising for the development of a differential sensing platform to be used for water quality monitoring.

The third and last part of this thesis describes the development of an ECL-based immunoassay for the sensing of anti-listeria antibodies. The work stems from a collaboration with Diatheva s.r.l.. The architecture of the immunoassay was taken

from a commercial ELISA test sold by Diatheva and modified to accommodate electrochemiluminescence as the analysis technique.

The general aim of the project was to evaluate the feasibility of employing an already existing assay architecture and, with minimal changes, translating it to use a different sensing technique, to enhance the assay performances. Promising results were obtained when translating the assay to chemiluminescence just by changing the color developing substrate (ABTS) typical of ELISA, with a commercial luminol-H_2O2 substrate.

Secondary antibody labeling with $Ru(bpy)_3^{2+}$, showed that over labeling of the antibodies can lead to instability issues. Precipitation of the antibodies was probably caused by electrostatic forces brought by the doubly charged ruthenium complex. This led us to investigate other luminophores to be employed for antibodies labelling; this optimization process is in progress.

Although many optimization steps are still required to obtain the desired performances of the assay, the insight gained from this work allowed us to better approach the study and development of sensors that make use of biological recognition elements such as antibodies or DNA.

In conclusion, this work was focused on the study and characterization of different sensing platforms, all based on optical methods, for the detection of water pollutants. The different systems all showed good performances, being capable of sensing the target analytes both in organic media (in the case of **L1-L7**) and in aqueous media (for **EuL1-EuL5** and the ECL-immunoassay). Above all, the results obtained in this PhD study show that optical chemosensors can offer a plethora of strategies to tackle water quality monitoring in its complexity. Therefore, this research represents one of many steps toward the development of new and efficient optical sensing platforms for water quality analysis.

6. Bibliography

1. Kumar, M., Khamis, K., Stevens, R., Hannah, D. M. & Bradley, C. In-situ optical water quality monitoring sensors—applications, challenges, and future opportunities. *Front. Water* **6**, (2024).

2. Markham, A. C. *A Brief History of Pollution*. (Routledge, London, 2019). doi:10.4324/9780429344879.

3. Kroehler, C. J. Potable Water Quality Standards and Regulations: A Historical and World Overview. in *Potable Water: Emerging Global Problems and Solutions* (eds. Younos, T. & Grady, C. A.) 1–36 (Springer International Publishing, Cham, 2014). doi:10.1007/978-3-319-06563-2_1.

4. Rajapaksha, P. *et al.* A review of methods for the detection of pathogenic microorganisms. *Analyst* **144**, 396–411 (2019).

5. Kruse, P. Review on water quality sensors. *J. Phys. Appl. Phys.* **51**, 203002 (2018).

6. Water Quality Parameters | IntechOpen. https://www.intechopen.com/chapters/69568.

7. Dulio, V. *et al.* Emerging pollutants in the EU: 10 years of NORMAN in support of environmental policies and regulations. *Environ. Sci. Eur.* **30**, 5 (2018).

8. Ramírez-Castillo, F. Y. *et al.* Waterborne Pathogens: Detection Methods and Challenges. *Pathogens* **4**, 307–334 (2015).

9. Leonard, P. *et al.* Advances in biosensors for detection of pathogens in food and water. *Enzyme Microb. Technol.* **32**, 3–13 (2003).

10. Cabral, J. P. S. Water Microbiology. Bacterial Pathogens and Water. *Int. J. Environ. Res. Public. Health* **7**, 3657–3703 (2010).

11. Anastasopoulos, P. & Akratos, C. S. A Review on Water Quality Indices. *Hydroecology Eng.* **2**, 10003 (2025).

12. Hulanicki, A., Glab, S. & Ingman, F. Chemical sensors: definitions and classification. *Pure Appl. Chem.* **63**, 1247–1250 (1991).

13. Lieberzeit, P. A. & Dickert, F. L. Chemosensors in environmental monitoring: challenges in ruggedness and selectivity. *Anal. Bioanal. Chem.* **393**, 467–472 (2009).

14. Molecular Probes, Chemosensors, and Nanosensors for Optical Detection of Biorelevant Molecules and Ions in Aqueous Media and Biofluids | Chemical Reviews. https://pubs.acs.org/doi/10.1021/acs.chemrev.1c00746.

15. (PDF) Optical Chemosensors: Principles, Chemistry, Strategies, and Applications. in *ResearchGate* doi:10.5772/intechopen.105968.

16. Fischer, E. Einfluss der Configuration auf die Wirkung der Enzyme. *Berichte Dtsch. Chem. Ges.* **27**, 2985–2993 (1894).

17. Lavigne, J. J. & Anslyn, E. V. Sensing A Paradigm Shift in the Field of Molecular Recognition: From Selective to Differential Receptors. *Angew. Chem. Int. Ed.* **40**, 3118–3130 (2001).

18. Stewart, S., Ivy, M. A. & Anslyn, E. V. The use of principal component analysis and discriminant analysis in differential sensing routines. *Chem. Soc. Rev.* **43**, 70–84 (2013).

19. Wong, S.-F. & Khor, S. M. State-of-the-art of differential sensing techniques in analytical sciences. *TrAC Trends Anal. Chem.* **114**, 108–125 (2019).

20. Krantz-Rülcker, C., Stenberg, M., Winquist, F. & Lundström, I. Electronic tongues for environmental monitoring based on sensor arrays and pattern recognition: a review. *Anal. Chim. Acta* **426**, 217–226 (2001).

21. Peng, G. *et al.* Diagnosing lung cancer in exhaled breath using gold nanoparticles. *Nat. Nanotechnol.* **4**, 669–673 (2009).

22. Bell, K. Y. *et al.* Emerging Pollutants. *Water Environ. Res.* **83**, 1906–1984 (2011).

23. Tyumina, E. A., Bazhutin, G. A., Cartagena Gómez, A. d. P. & Ivshina, I. B. Nonsteroidal Anti-inflammatory Drugs as Emerging Contaminants. *Microbiology* **89**, 148–163 (2020).

24. Castro-Pastrana, L. I., Palacios-Rosas, E., Toledo-Wall, M. L. & Cerro-López, M. Worldwide Occurrence, Detection, and Fate of Nonsteroidal Anti-inflammatory Drugs in Water. in *Non-Steroidal Anti-Inflammatory Drugs in Water: Emerging Contaminants and Ecological Impact* (ed. Gómez-Oliván, L. M.) 55–82 (Springer International Publishing, Cham, 2020). doi:10.1007/698_2020_542.

25. Świacka, K., Michnowska, A., Maculewicz, J., Caban, M. & Smolarz, K. Toxic effects of NSAIDs in non-target species: A review from the perspective of the aquatic environment. *Environ. Pollut.* **273**, 115891 (2021).

26. A robust and rapid liquid chromatography tandem mass spectrometric method for the quantitative analysis of 5-azacytidine - PubMed. https://pubmed.ncbi.nlm.nih.gov/26174363/.

27. Akdeniz, A., Mosca, L., Minami, T. & Anzenbacher, P. Sensing of enantiomeric excess in chiral carboxylic acids. *Chem. Commun.* **51**, 5770–5773 (2015).

28. Romano, G. M. *et al.* Polyamine receptors containing anthracene as fluorescent probes for ketoprofen in H2O/EtOH solution. *Chem. Commun.* **58**, 7022–7025 (2022).

29. Storer, R. I., Aciro, C. & Jones, L. H. Squaramides: physical properties, synthesis and applications. *Chem. Soc. Rev.* **40**, 2330–2346 (2011).

30. Marchetti, L. A., Kumawat, L. K., Mao, N., Stephens, J. C. & Elmes, R. B. P. The Versatility of Squaramides: From Supramolecular Chemistry to Chemical Biology. *Chem* **5**, 1398–1485 (2019).

31. Picci, G. *et al.* Anion-Responsive Fluorescent Supramolecular Gels. *Molecules* **27**, 1257 (2022).

32. Prohens, R. *et al.* Squaramido-based receptors: Molecular recognition of carboxylate anions in highly competitive media. *Tetrahedron Lett.* **39**, 1063–1066 (1998).

33. Picci, G., Montis, R., Lippolis, V. & Caltagirone, C. Squaramide-based receptors in anion supramolecular chemistry: insights into anion binding, sensing, transport and extraction. *Chem. Soc. Rev.* **53**, 3952–3975 (2024).

34. Picci, G. *et al.* Potentiometric Sensing of Nonsteroidal Painkillers by Acyclic Squaramide Ionophores. *ACS Sens.* **8**, 3225–3239 (2023).

35. Picci, G. *et al.* Fluorescent sensing of non-steroidal anti-inflammatory drugs naproxen and ketoprofen by dansylated squaramide-based receptors. *Org. Biomol. Chem.* **21**, 2968–2975 (2023).

36. Genovese, D., Cingolani, M., Rampazzo, E., Prodi, L. & Zaccheroni, N. Static quenching upon adduct formation: a treatment without shortcuts and approximations. *Chem. Soc. Rev.* **50**, 8414–8427 (2021).

37. Unusual Photophysical Properties of Coumarin-151 | The Journal of Physical Chemistry A. https://pubs.acs.org/doi/10.1021/jp003157m.

38. Mert, S. & Erdebil, Ö. Anion-Binding Properties of Aliphatic Symmetric Squaramide Receptors. *ACS Omega* **9**, 8333–8342 (2024).

39. Sofronov, O. O. & Bakker, H. J. Energy Relaxation and Structural Dynamics of Protons in Water/DMSO Mixtures. *J. Phys. Chem. B* **122**, 10005–10013 (2018).

40. Hibbert, D. B. & Thordarson, P. The death of the Job plot, transparency, open science and online tools, uncertainty estimation methods and other developments in supramolecular chemistry data analysis. *Chem. Commun.* **52**, 12792–12805 (2016).

41. Wolfbeis, O. S. Editorial: Probes, Sensors, and Labels: Why is Real Progress Slow? *Angew. Chem. Int. Ed.* **52**, 9864–9865 (2013).

42. The Development of a Continuous Intravascular Glucose Monitoring Sensor - Barry C. Crane, Nicholas P. Barwell, Palepu Gopal, Mannam Gopichand, Timothy Higgs, Tony D. James, Christopher M. Jones, Alasdair Mackenzie, Krishna Prasad Mulavisala, William Paterson, 2015. https://journals.sagepub.com/doi/10.1177/1932296815587937.

43. Silva, A. P. de, Vance, T. P., West, M. E. S. & Wright, G. D. Bright molecules with sense, logic, numeracy and utility. *Org. Biomol. Chem.* **6**, 2468–2480 (2008).

44. https://www.ijera.com/papers/Vol3_issue6/LV3620292035.pdf. https://www.ijera.com/papers/Vol3_issue6/LV3620292035.pdf.

45. Umali, A. P. & Anslyn, E. V. A general approach to differential sensing using synthetic molecular receptors. *Curr. Opin. Chem. Biol.* **14**, 685–692 (2010).

46. Parker, D. Luminescent lanthanide sensors for pH, *p*O2 and selected anions. *Coord. Chem. Rev.* **205**, 109–130 (2000).

47. Aletti, A. B., Gillen, D. M. & Gunnlaugsson, T. Luminescent/colorimetric probes and (chemo-) sensors for detecting anions based on transition and lanthanide ion receptor/binding complexes. *Coord. Chem. Rev.* **354**, 98–120 (2018).

48. Crease, A. E. & Legzdins, P. The Lewis acidity of organolanthanides. The interaction of cyclopenta-dienyl-lanthanides with some carbonyl and nitrosyl complexes. *J. Chem. Soc. Dalton Trans.* 1501–1507 (1973) doi:10.1039/DT9730001501.

49. Kovacs, D. *et al.* Coordination Environment-Controlled Photoinduced Electron Transfer Quenching in Luminescent Europium Complexes. *J. Am. Chem. Soc.* **142**, 13190–13200 (2020).

50. Supkowski, R. M. & Horrocks, W. DeW. On the determination of the number of water molecules, *q*, coordinated to europium(III) ions in solution from luminescence decay lifetimes. *Inorganica Chim. Acta* **340**, 44–48 (2002).

51. Kiraev, S. R. *et al.* Analysis of Anion Binding Effects on the Sensitized Luminescence of Macrocyclic Europium(III) Complexes. *Anal. Sens.* **2**, e202200015 (2022).

52. Shavaleev, N. M., Eliseeva, S. V., Scopelliti, R. & Bünzli, J.-C. G. Influence of Symmetry on the Luminescence and Radiative Lifetime of Nine-Coordinate Europium Complexes. *Inorg. Chem.* **54**, 9166–9173 (2015).

53. Bridou, L., Nielsen, L. G. & Sørensen, T. J. Using europium(III) complex of 1,4,7,10-tetraazacyclododecane-1,4,7-triacedic acid Eu.DO3A as a luminescent sensor for bicarbonate. *J. Rare Earths* **38**, 498–505 (2020).

54. Verani, M., Federigi, I., Donzelli, G., Cioni, L. & Carducci, A. Human adenoviruses as waterborne index pathogens and their use for Quantitative Microbial Risk Assessment. *Sci. Total Environ.* **651**, 1469–1475 (2019).

55. Ferreira, V., Wiedmann, M., Teixeira, P. & Stasiewicz, M. J. *Listeria monocytogenes* Persistence in Food-Associated Environments: Epidemiology, Strain Characteristics, and Implications for Public Health. *J. Food Prot.* **77**, 150–170 (2014).

56. Authority, E. F. S. & European Centre for Disease Prevention and Control (ECDC). The European Union summary report on trends and sources of zoonoses, zoonotic agents and food-borne outbreaks in 2014. *EFSA J.* **13**, 4329 (2015).

57. Arvanitidou, M., Papa, A., Constantinidis, T. C., Danielides, V. & Katsouyannopoulos, V. The occurrence of *Listeria* spp. and *Salmonella* spp. in surface waters. *Microbiol. Res.* **152**, 395–397 (1997).

58. Ryser, E. Listeria, listeriosis, and food safety. (1991).

59. Stea, E. C., Purdue, L. M., Jamieson, R. C., Yost, C. K. & Truelstrup Hansen, L. Comparison of the Prevalences and Diversities of Listeria Species and Listeria monocytogenes in an Urban and a Rural Agricultural Watershed. *Appl. Environ. Microbiol.* **81**, 3812–3822 (2015).

60. Hamon, M. A., Ribet, D., Stavru, F. & Cossart, P. Listeriolysin O: the Swiss army knife of *Listeria*. *Trends Microbiol.* **20**, 360–368 (2012).

61. Churchill, R. L. T., Lee, H. & Hall, J. C. Detection of Listeria monocytogenes and the toxin listeriolysin O in food. *J. Microbiol. Methods* **64**, 141–170 (2006).

62. Erdenlig, S., Ainsworth, A. J. & Austin, F. W. Production of Monoclonal Antibodies toListeria monocytogenes and Their Application To Determine the Virulence of Isolates from Channel Catfish. *Appl. Environ. Microbiol.* **65**, 2827–2832 (1999).

63. Darji, A. *et al.* Neutralizing monoclonal antibodies against listeriolysin: mapping of epitopes involved in pore formation. *Infect. Immun.* **64**, 2356–2358 (1996).

64. Forster, R. J., Bertoncello, P. & Keyes, T. E. Electrogenerated Chemiluminescence. *Annu. Rev. Anal. Chem.* **2**, 359–385 (2009).

65. Electrogenerated Chemiluminescence and Its Biorelated Applications | Chemical Reviews. https://pubs.acs.org/doi/10.1021/cr068083a.

66. Blancher, C. & Jones, A. SDS -PAGE and Western Blotting Techniques. in *Metastasis Research Protocols: Volume I: Analysis of Cells and Tissues* (eds. Brooks, S. A. & Schumacher, U.) 145–162 (Humana Press, Totowa, NJ, 2001). doi:10.1385/1-59259-136-1:145.

67. Zhang, Y., Cui, G., Meng, Y., Wang, Y. & Hun, X. Chemiluminescence assay for based on Cu/Co/Ni ternary nanocatalyst coupled with penicillin as generic capturing agent. *Luminescence* **36**, 11–19 (2021).

68. Montalti, M., Credi, A., Prodi, L. & Gandolfi, M. T. *Handbook of Photochemistry*. (CRC Press, Boca Raton, 2006). doi:10.1201/9781420015195.

69. *Principles of Fluorescence Spectroscopy*. (Springer US, Boston, MA, 2006). doi:10.1007/978-0-387-46312-4.

70. Electrogenerated chemiluminescence of bipyridine and phenanthroline complexes of osmium - ScienceDirect. https://www.sciencedirect.com/science/article/abs/pii/S0022072884803678?via%3Dihub.

71. Hesari, M. & Ding, Z. Review—Electrogenerated Chemiluminescence: Light Years Ahead. *J. Electrochem. Soc.* **163**, H3116 (2015).

72. Electrogenerated Chemiluminescence and Its Biorelated Applications | Chemical Reviews. https://pubs.acs.org/doi/10.1021/cr068083a.

7. APPENDIX

7.1 Principle of photophysics

7.1.1 Excited electronic state-Jablonski diagram

Electromagnetic radiation and matter can interact together in different ways. The field of photochemistry is interested in the processes that happen when a photon gets absorbed by a chemical species, and its energy (hv) is capable of promoting an electron into higher energy orbitals. The species from its ground state (A) turns into an excited state species (A*) which possesses a different electronic configuration, leading to such different physiochemical properties that A and A* can be considered totally different chemical species.

$$A + h\nu \rightarrow A^* \qquad (Eq.3)$$

To promote the formation of an excited state species, the energy of the absorbed photon (hv) must correspond exactly to the energy gap between the ground state and the excited state. Absorption electronic transition are fast processes that occur in the femtosecond time scale (10^{-15}s, Frank-Condon principle), and they create transient species capable of decay in different ways, shown in the Jablonsky diagram (Fig.50).

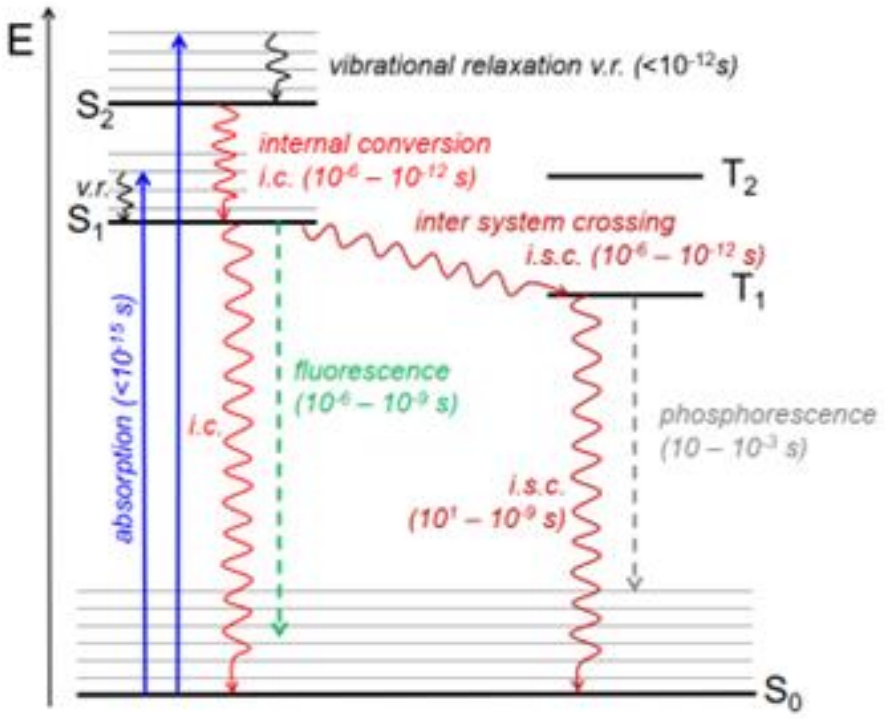

Figure 50. *General Jablonsky diagram for a simple organic molecule.*

The Jablonsky visually describes the electronic configuration and the possible transition of a chemical species. In this general diagram the thicker horizontal lines represent electronic states, which can be differentiated in singlet electronic states (S_0 is the ground state, S_1 and S_2, the first -lowest energy- and second singlet excited state) and triplets (T_1 and T_2, the first and second triplet excited states) according to their spin multiplicity. This distinction between single and triplet state is important because electronic transitions between different spin states are partially not allowed. The thinner lines represent the vibrational levels of the electronic state. The vertical lines represent electronic transitions between levels: the blue straight lines represent the absorption of energy, the undulated red lines represent non-radiative (no light emission) deactivation pathways where the energy gets dissipated as vibrational energy that generates heat, while the straight dashed lines are for radiative deactivation pathways, where excess energy gets released as light emission (luminescence). After absorption of energy, an excited vibration level of an electronic excited state (S_1 or S_2, according to the energy of the photon) is reached, the molecule then goes rapidly ($< 10^{-12}$ s) to the ground

vibrational level of that excited state with a vibrational relaxation. Afterwards, if S_2 is the reached excited state, an internal conversion occurs, passing from the ground vibrational level of S_2 to the isoenergetic vibrational level of S_1 (< 10^{-12} s), where another vibrational relaxation is then observed toward the ground vibrational state of S_1; from S_1 vibrational ground state the molecule can deactivate following two main paths, radiative or non-radiative.

Following the non-radiative deactivation path, the energy gets released as vibrational energy generating heat. In the process occurs between two excited states with the same spin-multiplicity this process is called internal conversion (IC, 10^{-12}-10^{-6} s), while if between different spin-multiplicity states the process is referred to as inter-system crossing (ISC, 10^{-12}-10^{-6} s from S_1 to T_1, 10^{-9}-10 s from T_1 to S_0).

Radiative deactivation processes involve the emission of energy as light (emission of a photon); if the transition happens between states with the same spin the light emission is called fluorescence, while phosphorescence happens when the transition is between different spin multiplicity states.

Similarly to S_1, T_1 can deactivate to S_0 by radiative deactivation (phosphorescence, 10^{-4}-10^{2} s) or by non-radiative deactivation (intersystem crossing, 10^{-3}-10 s, and successive vibrational relaxation to S_0). Long-lived states such as T_1 can undergo photochemical reactions, for example with oxygen, producing other chemical species. Since the time scale to decay to S_1 and T_1 are shorter than that necessary to pass from S_1 and T_1 to S_0, only the lowest energetic states of each spin multiplicity (that is S_1 and T_1) live enough to undergo luminescence (Kasha's rule) or photochemical reactions.[68]

7.1.2 Energy transfer processes

The term "electronic excitation energy transfer" sometimes called just "energy transfer" (ET) is used to indicate the process in which an excited molecule of a

donor D* decays to its ground state with a simultaneous transfer of excitation energy to an acceptor molecule in its ground state A, with the formation of the excited state A*.

$$D^* + A \rightarrow D + A^* \qquad (Eq.4)$$

This phenomenon is easily observable by exciting the donor D in a spectral region where the acceptor A does not absorb light: if energy transfer occurs, the emission of D* gets quenched while the emission of A* can be observed; this phenomenon is referred to as "sensitized emission". Energy transfer processes can occur between two different molecules of the same energy species, in which case is called homo-energy transfer. It is also possible to observe intramolecular energy transfer in the case of (super)molecules containing both a donor and an acceptor part separate by a linking moiety L.

$$D^* - L - A \rightarrow D - L - A^* \qquad (Eq.5)$$

Energy transfer can occur following two different mechanisms: radiative and non-radiative. The radiative ET, often referred to as "trivial energy transfer" does not require direct interaction between A and D and it's mediated by the electromagnetic field produced by the photons emitted by D*, which can be absorbed by A, provided that the energy of the photon emitted by D is adequate to promote A to A*. The mechanism consists of two distinct processes: light emission from D* and light absorption from A.

$$D^* \rightarrow D + h\nu' \qquad (Eq.6)$$

$$A + h\nu' \rightarrow A^* \qquad (Eq.7)$$

The probability of the energy transfer, defined as the probability of absorption by A of a photon emitted by D*, is correlated with the overlap between the emission spectrum of D and the absorption one of A. In particular, a relation stands between the probability of absorption with the overlap integral J:

$$J = \int_{\infty}^{0} F_D\,(\lambda)\varepsilon_A(\lambda)\lambda^4 d\lambda \qquad (Eq.8)$$

Where F_D is the normalized emission spectrum of D and ε_A is the absorption spectrum of A. So, if J increases, the probability of radiative ET linearly increases. The probability also increases with the concentration of A, it is directly proportional to the optical path length and inversely proportional to the luminescence quantum yield of D. It is also necessary that the transition of absorption in the acceptor is spin-allowed so that the radiative energy transfer can occur: thus singlet(D*)-singlet(A*) and triplet(D*)-singlet(A*) transfers are allowed, while singlet(D*)-triplet(A*) and triplet(D*)-triplet (A*) transfers are not allowed.

Non radiative ET processes, on the other hand, require an intermolecular interaction between A and D, mediated by the electromagnetic field. In this case, for ET to occur, A and D must be in resonance condition, involving isoenergetic non-radiative transition between D* and A. The theoretical description of this process reveals that two different terms play a role: one is a Columbic term (Foster mechanism) the other is an exchange term (Dexter mechanism). (Fig.51)

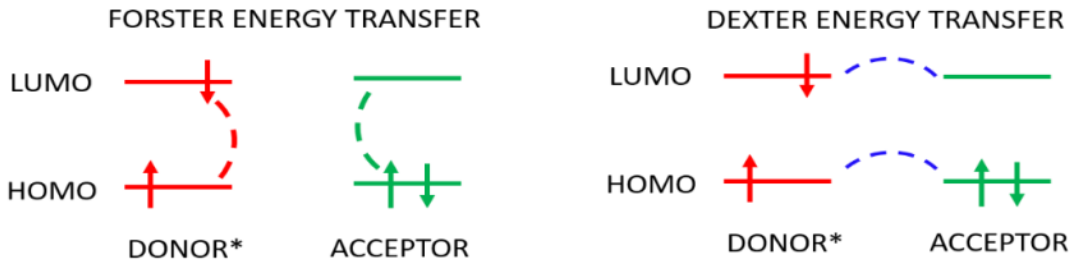

Figure 51. *Energy transfer via Coulombic mechanism (left) and with exchange mechanism (right).*

The Coulombic term arises from the coupling of the electronic transition moments of electric dipole of the transitions D*→D and A→A*. This kind of energy transfer is governed by the Förster's equation, which correlates the energy transfer kinetic constant (k_{ET}) with the distance between the donor and the acceptor (R_{DA}):

$$k_{ET} = \frac{1}{\tau_D}\frac{{R_0}^6}{{R_{DA}}^6} \qquad (Eq.9)$$

Where τ_D is the lifetime of the donor in the absence of the acceptor. and R_0 is the Förster distance. The Förster distance is the distance between the donor and the acceptor at which the energy transfer rate (k_{ET}) is equal to the decay rate of the donor in the absence of the acceptor ($k_{ET} = 1/\tau_D$). At this distance half of the molecules of D decay via energy transfer. The Förster distance is directly proportional to the overlap integral J, according to the relation:

$$R_0{}^6 = 2.302 \frac{9000\chi^2\Phi_D}{n^4 N_A 128\pi^5} J \qquad (Eq.10)$$

Where χ is the orientational factor which describes the relative orientation of the electric dipole moment of D and A (it is assumed to be equal to 2/3 in the case of freely rotating D and A), Φ_D is the fluorescence quantum yield of D in the absence of A, n is the refractive index of the solvent, and N_A is the Avogadro's constant. Typically, R_0 is about 3-7 nm. The efficiency of the energy transfer (η) is defined as:

$$\eta = \frac{k_{ET}}{k_{ET} + k_D} = \frac{R_0{}^6}{R_0{}^6 + R_{DA}{}^6} \qquad (Eq.11)$$

This relation reveals that when $R_{DA} = R_0$, the efficiency of the energy transfer is equal to 0.5. Experimentally, the efficiency of the energy transfer can be obtained from the fluorescence quantum yield of D in the presence of A (Φ_{DA}) and in its absence (Φ_D), or from lifetimes in these two conditions (τ_{DA} and τ_D):

$$\eta = 1 - \frac{\Phi_A}{\Phi_D} \qquad (Eq.12)$$

$$\eta = 1 - \frac{\tau_{DA}}{\tau_D} \qquad (Eq.13)$$

The Förster energy transfer is generally allowed if the transition does not involve spin variations of the donor and the acceptor. If the spin of D and A change, Dexter energy transfer dominates. In this case, the process requires a simultaneous double electronic exchange involving the LUMO of D and the HOMO of A. For this

reason, this kind of energy transfer is a shortrange interaction, becoming important only when R_{DA} is ≤ 5 Å. In the Dexter model, the kinetic constant for the exchange mechanism (k_{ET}^{ex}) decays exponentially with R_{DA}:

$$k_{ET}{}^{ex} = \frac{2\pi}{\hbar} K J^{ex} e^{\frac{2R_{DA}}{L}} \qquad (Eq.14)$$

Where K is a factor related to the specific orbitalic interaction, J^{ex} is the normalized overlap integral, and L is an average Van der Waals radius which simulates molecular dimensions.[69]

7.1.3 Electronic absorption spectra

To quantify the amount of light absorbed by a chemical species, absorbance (A) is often used. A is defined by the ratio between the intensity of incident light (I_0) and the intensity of the transmitted light (I_t) following the relation:

$$A = log_{10} \frac{I_0}{I_t} \qquad (Eq.15)$$

Absorbance is linearly correlated to the concentration of the species absorbing light; this relation is expressed by the Lambert-Beer law.

$$A = \varepsilon bc \qquad (Eq.16)$$

Where ε is the molar extinction coefficient $(mol/L)^{-1}cm^{-1}$, b is the optical path of the sample (for a typical cuvette, b = 1 cm), and c is the dye concentration express in mol/L.

The instrument used to obtain absorption spectra is called a spectrophotometer. There are two important types of spectrophotometers. A dual beam spectrophotometer measures the ratio of the light intensity of two different light rays, the one coming from the sample and the one coming from the reference, while a single beam spectrophotometer measures an absolute light intensity, that is only the beam coming from the sample. Consequently, a double beam

spectrophotometer allows to make more stable, precise, and fast measurements compared to a single beam spectrophotometer, in which the execution of the measurements relating to the reference and the sample at different times involves less rapidity and less precision for the error relating to possible fluctuations in the light source. A generic dual beam spectrophotometer is shown in Fig.52:

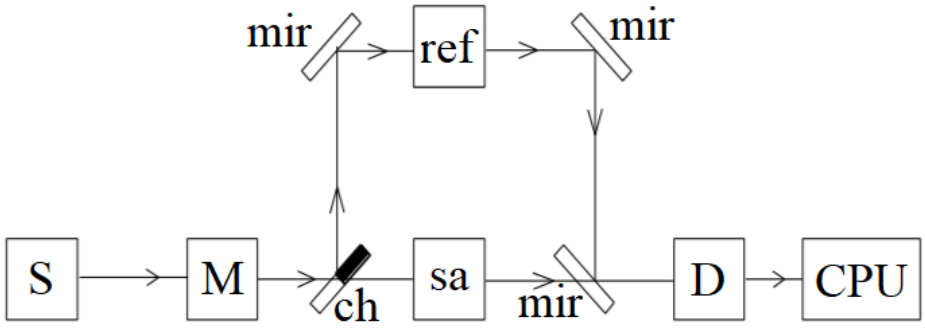

Figure 52. *Block diagram of a spectrophotometer.*

It consists of:

- A light source (S) which produces polychromatic radiation in a certain range of wavelengths: tungsten filament lamp for visible and near infrared light (350-2200 nm), deuterium lamp for ultraviolet radiation (160-380 nm), xenon lamp covering the whole UV-vis range (190-1100 nm);
- A wavelength selector or monochromator (M) that solves the polychromatic beam in radiation at a determined wavelength.
- A holder for the introduction of the sample cuvette (sa) and a holder for the reference cuvette (ref).
- A circular rotating mirror or chopper (ch) – which presents a transparent half and a reflecting half – that reflects light alternately on the sample and on the reference.
- Several mirrors (mir) before and after the holders to direct the beams.
- A detector (D), usually a photomultiplier, composed of (i) a photoelectric cell, which can transform the light signal into an electrical signal, (ii) a

system for amplifying the electric current emitted by the photocell and (iii) a galvanometer for measuring this current.

- A computer for recording and viewing the results.

In this thesis, for the acquisition of electronic absorption spectra, a double beam spectrophotometer UV/Vis Perkin Elmer Lambda 850+ was used. All the spectroscopic measurements (absorbance, emission, TCSPC) were conducted using spectroscopy-grade solvents purchased from Merck, and using 1 cm optical path quartz cuvettes purchased from Hellma.

7.1.4 Emission spectroscopy

The emitted light intensity depends on the absorption coefficient (so related to absorbance) and the emission quantum yield of the sample, together with the intensity of incident light:

$$I_{em} = k\Phi I_0(1 - 10^A) \qquad (Eq. 17)$$

Where I_{em} and I_0 represent the intensity of the fluorescent and incident radiation respectively, k is an instrumental paramether, Φ is the fluorescence quantum yield of the sample, and A is the absorbance. Therefore, fluorescence intensity increases as the absorbance and the concentration of the analysed substance increase. This dependence is not linear, but if the analyte concentration is sufficiently low to obtain an absorbance lower than 0.1, the relationship between fluorescence intensity, absorbance and concentration can be considered as a linear approximation:

$$if\ A \leq 0.1\ \rightarrow\ I_{em} \propto A \propto c \qquad (Eq. 18)$$

The acquisition of emission and excitation spectra can be performed using a spectrofluorimeter. For collecting an emission spectrum, the excitation wavelength is kept fixed, and a scan of the emission monochromator is performed. For the registration of an excitation spectrum, on the contrary, the emission wavelength is

kept fixed, and scanning is performed along the excitation monochromator. The signal acquired through excitation spectrum acquisition correlates directly with the probability, upon sending a photon of appropriate wavelength, of populating the excited state responsible for the observed emission.

It is important to note that, contrary to spectrophotometers, in which the recorded absorbance is expressed on an absolute scale, as the ratio between transmitted light and incident light, spectrofluorometers determine the emission intensity only on an arbitrary scale, as it depends on the instrument and the measurement conditions. This implies that the signal detected for the same sample varies from instrument to instrument and from measurement to measurement, and that the numerical value of the emission intensity has no physical meaning. If a comparison between two different emission phenomena is needed, quantum yields are more suited, since they are absolute quantities.

Depending on the complexity and configuration of the equipment, spectrofluorimeters can be distinguished in various types. A generic spectrometer with 90° configuration is shown in Fig.53:

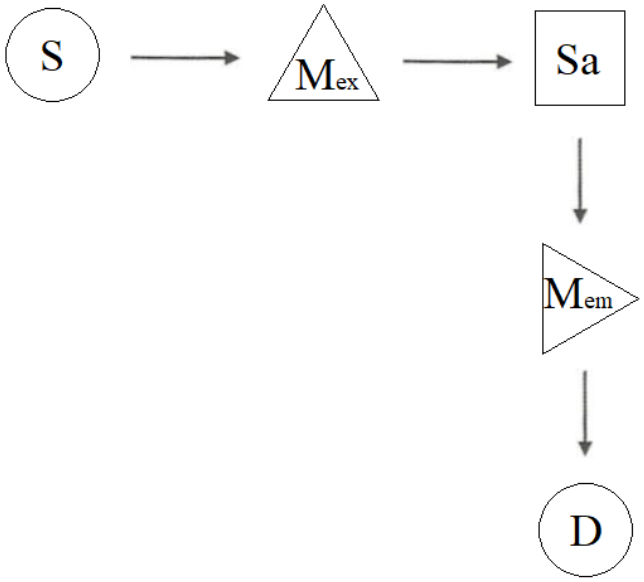

Figure 53. *Block diagram of a spectrofluorimeter.*

It consists of:

- A light source (S) that produces exciting energy in the form of polychromatic radiation, generally, xenon lamp, whose spectrum is continuous from 250 to over 1000 nm. The sources can be both continuous and pulsed, depending on the needs.
- An excitation monochromator (M_{ex}) that solves the polychromatic beam of the source in radiation at a determined wavelength.
- A holder for the sample (Sa).
- An emission or monochromator (M_{em}) which solves the polychromatic beam emitted by the sample in radiation at a determined wavelength. The monochromator is positioned commonly, at 90° with respect to the direction of the excited light to avoid receiving the excitation light that passes through the sample.
- A detector (D), usually a photomultiplier, composed of (i) a photoelectric cell that can transform the light signal into an electrical signal, (ii) a system for amplifying the electric current emitted by the photocell and (iii) a galvanometer for measuring this current
- A computer for recording and viewing the results.

In this thesis, the registration of the emission and excitation spectra were performed using a spectrofluorimeter Perkin Elmer LS55, a spectrofluorimeter Horiba Fluoromax-4P and a spectrofluorimeter Edinburgh Instruments FLS1000.

7.1.5 Luminescence quantum yields

The luminescence quantum yield (Φ) of a sample is defined as the ratio between the number of emitted photons and the number of photons absorbed by a species at the same excitation wavelength:

$$\Phi = \frac{number\ of\ emitted\ photons}{number\ of\ absorbed\ photons} \qquad (Eq.19)$$

A fast and useful method to determine the luminescence quantum yield is to compare the emission of a sample with a reference species having a known quantum yield, upon excitation of both reference and sample at the same wavelength. The chosen reference should emit in the same spectral region of the sample and the emission spectra must be recorded in the same experimental conditions. For the assessment of Φ_{PL} we adopted the following experimental procedure: the absorption spectra of the sample and of the reference were registered and, when possible, isoabsorbing points were used as excitation wavelength for the registration of emission spectra. Then, to obtain the luminescence quantum yield the following equation can be used:

$$\Phi = \Phi_R \frac{I_x}{I_R} \frac{A_R}{A_x} \frac{{n_x}^2}{{n_R}^2} \qquad (Eq. 20)$$

Where Φ_R is the quantum yield of the reference, I_R and I_X are the emission intensities of the reference and the sample, respectively; A_R and A_X are the absorbance at the excitation wavelength of the reference and the sample; n_R and n_X are the refractive index of the solvents.

7.1.6 Excited state lifetime decay measurement-TCSPC and MCS

Emission lifetimes can be measured with a time-correlated single-photon counting. This kind of instrument is based on the probability that a single photon emitted by a luminescent sample is collected by a proper high-sensitive detector. This probability is statistically correlated with the variation over time of the concentration of the excited states in the sample.

$$[A^*] = [A^*]_0 \, e^{-\sum_i k_i \, t} \qquad (Eq. 21)$$

Where [A*] is the concentration of the excited states at a certain time t, $[A^*]_0$ is the concentration of the excited states at the initial time (t = 0), and k_i are the kinetic constants of the all the i deactivation pathways that are involved in the relaxation

of the excited states. The instrumentation of a time-correlated single-photon counting (TCSPC) is schematized in Fig.54.

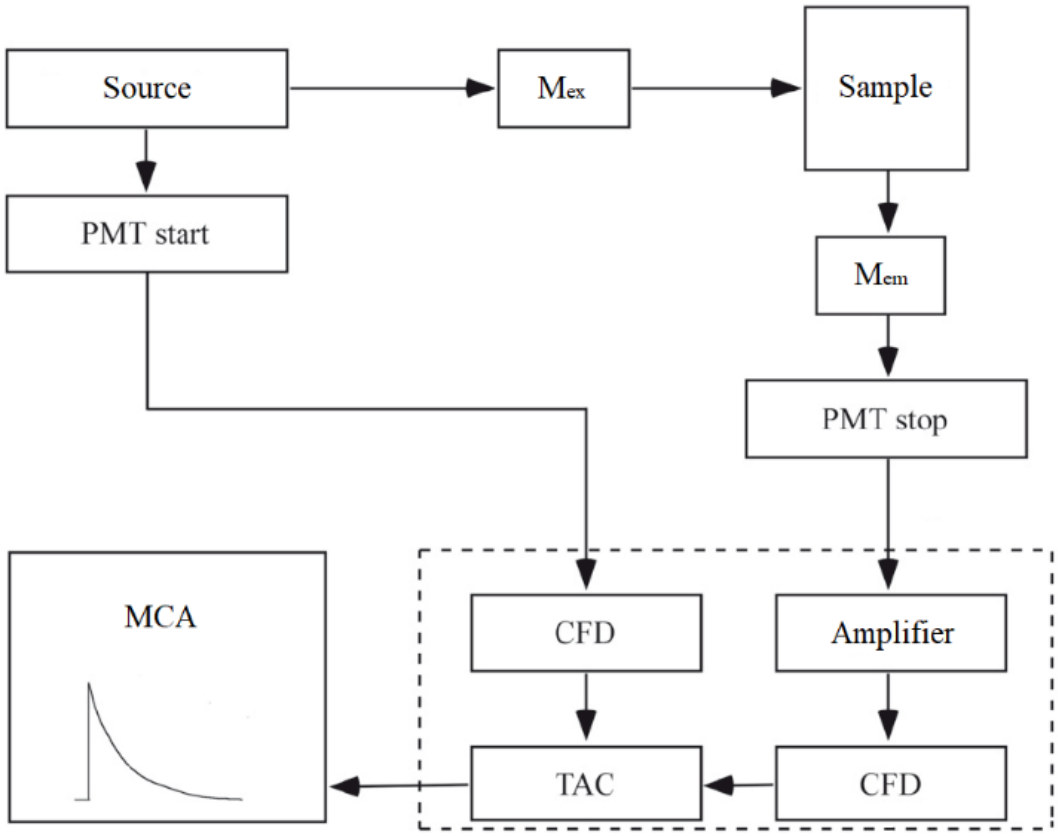

Figure 54. *Block diagram of a time-correlated single-photon counting instrument.*

The light sources are high-frequency pulsed lasers or pulsed lamps, depending on the magnitude of the lifetime measured. PMT_{start} is the start photomultiplier, which receives the photons emitted by the source, causing the starting of the multichannel analyser (MCA). PMT_{stop} is the stop photomultiplier, which stops the MCA once it receives a photon from the sample, guaranteeing the collection of a single photon. The CFD is a constant fraction discriminator, which eliminates light interferences, while TAC is a time-to-amplitude converter, which can convert into time the value of a voltage – which increases linearly with time – that is reached during the delay between the arrival of the photon emitted by the source and the arrival of the photon emitted by the sample. By measuring this delay and by accumulating these signals in various channels according to their delays, the emission decay curve can be created and thus the lifetime can be calculated. The

instrument presents a measuring range that can extends over lifetimes from 350ps to 1 μs and the error associated with the lifetime is approximately ± 10%. This fluorimeter setup can be also used to measure longer lifetimes (from 1 μs and over) using Multi-Channel Scaling (MCS) technique; the only difference is that rather than collecting a single photon per cycle, multiple are collected to reconstruct the full decay.

Fluorescence lifetime measurements were performed using a spectrofluorimeter Edinburgh Analytical Instruments FLS920, equipped with a time-correlated single-photon counting device, which is able to measure lifetimes in a range between 300 ps and 30 μs. Phosphorescence lifetime decay measurement were performed on an Edinburgh Analytical Instruments FLS1000 equipped with a μF pulsed xenon lamp. The fitting procedure for determining the emission lifetimes has been carried out with the software distributed with the instruments, using the default algorithm.

7.2 Electrochemiluminescence (ECL) technique

Electrochemiluminescence is a light emission phenomenon in which luminescence is generated by the reaction of chemical species, that can undergo high energy electron transfer reaction to form excited state luminescent species. ECL essentially implies the emission of light by species formed on an electrode surface. In most ECL reactions four steps are generally involved (graphically represented in Fig.55)[70]:

1. Redox reactions on the electrode surface
2. Homogeneous chemical reaction
3. Excited state species formation
4. Light emission

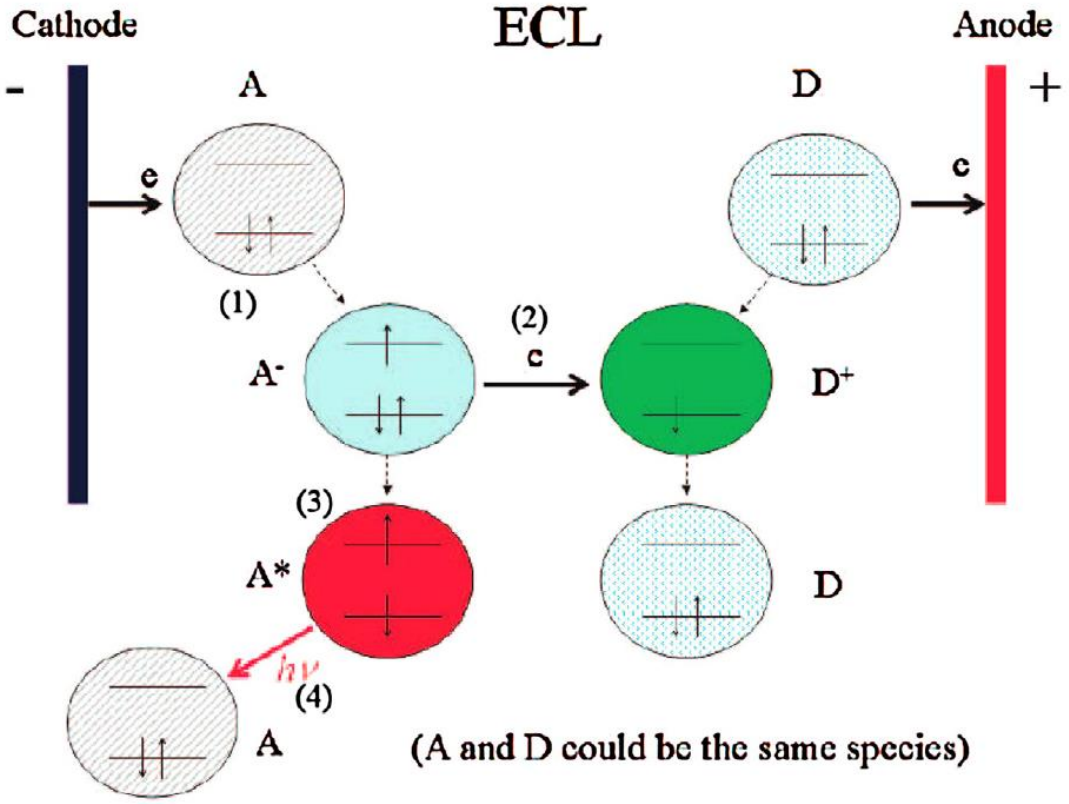

Figure 55. *Graphic representation of ECL reactions.*

Looking more in detail at the mechanism characteristic of the presented technique, there are two dominant pathways through which ECL can be produced, namely the

"annihilation" and "co-reactant" pathway.[71] In each case, two species are generated electrochemically, and those two species undergo an electron-transfer reaction to produce an emissive species. Particularly, ion annihilation (or radical ion annihilation) ECL involves the formation of excited states as a result of exergonic electron-transfer (in the diffusion layer) between electrochemically generated species (typically radical ions) at the surface of electrodes during potential pulsing or cycling. Let us consider a luminophore (emitter) species, R, which is oxidised and reduced at the electrode. Light emission occurs when electrogenerated reduced species ($A^{\cdot -}$) collides with oxidized species ($D^{\cdot +}$) in an annihilation process that produces excited species (R^*). The *ion annihilation* ECL occurs through the following steps:

$$R - e^- \rightarrow D^{\cdot +} \qquad \text{(Eq. 22)}$$

$$R + e^- \rightarrow A^{\cdot -} \qquad \text{(Eq. 23)}$$

$$A^{\cdot -} + D^{\cdot +} \rightarrow R + R^* \qquad \text{(Eq. 24)}$$

$$R^* \rightarrow R + h\nu \qquad \text{(Eq. 25)}$$

Annihilation occurs in the third step with the formation of the excited species, R^*. Furthermore, it must be considered that annihilation reactions can also occur with different species, i.e., when the radical cation and the radical anion derive from different molecules.

On the other hand, considering the co-reactant pathway, ECL emission can take place during a single direction potential sweep with ECL emitter and co-reactant in solution. Typically, depending on the polarity of the applied potential, both luminophore and co-reactant species can be oxidised or reduced at the electrode to form radical ions and intermediates species, followed by decomposition and formation of excited states that emit light. Because highly reducing intermediate species are generated after electrochemical oxidation of co-reactant or highly oxidising intermediates are produced after electrochemical reduction, the

corresponding ECL reactions are often defined as “oxidative-reduction” for the former and “reductive-oxidation” ECL for the latter, respectively.

The coreactant pathway simply requires sacrificial reagents and the application of a single potential step or its sweeping in one direction. A coreactant is a chemical species that undergoes electrochemical oxidation or reduction at the electrode surface producing very reactive intermediates that react with the luminophore to generate the excited state.14,24 Typical coreactants are amines, such as TPrA and 2-(dibutylamino)ethanol (DBAE), oxalate ion, peroxydisulfate, NADH, H2O2 or carbon nanomaterials and, they may generate ECL through the so-called ‘oxidative-reduction’ or ‘reductive-oxidation’ mechanisms. Unlike the coreactant, which gets irreversibly consumed, the luminophore can be regenerated and used for a new cycle.[72]

The coreactant mechanism can be divided into homogeneous and heterogeneous mechanism and they mainly use the couple [Ru(bpy)3]2+ / TPrA. The “homogenous ECL” is the mainly applied and involves the direct oxidation of both the luminophores and the coreactant at the electrode surface followed by the deprotonation reaction of the oxidised coreactant that generates TPrA●, which reacts with [Ru(bpy)3]3+, forming the excited state [Ru(bpy)3]2+*. Then, it returns to the ground state after the release of a photon, thus emitting light. The ECL homogeneous mechanism is schematized in Fig.56.

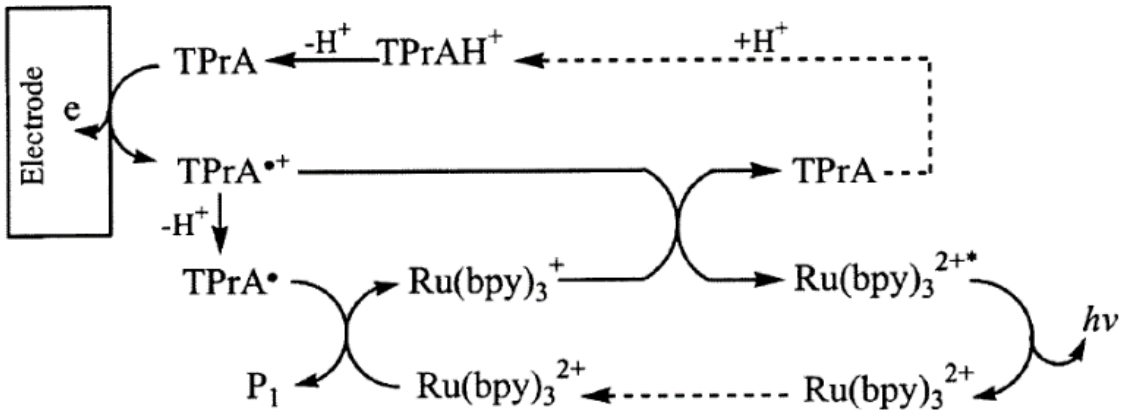

Figure 56. *Graphic representation of homogeneous coreactant ECL reactions.*

However, in most of the analytical methods, the luminophore is constrained close to the electrode because it is attached to a sensing element (i.e. antibody, bead, DNA probe, ecc..) and thus not free to diffuse to the electrode. In this case, ECL emission is therefore triggered exclusively by the radicals obtained by the anodic oxidation of TPrA, i.e. $TPrA^{\bullet+}$ and $TPrA^{\bullet}$ that would react with the immobilized luminophore generating the excited state. The oxidation and deprotonation steps of coreactant are the same as homogeneous mechanism, while the reduction and oxidation of luminophore were performed directly by the products of coreactant oxidation and not at the electrode surface. Compared with annihilation, co-reactant ECL presents unique advantages in all bioanalytical applications. First, a key advantage is that it facilitates ECL generation in aqueous solution (i.e., where hydrogen evolution may strongly compete with the generation of the reduced luminophore, thus inhibiting the annihilation procedure), opening up a wide range of assays for molecules of diagnostic or biological relevance. Furthermore, a high stability of both the oxidised and reduced forms of the luminophore is no longer required through this pathway, thus increasing the number of potential ECL reporters that may be used in the analysis. Additionally, the use of a co-reactant can make ECL possible even for some fluorescent compounds that have only a reversible electrochemical reduction or oxidation. Therefore, when the annihilation reaction between oxidized and reduced species is not efficient, the use of a co-reactant may produce more intense ECL. To mention also an additional advantage, the possibility to operate only in the region of positive potentials (*oxidative-reduction* mechanism) avoids any possible interference of oxygen (that is a reducible species) in the generation of ECL partners, thus permitting in principle to perform analysis in air-equilibrated solutions.

Electrochemical measurements were conducted using a custom glass cell filled with a solutions of 0.3 M phosphate buffer, variable TPrA concentrations (pH 6.8) with a potentiostat SP-150 (Biologic science instruments). The working electrodes were purchased from MetrOhm; a Pt counter electrode (0.072 cm2), and a

reference electrode Ag/AgCl (3 M NaCl) were used. The ECL signals were measured with a photomultiplier tube (PMT, Hamamatsu R928) placed at a fixed height above the electrochemical cell. Both the electrochemical cell and the PMT were placed inside a dark box. A high-voltage power socket assembly with a transimpedance amplifier (Hamamatsu C6271) was used to supply the voltage to the PMT, using an external trigger connection to the potentiostat DAC module. Light/current/voltage curves were recorded by collecting the amplified PMT output signal with the ADC module of the potentiostat. The experimental setup used is depicted in Fig.57.

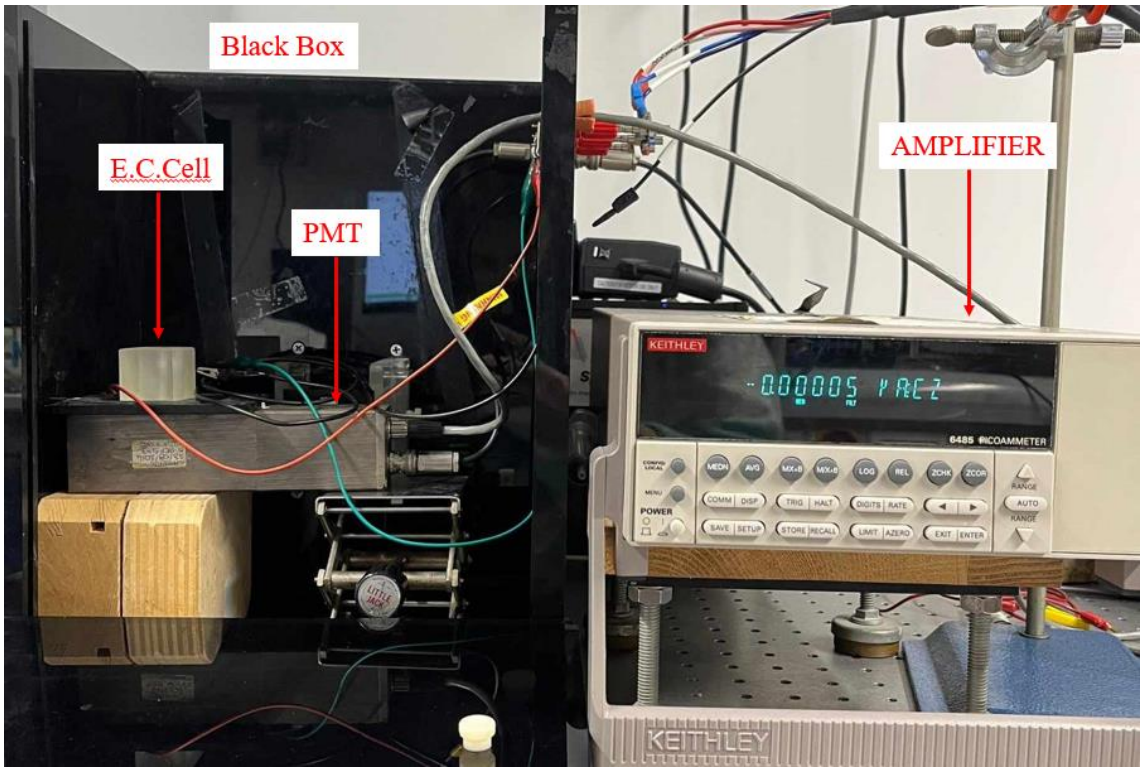

Figure 57. *Experimental setup used for ECL measurements*

Funding acknowledgements

Borsa di dottorato del Programma Operativo Nazionale Ricerca e Innovazione 2014-2020 (CCI 2014IT16M2OP005), risorse FSE REACT-EU, Azione IV.4 “Dottorati e contratti di ricerca su tematiche dell’innovazione” e Azione IV.5 “Dottorati su tematiche Green."

Codice CUP: J35F21003220006